70-21,605

ADAMS, Wade J., 1940-
THE MOLECULAR STRUCTURES OF GASEOUS CYCLOPENTANE, TETRAHYDROFURAN, IODINE HEPTAFLUORIDE, CYCLOBUTANECARBOXYLIC ACID CHLORIDE AND PHOSPHORUS PENTACHLORIDE AS DETERMINED BY ELECTRON DIFFRACTION.

The University of Michigan, Ph.D., 1969
Chemistry, physical

University Microfilms, A XEROX Company, Ann Arbor, Michigan

THIS DISSERTATION HAS BEEN MICROFILMED EXACTLY AS RECEIVED

THE MOLECULAR STRUCTURES OF GASEOUS CYCLOPENTANE, TETRAHYDROFURAN, IODINE HEPTAFLUORIDE, CYCLOBUTANECARBOXYLIC ACID CHLORIDE AND PHOSPHORUS PENTACHLORIDE AS DETERMINED BY ELECTRON DIFFRACTION

by

Wade J. Adams

A dissertation submitted in partial fulfillment
of the requirements for the degree of
Doctor of Philosophy in
The University of Michigan
1969

Doctoral Committee:

Professor Lawrence S. Bartell, Chairman
Professor Lawrence O. Brockway
Professor Philip J. Elving
Professor Richard H. Sands
Assistant Professor James F. Verdieck

ABSTRACT

THE MOLECULAR STRUCTURES OF GASEOUS CYCLOPENTANE, TETRAHYDROFURAN, IODINE HEPTAFLUORIDE, CYCLOBUTANECARBOXYLIC ACID CHLORIDE AND PHOSPHORUS PENTACHLORIDE AS DETERMINED BY ELECTRON DIFFRACTION

by

Wade J. Adams

Chairman: Lawrence S. Bartell

The structural characteristics of cyclopentane and tetrahydrofuran have been compared and discussed with respect to their structural characteristics determined by other methods. Experimental diffraction intensities can be accounted for by a pseudorotation model similar to that proposed by Kilpatrick, Pitzer and Spitzer. Kilpatrick's model was modified to maintain the constancy of the ring bond lengths, independent of the puckering amplitude and pseudorotation phase angle. The one-dimensional structural information implicit in the diffraction intensities does not distinguish between the case of molecules undergoing dynamic pseudorotation and the case of molecules existing in a single puckered conformation. The diffraction intensities are sufficiently sensitive to the puckering amplitude, q_g, in both molecules, to yield an accurate determination of its value. Selected structural parameters determined for cyclopentane were r_g(C-H) = $1.113_5 \pm 0.001_5$ Å, r_g(C-C) = $1.546 \pm 0.001_2$ Å, $\angle$ CCH = $111.7 \pm 0.2°$ and $q_g = 0.43_5 \pm 0.01$ Å. Structural parameters determined for tetrahydrofuran were r_g(C-H) = $1.114 \pm 0.001_3$ Å, r_g(C-O) = $1.429 \pm 0.001_2$ Å, r_g(C-C) = $1.538 \pm 0.001_2$ Å,

$\angle$ CCH = 110.9 ± 0.2° and q_g = 0.38 ± 0.02 Å.

As was the case for the foregoing cyclic molecules, electron diffraction intensities of iodine heptafluoride may be accounted for in terms of structures with C_2 or C_s symmetry or, alternatively, in terms of a dynamic pseudorotation model. In either interpretation the deformations from D_{5h} symmetry are small, and characterized by a correlation in phase of displacements along e_2'' (equatorial puckering) and e' (axial bending) symmetry coordinates. The amplitudes of the e_2'' and e' angular displacements found were α_{eq} = 7.5 ± 1° and α_{ax} = 4.5 ± 1°. The mean bond length was determined to be 1.837 ± 0.002 Å with the equatorial bonds 0.07_2 ± 0.01 Å longer than the axial bonds.

Rotational isomerization about the C-CClO bond in cyclobutanecarboxylic acid chloride was found to be similar to that in unstrained alkyl carboxaldehydes, exhibiting gauche-like isomerization ($100 \pm {}^{0}_{15}$%) with no evidence for the cis isomerization observed in highly strained cyclopropyl compounds. This molecule provides an additional example in which the carbonyl oxygen exhibits a propensity to eclipse a methyl or methylene group in preference to a hydrogen atom. A crude estimate of the rotational barrier of 2.5 to 4.0 kcal/mole was derived from the breadth of the distribution in internal rotation angle. Normal values for bond lengths, bond angles and amplitudes of vibration were found.

The molecular structure of PCl_5 has been re-examined and the mean amplitudes of vibration were determined for the first time. The mean bond length was found to be r_g(P-Cl) = 2.061 ± 0.002 Å with the axial bonds of this trigonal bipyramid molecule 0.10_4 ± 0.01 Å longer than the equatorial bonds. Mean amplitudes of vibration showed that the axial bending frequency is higher than the in-plane equatorial bending

frequency, an assignment which has been in doubt, since insufficient data are available from vibrational spectroscopy to make an unambiguous assignment.

ACKNOWLEDGMENTS

I sincerely thank Dr. L. S. Bartell for his helpful discussions during the course of this research and for his generous advice during the writing of this dissertation.

I also express my thanks to the members of Dr. Bartell's research group for their aid and valuable discussions, particularly, Dr. F. B. Clippard, Jr., Miss E. J. Jacob and Dr. J. Janzen. Special thanks go to Dr. H. J. Geise for his assistance in recording the cyclopentane and tetrahydrofuran diffraction patterns and for help in the analysis of the data. Special thanks also go to Dr. H. B. Thompson for recording the iodine heptafluoride diffraction patterns.

I also thank my wife, Sandra, for encouragement and for giving so much of her time typing, plotting data and drawing illustrations.

For financial support, I am indebted to the National Science Foundation, the Minnesota Mining and Manufacturing Company and the Stauffer Chemical Company.

ABSTRACT

The structural characteristics of cyclopentane and tetrahydrofuran have been compared and discussed with respect to their structural characteristics determined by other methods. Experimental diffraction intensities can be accounted for by a pseudorotation model similar to that proposed by Kilpatrick, Pitzer and Spitzer. Kilpatrick's model was modified to maintain the constancy of the ring bond lengths, independent of the puckering amplitude and pseudorotation phase angle. The one-dimensional structural information implicit in the diffraction intensities does not distinguish between the case of molecules undergoing dynamic pseudorotation and the case of molecules existing in a single puckered conformation. The diffraction intensities are sufficiently sensitive to the puckering amplitude, q_g, in both molecules, to yield an accurate determination of its value. Selected structural parameters determined for cyclopentane were r_g(C-H) = $1.113_5 \pm 0.001_5$ Å, r_g(C-C) = $1.546 \pm 0.001_2$ Å, $\angle$ CCH = $111.7 \pm 0.2°$ and $q_g = 0.43_5 \pm 0.01$ Å. Structural parameters determined for tetrahydrofuran were r_g(C-H) = $1.114 \pm 0.001_3$ Å, r_g(C-O) = $1.429 \pm 0.001_2$ Å, r_g(C-C) = $1.538 \pm 0.001_2$ Å, $\angle$ CCH = $110.9 \pm 0.2°$ and $q_g = 0.38 \pm 0.02$ Å.

As was the case for the foregoing cyclic molecules, electron diffraction intensities of iodine heptafluoride may be accounted for in terms of structures with C_2 or C_s symmetry or, alternatively, in terms of a dynamic pseudorotation model. In either interpretation the deformations from D_{5h} symmetry are small, and characterized by a correlation

in phase of displacements along e_2'' (equatorial puckering) and e' (axial bending) symmetry coordinates. The amplitudes of the e_2'' and e' angular displacements found were $\alpha_{eq} = 7.5 \pm 1°$ and $\alpha_{ax} = 4.5 \pm 1°$. The mean bond length was determined to be 1.837 ± 0.002 Å with the equatorial bonds 0.07_2 ± 0.01 Å longer than the axial bonds.

Rotational isomerization about the C-CClO bond in cyclobutanecarboxylic acid chloride was found to be similar to that in unstrained alkyl carboxaldehydes, exhibiting gauche-like isomerization ($100 \pm {}^{0}_{15}\%$) with no evidence for the cis isomerization observed in highly strained cyclopropyl compounds. This molecule provides an additional example in which the carbonyl oxygen exhibits a propensity to eclipse a methyl or methylene group in preference to a hydrogen atom. A crude estimate of the rotational barrier of 2.5 to 4.0 kcal/mole was derived from the breadth of the distribution in internal rotation angle. Normal values for bond lengths, bond angles and amplitudes of vibration were found.

The molecular structure of PCl_5 has been re-examined and the mean amplitudes of vibration were determined for the first time. The mean bond length was found to be r_g(P-Cl) = 2.061 ± 0.002 Å with the axial bonds of this trigonal bipyramid molecule 0.10_4 ± 0.01 Å longer than the equatorial bonds. Mean amplitudes of vibration showed that the axial bending frequency is higher than the in-plane equatorial bending frequency, an assignment which has been in doubt, since insufficient data are available from vibrational spectroscopy to make an unambiguous assignment.

TABLE OF CONTENTS

	Page
ACKNOWLEDGMENTS	ii
ABSTRACT	iii
LIST OF TABLES	viii
LIST OF FIGURES	x
LIST OF APPENDICES	xii
PART I. Molecular Structure of Cyclopentane	1
INTRODUCTION	2
EXPERIMENTAL	3
ANALYSIS OF DATA	4
Molecular Model	5
CONFORMATIONAL ENERGY CALCULATIONS	12
RESULTS	13
DISCUSSION	24
PART II. Molecular Structure of Tetrahydrofuran	26
INTRODUCTION	27
EXPERIMENTAL	28
ANALYSIS OF DATA	29
Molecular Model	30
RESULTS	36
DISCUSSION	46

		Page
PART III.	Molecular Structure of Iodine Heptafluoride	50
	INTRODUCTION	51
	EXPERIMENTAL	52
	ANALYSIS OF DATA	54
	RESULTS	56
	Models of Static Deformation from D_{5h} Symmetry	61
	Model of Dynamic Pseudorotation	69
	Coupling of e_1' and e_2'' Modes	70
	DISCUSSION	75
PART IV.	Molecular Structure of Cyclobutanecarboxylic Acid Chloride	80
	INTRODUCTION	81
	EXPERIMENTAL	81
	ANALYSIS OF DATA	83
	RESULTS	87
	Internal Rotation and Ring Puckering	87
	Molecular Parameters	98
	DISCUSSION	100
PART V.	Molecular Structure of Phosphorus Pentachloride	112
	INTRODUCTION	113
	EXPERIMENTAL	113
	ANALYSIS OF DATA	115
	RESULTS	117
	DISCUSSION	125

Page

REFERENCES 128

APPENDIX A 135

APPENDIX B 139

APPENDIX C 143

APPENDIX D 148

APPENDIX E 153

APPENDIX F 157

LIST OF TABLES

Table		Page
1.1	Experimental conditions under which C_5H_{10} diffraction patterns were recorded.	3
1.2	Molecular distances calculated by the C_5H_{10} pseudorotation model for a puckering amplitude q = 0.435 Å.	14
1.3	Valency and torsional angles calculated by the C_5H_{10} pseudorotation model for a puckering amplitude q = 0.435 Å.	15
1.4	Structural parameters and estimated standard errors for C_5H_{10}.	16
1.5	Matrix of correlation coefficients for C_5H_{10}.	21
2.1	Experimental conditions under which C_4H_8O diffraction patterns were recorded.	28
2.2	Structural parameters calculated by the C_4H_8O pseudorotation model for a puckering amplitude q = 0.38 Å.	37
2.3	Results of least squares analyses of the composite molecular intensity for C_4H_8O.	41
2.4	Structural parameters and estimated standard errors for C_4H_8O.	45
2.5	Matrix of correlation coefficients for C_4H_8O.	47
3.1	Experimental conditions under which IF_7 diffraction patterns were recorded.	53
3.2	Results of least squares analyses of the composite molecular intensity for IF_7.	62
3.3	Matrix of correlation coefficients for IF_7.	67
3.4	Atomic coordinates of IF_7 for $\alpha_{eq} = 7.55°$ and $\alpha_{ax} = 4.5°$.	71
3.5	Molecular distances calculated by the IF_7 pseudorotation model for an equatorial angular amplitude $\alpha_{eq} = 7.55°$ and an axial bending amplitude $\alpha_{ax} = 4.5°$.	72
3.6	Structural parameters and estimated standard errors for IF_7.	74

Table		Page
4.1	Experimental conditions under which C_4H_7CClO diffraction patterns were recorded.	82
4.2	Distribution in angle of internal rotation and ring puckering for C_4H_7CClO. Results of least squares minimization with respect to three internal rotation isomers for various assumed isomeric concentrations and ring conformations.	94
4.3	Structural parameters and estimated standard errors for C_4H_7CClO.	99
4.4	Comparison of parameters for C_4H_7CClO and related molecules.	101
4.5	Matrix of correlation coefficients for C_4H_7CClO.	107
5.1	Experimental conditions under which PCl_5 diffraction patterns were recorded.	115
5.2	Structural parameters and estimated standard errors for PCl_5.	123
5.3	Comparison of electron diffraction studies of PCl_5.	124
5.4	Matrix of correlation coefficients for PCl_5.	126

LIST OF FIGURES

Figure		Page
1.1	Comparison of the C_5H_{10} experimental radial distribution function with the calculated function for a planar, D_{5h} symmetry, model.	7
1.2	Pseudorotation model for C_5H_{10} with the $\phi = 108°$ (C_s symmetry) conformation shown.	10
1.3	Comparison of experimental and calculated molecular intensity functions for C_5H_{10}.	17
1.4	Experimental radial distribution function for C_5H_{10}.	19
2.1	Experimental radial distribution function for C_4H_8O.	32
2.2	Pseudorotation model for C_4H_8O with the $\phi = 108°$ (C_s symmetry) conformation shown.	34
2.3	Comparison of experimental and calculated molecular intensity functions for C_4H_8O.	40
2.4	Experimental and calculated radial distribution functions for the $\phi = 18°$ (C_s conformation), $\phi = 63°$ (C_2 conformation), 50% $\phi = 18°$ + 50% $\phi = 63°$ and $\phi = 40.5°$ pseudorotation conformers of C_4H_8O.	44
3.1	Comparison of the IF_7 experimental radial distribution function with the calculated function for a D_{5h} symmetry model.	58
3.2	Molecular models of IF_7 having D_{5h}, C_2 and C_s symmetry.	59
3.3	Comparison of experimental and calculated molecular intensity functions for IF_7.	64
3.4	Experimental radial distribution function for IF_7.	66
4.1	Axial and equatorial conformations of C_4H_7CCl0.	86
4.2	Experimental and calculated radial distribution functions of C_4H_7CCl0 for different internal rotation angles assuming a planar cyclobutane ring.	90

Figure		Page
4.3	Experimental and calculated radial distribution functions showing the results of least squares minimization with respect to three internal rotation isomers for various assumed isomeric concentrations and ring conformations.	92
4.4	Experimental and calculated molecular intensity functions for C_4H_7CClO.	104
4.5	Experimental radial distribution function for C_4H_7CClO.	106
5.1	Comparison of experimental and calculated molecular intensity functions for PCl_5.	118
5.2	Experimental radial distribution function for PCl_5.	120
5.3	Summary of results of least squares analyses on corrected and uncorrected 21 cm, 11 cm and 6.5 cm camera distance intensities.	122

LIST OF APPENDICES

APPENDIX		Page
A	Experimental Leveled Intensity and Background Intensity Functions for C_5H_{10}	135
	21 cm Camera Distance (r^3 Sector)	136
	11 cm Camera Distance (r^3 Sector)	137
	6.5 cm Camera Distance (r^3 Sector)	138
B	Experimental Leveled Intensity and Background Intensity Functions for C_4H_8O	139
	21 cm Camera Distance (r^3 Sector)	140
	11 cm Camera Distance (r^3 Sector)	141
	6.5 cm Camera Distance (r^3 Sector)	142
C	Experimental Leveled Intensity and Background Intensity Functions for IF_7	143
	21 cm Camera Distance (r^2 Sector)	144
	21 cm Camera Distance (r^3 Sector)	145
	11 cm Camera Distance (r^3 Sector)	146
	6.5 cm Camera Distance (r^3 Sector)	147
D	Experimental Leveled Intensity and Background Intensity Functions for C_4H_7CC1O	148
	21 cm Camera Distance (r^2 Sector)	149
	21 cm Camera Distance (r^3 Sector)	150
	11 cm Camera Distance (r^3 Sector)	151
	6.5 cm Camera Distance (r^3 Sector)	152

APPENDIX		Page
E	Experimental Leveled Intensity and Background Intensity Functions for PCl_5	153
	21 cm Camera Distance (r^3 Sector)	154
	11 cm Camera Distance (r^3 Sector)	155
	6.5 cm Camera Distance (r^3 Sector)	156
F	Corrected Experimental Leveled Intensity and Background Intensity Functions for PCl_5	157
	21 cm Camera Distance (r^3 Sector)	158
	11 cm Camera Distance (r^3 Sector)	159
	6.5 cm Camera Distance (r^3 Sector)	160

PART I

Molecular Structure of Cyclopentane

INTRODUCTION

Thermodynamic studies (1) gave the first experimental evidence that cyclopentane is non-planar. Semi-quantitative calculations (2,3) relating structure and strain energy suggested, in addition, that the deformation is not static, but dynamic, with the puckering displacements progressing (pseudorotating) around the five-membered ring. Later thermodynamic studies (3,4,5) and energy calculations (6,7,8) have provided further support for pseudorotation. Perhaps the most direct evidence for pseudorotation has come from a recent infrared spectroscopic study (9). In addition, a number of related five-membered ring systems have now been found to undergo pseudorotation (10). Cyclopentane has previously been studied by electron diffraction by both Hassel, et al., (11) (visual method) and Bastiansen, et al., (12). While the latter work indicated that the molecule was non-planar, no estimate was given of the degree of non-planarity.

It was therefore thought worthwhile to reinvestigate the structure of this molecule to establish the amplitude of puckering involved in the pseudorotation. It also seemed desirable to make use of an existing potential energy minimization computer program to calculate energies as a function of both the amplitude and phase angle of puckering according to a proposed pseudorotation model.

EXPERIMENTAL

Research grade cyclopentane of 99.99 mole percent purity was obtained from the Phillips Petroleum Corp., Bartlesville, Oklahoma, and used without further purification. Diffraction patterns were recorded on 4 X 5 in. Kodak process plates at camera distances of 21, 11 and 6.5 cm using an electron diffraction apparatus (13) equipped with an r^3 rotating sector. The gas was introduced into the diffraction chamber through a nickel nozzle having a throat 0.29 mm in diameter and 0.70 mm in length. The experimental conditions under which the diffraction patterns were recorded using 40 kV electrons are given in Table 1.1. Plates were developed at 20°C for 5 min. with Kodak D-11 developer.

Table 1.1 Experimental conditions under which C_5H_{10} diffraction patterns were recorded.

Camera distance (cm)	21.048	11.115	6.585
Sample temperature (°C)	-26	-26	-26
Vapor pressure (torr)	27	27	27
Exposure time (sec)	5-6	15-20	35-40
Beam current (μA)	0.46	0.46	0.47

Photographic densities, measured with an automatic recording microphotometer with digital output (14), were converted to absorbancies and corrected for the radial variation of plate sensitivity (15). Intensi-

ties were calculated from the corrected absorbancies according to

$$I = A(1 + 0.05A^2)^*$$

as recommended by Janzen (15). Six plates at the 21 and 6.5 cm distances and four plates at the 11 cm distance were averaged and used in the structural analysis.

ANALYSIS OF DATA

Experimental intensities were leveled (16) using the analytical elastic scattering factors of Strand and Bonham (17) and the inelastic scattering factors of Heisenberg and Bewilogua (18). Corrections were also made for sector imperfections and extraneous scattering. Experimental leveled intensity, $I_0(s)$, and background intensity, $I_B(s)$, functions (16) for the three camera distances are given in Appendix A. Indices of resolution (19) were 1.03_5, 1.08 and 1.05 for the 21, 11 and 6.5 cm camera distances respectively.

Experimental and calculated molecular intensities and radial distribution functions were computed as previously described (16,19,20) with the usual corrections applied for scattering by planetary electrons (19), the failure of the Born approximation (21), anharmonicity of vibrations (22) and integral termination errors (23). Radial distribution functions were calculated using a Degard damping factor [$\exp(-0.0015s^2)$]. Atomic scattering factors used in the calculations were the partial wave elastic factors of Cox and Bonham (24) and the inelastic factors of Tavard (25). Anharmonicity constants (22) were estimated (26) to be

---

* Least squares analyses (15) on plates processed in the present manner supported the empirical I(A) function used. This function probably does not have general validity (R. A. Bonham, private communication).

2.0 $Å^{-1}$ for the bonded distances and taken to be 1.0 $Å^{-1}$ for nonbonded distances.

The anharmonic radial distribution function, the molecular intensity of each camera distance, and the composite molecular intensity were fitted with the appropriate calculated expressions in least squares analyses (27). The composite molecular intensity was calculated by interpolating the molecular intensity of each camera distance, divided by its index of resolution, to integral values of the scattering variable q prior to combination of the data. Data in the scattering range in which two camera distances overlapped were combined as in the construction of experimental radial distribution functions (16).

The effects of both random and systematic errors were included in calculated standard errors as discussed by Bartell (28). Systematic errors in bond lengths and mean amplitudes of vibration were estimated to be 0.07% and 2.0% respectively. The principal systematic error in the mean amplitude of vibration arises from the uncertainty in the index of resolution.

Molecular Model

Comparison of the experimental radial distribution function and the calculated distribution function for a planar (D_{5h} symmetry) model of cyclopentane, Figure 1.1, shows the ring to be decidedly non-planar. First, the 2.4 Å C...C nonbonded peak is closer to the C-C bonded peak than would be possible in a planar ring. Secondly, the C...H nonbonded distribution near 3.2 Å is split into two components instead of appearing as the single nearly Gaussian peak characteristic of a planar skeleton. A molecular model was therefore adopted which allowed the calcu-

Figure 1.1 Comparison of the C_5H_{10} experimental radial distribution function (solid curve) with the calculated function (dashed curve) for a planar, D_{5h} symmetry, model.

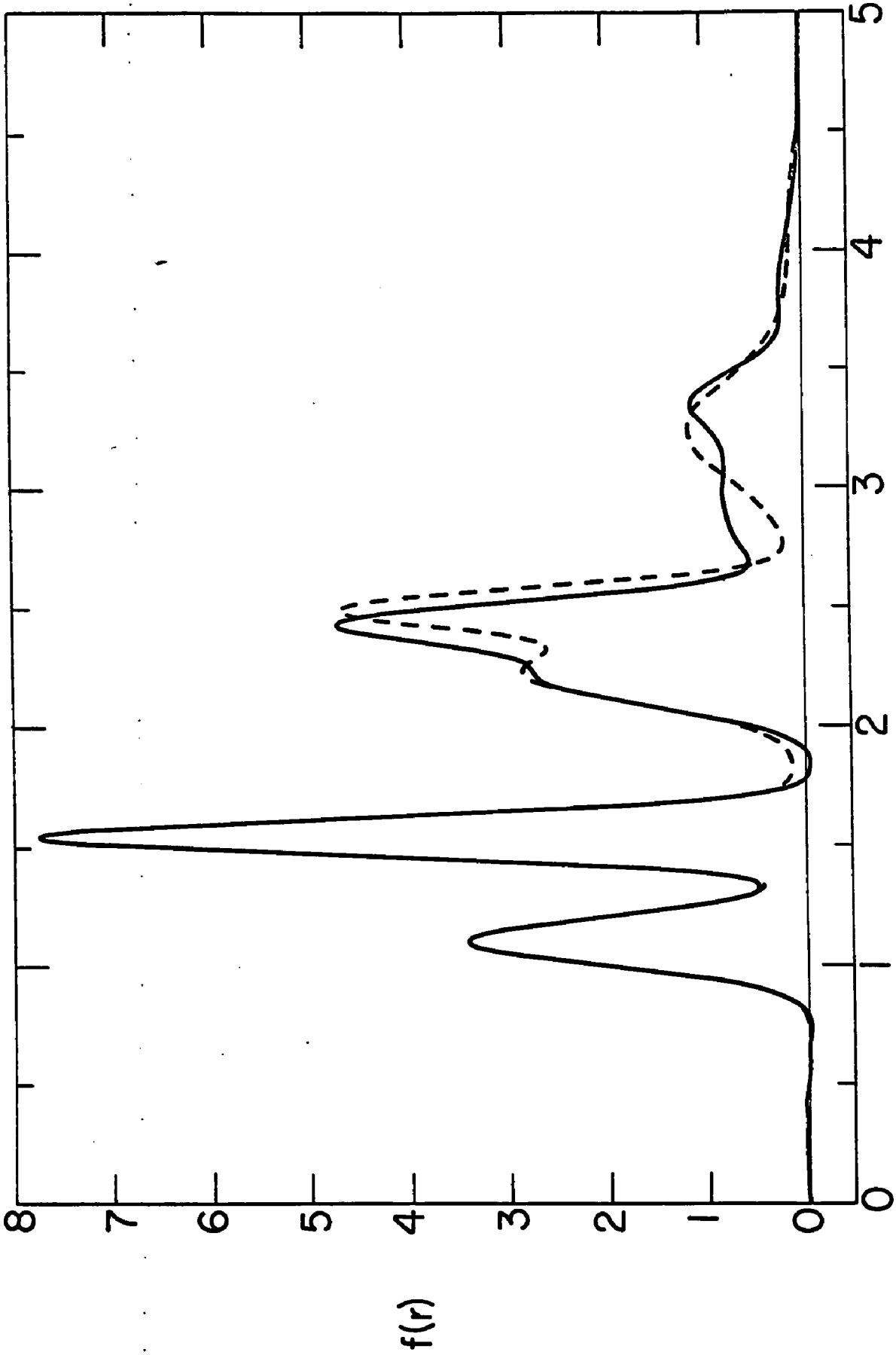


Figure 1.1

lation of all conformations of a freely pseudorotating molecule and made possible a comparison with previous thermodynamic (3,4,5) and infrared (9) studies. The model was modified somewhat from that suggested by Kilpatrick, et al., (3) as described below.

The pseudorotation model adopted is shown in Figure 1.2. The puckering displacements in cyclopentane are described relative to the plane of the unpuckered, D_{5h} symmetry, configuration of the carbon atom skeleton. An origin is centered on the carbon atom skeleton and a z-axis is defined to be perpendicular to the plane of the skeleton. The dotted lines are hypothetical spokes of length

$$S_o = (r_{CC}/2) \text{ cosec } (2\pi/10)$$

extending from the origin to the carbon atoms (1,...,5) in their reference positions. The vectors $\vec{S}_j$, radiating from the origin, define the instantaneous atomic positions of the carbon atoms. During the pseudorotation, each carbon atom is constrained to move in its respective vertical plane. The angular separation between adjacent vertical planes is $2\pi/5$.

An angular displacement of the vector $\vec{S}_j$ from the horizontal reference plane is defined by

$$\alpha_j = \tan^{-1}(z_j/S_o) \qquad j = 1,...,5$$

in which z_j corresponds to the hypothetical perpendicular displacement

$$z_j = \sqrt{2/5}\ q \cos[2(2\pi j/5 + \phi)].$$

The parameters q and ϕ are the pseudoradial puckering amplitude and pseudorotational phase angle respectively. In the model of Kilpatrick, et al., (3) z_j corresponds to the actual perpendicular displacement of carbon atom j from the reference planar configuration. In Kilpatrick's displacements the Eckart conditions are satisfied, but unfortunately,

Figure 1.2 Pseudorotation model for C_5H_{10} with the $\phi = 108°$ (C_s symmetry) conformation shown.

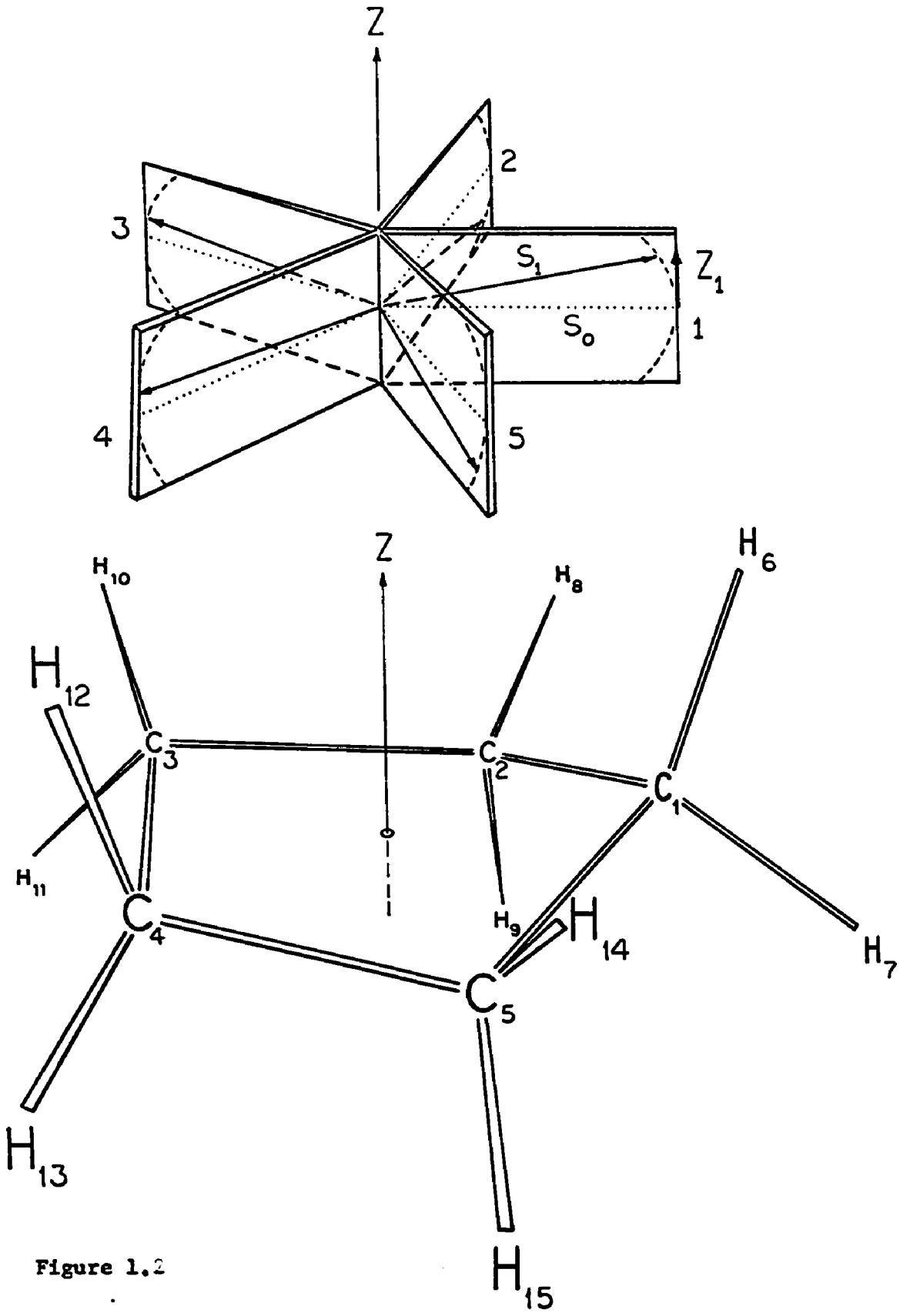


Figure 1.2

the individual C-C bond lengths in the molecule are appreciably dependent on both q and ϕ. A scheme to circumvent the problem of nonconstant bond lengths was devised for the present investigation. Atomic displacements are constrained to the vertical planes of the Kilpatrick model, but the actual displacement amplitudes are described in terms of the angles α_j rather than the distances z_j. The vectors $\vec{S}_j$ are then varied in length as q and ϕ vary, in order to preserve all C-C bond lengths. That is, for any given q and ϕ, the individual α_j are unambiguously specified, as are the five angles between adjacent $\vec{S}_j$. These five angles relate the $\vec{S}_j$ to the individual r_{CC} and give five simultaneous equations for the $|S_j|$ which must be satisfied if the C-C bonds are to remain invariant. A solution yields trajectories of carbon atoms which, for a given q, are nearly parabolic instead of linear as in the model of Kilpatrick, et al. It is notable, however, that the actual distance traveled by atom j from the reference configuration is equal (within 0.3%) to the perpendicular displacement z_j in the Kilpatrick, et al., model.

Although the present scheme rigorously preserves the C-C bond lengths, it does not satisfy the Eckart conditions exactly. The center of mass of the molecule rotates about the defined z-axis in a pseudorotational cycle, with a radius of 0.0236 ± 0.00005 Å for $q = 0.43_5$ Å. This has no influence on the diffraction analysis, but shows the need for a very minor correction to the displacement coordinates in treatments of dynamical properties.

The hydrogen atoms (6,...,15), Figure 1.2, were constrained to follow the motion of the carbon atoms in order to preserve local C_{2v} symmetry at each methylene group. All C-C-H valency angles were assumed to

be equal.

CONFORMATIONAL ENERGY CALCULATIONS

Conformational energy calculations were carried out as previously described (29) using a modified Urey-Bradley potential energy function composed of quadratic terms for bond stretches and bond angle bends, a three-fold cosine function for rotations about C-C bonds, and anharmonic analytical functions for pairwise nonbonded interactions between all nonbonded pairs. Quadratic force constants for bond stretches and bond angle bends were taken from the spectroscopic Urey-Bradley analysis of acyclic paraffins by Schachtschneider and Snyder (30), the torsional barrier was treated as an adjustable parameter, and the nonbonded functions adopted were those proposed by Bartell (31). Reference values of the bond lengths and valency angles were the same as those previously derived (29).

The computer program used in the energy minimization procedure was specifically written to handle acyclic molecules (29) and included no provision for maintaining geometrical consistency in a cyclic molecule if all internal coordinates were allowed to vary. In order to maintain geometrical consistency, the C-C-C valency angles and torsional angles about C-C bonds were calculated using the described pseudorotation model and were not allowed to vary in the minimization. The constraints on the valency and torsional angles permitted conformational energies to be calculated as functions of both the amplitude and phase angle of puckering as defined by the pseudorotation model. The total potential energy

according to this model force field, less the torsional energy,* was minimized with respect to the independent structural parameters r_{CC}, r_{CH} and ∢ HCH.

RESULTS

Intramolecular distances (excepting H...H distances) calculated by the pseudorotation model for a puckering amplitude, q = 0.43$_5$ Å, at three different pseudorotational phase angles are given in Table 1.2. Included in Table 1.3 are the C-C-H and C-C-C valency angles and torsional angles for these conformations as well as the sums

$$1/2 \sum_{i=1}^{5} (\theta^i - \theta^o)^2 \quad \text{and} \quad 1/2 \sum_{i=1}^{5} [1 + \cos(3\beta^i)]$$

over the C-C-C valency angles, θ^i, and torsional angles, β^i, for each of these conformations. The reference C-C-C valency angle, θ^o, was taken to be tetrahedral.

The composite experimental molecular intensity, sM(s), and its calculated counterpart computed using the parameters given in Table 1.2 (but including H...H distances) for the $\phi = 0^\circ$ model, are compared in Figure 1.3. The experimental radial distribution function is shown in Figure 1.4 and is compared with the distribution function calculated using the parameters of the same $\phi = 0^\circ$ model. Equally excellent fits were obtained using the parameters given for the $\phi = 5^\circ$ and $\phi = 9^\circ$ model indicating that the experimental diffraction intensities are independent of the phase angle of puckering. However, the experimental diffraction

---

*The neglect of the torsional energy in the minimization has a negligible effect on the derived structural parameters (E.J. Jacob, private communication).

Table 1.2 Molecular distances (in Å) calculated by the C_5H_{10} pseudorotation model for a puckering amplitude q = 0.435 Å.

Parameter	Pseudorotational Phase Angle		
	$\phi = 0^\circ$ (C_s symmetry)	$\phi = 5^\circ$	$\phi = 9^\circ$ (C_2 symmetry)
C-H	1.1135	1.1135	1.1135
C-C	1.5460	1.5460	1.5460
C...H	2.2140	2.2140	2.2140
$C_1...C_3$	2.4716	2.4647	2.4573
$C_1...C_4$	2.4052	2.4082	2.4144
$C_2...C_4$	2.4716	2.4754	2.4764
$C_2...C_5$	2.4357	2.4230	2.4144
$C_3...C_5$	2.4357	2.4483	2.4573
$(C...C)_{ave}$	2.4440	2.4439	2.4444
$C_1...H_{13}, C_4...H_7$	2.8350 (2X)	2.8695,2.8186	2.9084,2.8188
$C_2...H_{14}, C_3...H_{14}$	2.8584 (2X)	2.8302,2.8994	2.8188,2.9395
$C_5...H_8, C_5...H_{10}$	3.0208 (2X)	2.9552,3.0899	2.9084,3.1445
$C_2...H_{13}, C_3...H_7$	3.0449 (2X)	3.1073,2.9844	3.1565,2.9395
$C_1...H_{10}, C_1...H_{11}$	3.2557 (2X)	3.3000,3.1966	3.3285,3.1445
$C_4...H_8, C_4...H_9$	3.2557 (2X)	3.2031,3.3065	3.1565,3.3402
$C_5...H_9, C_5...H_{11}$	3.3695 (2X)	3.3808,3.3505	3.3861,3.3285
$C_2...H_{12}, C_3...H_6$	3.3925 (2X)	3.3674,3.4083	3.3402,3.4150
$C_1...H_{12}, C_4...H_6$	3.3939 (2X)	3.3897,3.3993	3.3861,3.4045
$C_2...H_{15}, C_3...H_{15}$	3.4153 (2X)	3.4098,3.4173	3.4045,3.4150

Table 1.3 Valency and torsional angles[a] calculated by the C_5H_{10} pseudorotation model for a puckering amplitude q = 0.435 Å.

Parameter	Pseudorotational Phase Angle		
	$\phi = 0^\circ$ (C_s symmetry)	$\phi = 5^\circ$	$\phi = 9^\circ$ (C_2 symmetry)
$\angle C_2-C_1-C_5$	103.947	103.191	102.676
$\angle C_1-C_2-C_3$	106.134	105.714	105.257
$\angle C_2-C_3-C_4$	106.134	106.373	106.432
$\angle C_3-C_4-C_5$	103.947	104.709	105.257
$\angle C_4-C_5-C_1$	102.134	102.309	102.676
$1/2\sum_{i=1}^{5}(\theta^i - \theta^o)^2$ [b]	68.5716±0.0002	68.5665±0.0002	68.5531±0.0002
$\angle C_5-(C_1-C_2)-C_3$	25.012	30.572	34.342
$\angle C_1-(C_2-C_3)-C_4$	0.0	7.398	13.164
$\angle C_2-(C_3-C_4)-C_5$	25.012	18.669	13.164
$\angle C_3-(C_4-C_5)-C_1$	40.265	37.433	34.342
$\angle C_4-(C_5-C_1)-C_2$	40.265	41.888	42.290
$1/2\sum_{i=1}^{5}[1 + \cos(3\beta^i)]$ [c]	2.74625±0.00001	2.74629±0.00001	2.74632±0.00001

[a] Angles are in degrees, with the absolute values of torsional angles reported.

[b] θ^i corresponds to the C-C-C valency angles, with the reference C-C-C valency angle, θ^o, taken to be tetrahedral.

[c] β^i corresponds to the C-(C-C)-C torsional angles.

Table 1.4 Structural parameters[a] and estimated standard errors[b] for C_5H_{10}.

Parameter	r_g	l_g	∠
C-H	$1.113_5 \pm 0.001_5$	$0.081_5 \pm 0.002_1$	
C-C	$1.546 \pm 0.001_2$	$0.053_5 \pm 0.001_1$	
$(C...H)_{short}$	$2.214 \pm 0.002_1$	0.110 ± 0.003	
$(C...C)_{mean}$	$2.444 \pm 0.001_5$	$0.071_5 \pm 0.001_6$	
$(C...H)_{long}$[c]		0.113 ± 0.004	
q_g	$0.43_5 \pm 0.01$		
C-C-H[d]			$111.7 \pm 0.1_5$

[a] Distances and amplitudes in Å, angle in degrees.

[b] The effects of both random and systematic errors (28) were included in calculated standard errors.

[c] Constrained to be the same as those given in Table 1.2.

[d] Not corrected for shrinkage effects.

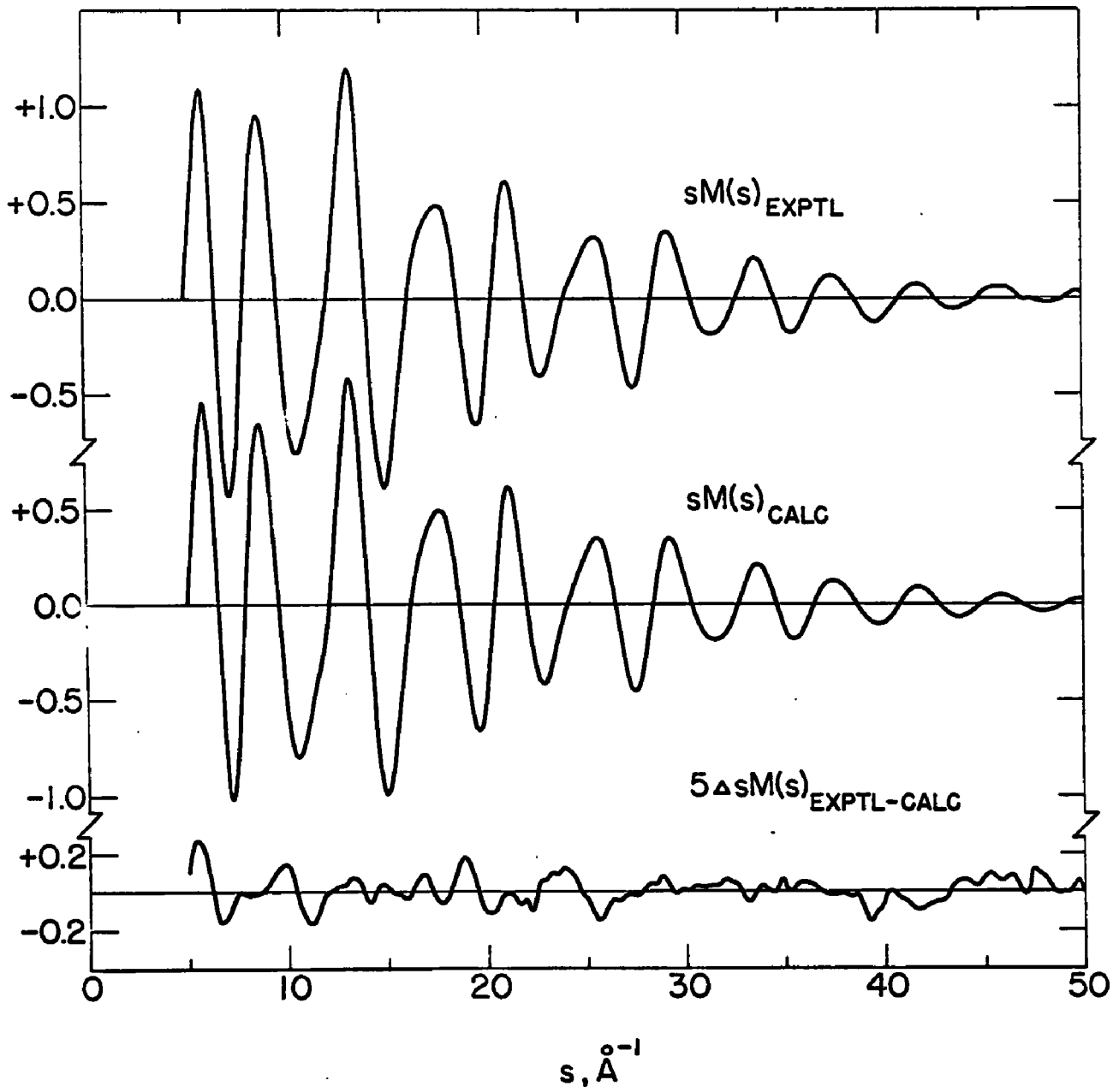


Figure 1.3 Comparison of experimental and calculated molecular intensity functions for C_5H_{10}. $\Delta sM(s) = sM(s)_{exptl} - sM(s)_{calc}$.

Figure 1.4 Experimental radial distribution function for C_5H_{10}. $\Delta f(r) = f(r)_{exptl} - f(r)_{calc}$.

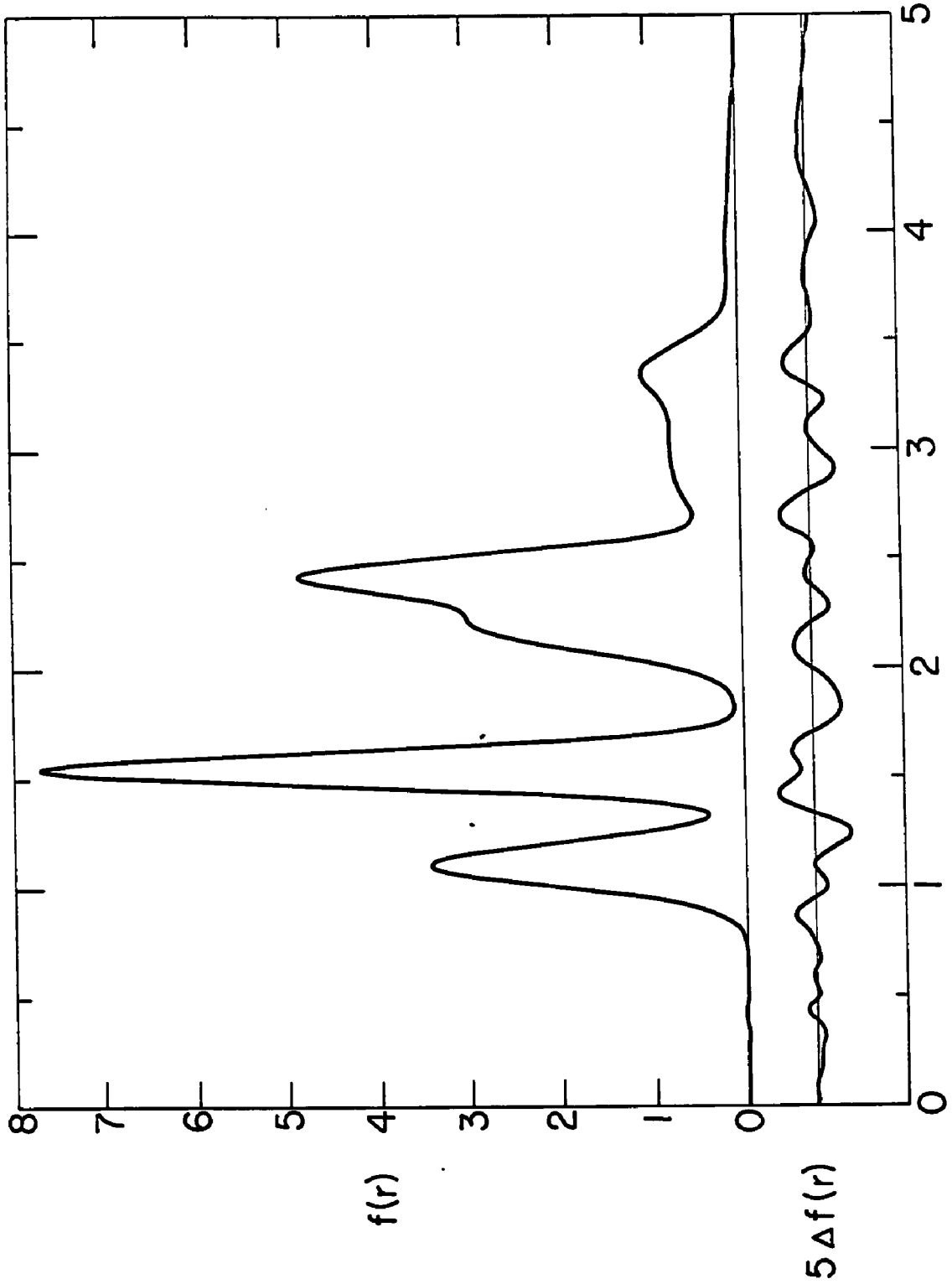


Figure 1.4

intensities are sufficiently sensitive to the amplitude of puckering, so that the value of q_g is readily derivable. Alternatively, q_g may be determined from the radial distribution function by comparing the mean C-C bonded and C...C nonbonded distances. The C-C-H valency angle is derived from the mean C...H nonbonded distance at 2.2 Å, while the spectrum of long C...H nonbonded distances centered around 3.2 Å checks the consistency of the model and the derived parameters. The converged set of structural parameters and their estimated standard errors are given in Table 1.4. It may be noted that the spectrum of C...H nonbonded distances computed using the pseudorotation model allows the broad asymmetric composite peak centered near 3.2 Å to be well fitted with a single value for the amplitude of vibration assigned to each component C...H distance.

A matrix of correlation coefficients based on the least squares fit of the composite molecular intensity using a diagonal weight matrix

$$W(s) = 1 - \exp[-0.00828(s - 2.827)^2]$$

is given in Table 1.5.

Calculated potential energies using the modified Urey-Bradley potential function of Jacob, Thompson and Bartell (29), were found to be the same for any phase angle of puckering to within 3 cal/mole. However, the present calculations show that the potential function proposed by these authors in their investigation of acyclic alkanes gives a poor representation of the cyclopentane force field. It yielded an unrealistically low equilibrium puckering amplitude of $q_e = 0.33$ Å. If the valence and nonbonded components of the Jacob, et al., model force field were retained, it was necessary to increase the intrinsic torsional barrier from 2.7 kcal/mole to 5.9 kcal/mole in order to achieve an equili-

Table 1.5 Matrix of correlation coefficients[a] for C_5H_{10}.

	r(C-H)	r(C-C)	$r(C...H)_{short}$	r(C...C)	ℓ(C-H)
r(C-H)	1.0	0.03	-0.09	-0.01	0.02
r(C-C)		1.0	-0.12	-0.07	0.12
$r(C...H)_{short}$			1.0	0.48	-0.18
r(C...C)				1.0	-0.03
ℓ(C-H)					1.0
ℓ(C-C)					
$ℓ(C...H)_{short}$					
ℓ(C...C)					
$ℓ(C...H)_{long}$					
R					

[a]Based on 149 intensity values interpolated from 328 experimentally observed data points. Matrix elements are given by

$$\rho_{ij} = B_{ij}^{-1}/(B_{ii}^{-1}\ B_{jj}^{-1})^{1/2}$$

where the notation corresponds to that of O. Bastiansen, L. Hedberg, and K. Hedberg, J. Chem. Phys. 27, 1311 (1957).

Table 1.5 (Continued)

	ℓ(C-C)	ℓ(C...H)$_{short}$	ℓ(C...C)	ℓ(C...H)$_{long}$	R
r(C-H)	0.09	0.09	0.10	-0.00	0.20
r(C-C)	-0.00	0.05	0.03	0.00	0.04
r(C...H)$_{short}$	-0.30	-0.23	-0.12	-0.08	-0.42
r(C...C)	-0.04	-0.20	-0.06	-0.16	-0.05
ℓ(C-H)	0.23	0.15	0.18	0.02	0.38
ℓ(C-C)	1.0	0.25	0.32	0.04	0.70
ℓ(C...H)$_{short}$		1.0	0.57	-0.04	0.37
ℓ(C...C)			1.0	-0.06	0.46
ℓ(C...H)$_{long}$				1.0	0.05
R					1.0

brium puckering amplitude of q_e = 0.44 Å. Structural parameters computed for an equilibrium puckering amplitude, q_e = 0.44 Å, were r_{CH} = 1.116 Å, r_{CC} = 1.557 Å and ∠CCH = 111.6°. These parameters may be compared with experiment by correcting the computed parameter according to a linear relation between experimental and computed parameters found to hold reasonably well for a large number of n-alkane molecules by Jacob, et al. The corrected parameters are r_{CH} = 1.115$_5$ Å, r_{CC} = 1.551 Å and ∠CCH = 111.6°, which agree well with the experimental results.

An equilibrium amplitude of puckering, q_e = 0.44$_6$ Å, was calculated from the observed mean amplitude, q_g = 0.43$_5$ Å, using the relation (22)

$$q_e = q_g - 3/2(a\ell_q^2).$$

The asymmetry of vibration in the puckering coordinate was estimated from potential energies calculated as a function of q, using the data of Pitzer and Donath (6). The Morse-like asymmetry constant

$$a = -1/3[(\partial^3V(q)/\partial q^3)/(\partial^2V(q)/\partial q^2)]_{q = q_e}$$

was estimated to be -2.0 Å^{-1}. The mean square amplitude of vibration of the puckering coordinate, ℓ_q^2, was calculated from the well known hyperbolic cotangent function (32) relating vibrational frequencies to mean square amplitudes of vibration

$$\ell^2 = (h/8\pi^2\mu\nu)\coth(h\nu/2kT).$$

A value of 283 cm^{-1}, the observed frequency of ring puckering (6), was assigned to ν and the effective reduced mass for this vibration, μ = 28.1 amu, was taken from Kilpatrick, et al., (3). The temperature was taken to be that of the diffraction nozzle during the experiments, 298°K.

DISCUSSION

The C-C bond length in cyclopentane is 0.013 Å longer than the average C-C bond length in n-hydrocarbons, r_g = 1.533 Å (33). The lengthening may in part be due to nonbonded interactions, specifically C...C interactions since the average C...C nonbonded distance in cyclopentane is 2.444 Å as compared to the average value in n-hydrocarbons of 2.545 Å (33). The observed bonded and nonbonded C-C mean amplitudes of vibration are somewhat smaller in this slightly strained cyclic system than in n-hydrocarbons (33), while all bonded and nonbonded C-H mean amplitudes are normal.

An inspection of the spectrum of nonbonded distances for a given puckering amplitude, as given in Table 1.2, shows that although the individual nonbonded distances vary with the pseudorotational phase angle, the envelope of the distribution function remains unchanged. Accordingly, the diffraction intensities are independent of the pseudorotational phase angle, and it is not possible to establish by electron diffraction whether the molecule is undergoing dynamic pseudorotation or exists in a single static conformation. However, certain quantities computed by the pseudorotation model do provide an interesting insight into pseudorotation. It is found that the sums

$$1/2 \sum_{i=1}^{5} (\theta^i - \theta^o)^2 \quad \text{and} \quad 1/2 \sum_{i=1}^{5} [1 + \cos(3\beta^i)]$$

over C-C-C valency angles and torsional angles, which are a representation of the potential energy of bending C-C-C valency angles and of rotation about C-C bonds, are nearly independent of ϕ (to within 0.3ppt and 0.025 ppt respectively). As previously indicated, the spectrum of nonbonded distances in the molecule is nearly independent of ϕ, suggesting that the nonbonded contribution to the potential energy is also nearly independent

of ϕ. These results give an indication as to why potential energy calculations (2,3,6,7,8), in which significantly different force fields were used, all found the potential energy to be essentially independent of the pseudorotational phase angle. These findings provide support for the conclusion of Lifson and Warshel (8) that "the existence of an equal potential path is more due to the geometry of cyclopentane than to the exact nature of the intermolecular forces".

The puckering amplitude determined by electron diffraction is approximately 10% lower than that determined by thermodynamic (3,4,5) and published* infrared (9) studies, but is in much better agreement with puckering amplitudes computed from optimized model force fields by machine calculation (7,8). The maximum torsional angle, which is related to the puckering amplitude (35), was found to be 44° by Hendrickson (7) and 42° by Lifson and Warshel (8), as compared to the 42.3° maximum torsional angle found by electron diffraction. This amount of puckering is somewhat less than that found in the D-ring of steroids thus far investigated(36), the five-membered ring in this case being trans-fused to the chair form of cyclohexane.

---

*A recent unpublished infrared study of cyclopentane by Hirakawa, et al., (34) is in much better agreement with the present work, with a preliminary result q_o = 0.45 Å.

PART II

Molecular Structure of Tetrahydrofuran

INTRODUCTION

Thermodynamic (37) and infrared (38) studies of tetrahydrofuran have given evidence of free pseudorotation similar to that in cyclopentane, despite the perturbing effect of substituting an oxygen atom for a methylene group. This is in disagreement with calculations of Pitzer and Donath (6), which indicated that a significant barrier to free pseudorotation exists due to the difference in torsional barriers about C-C and C-O bonds.* Thermodynamic data have also been interpreted in terms of free, or nearly free, pseudorotation in pyrrolidine (40), but restricted pseudorotation in tetrahydrothiophene (41). The barrier to free pseudorotation calculated for tetrahydrothiophene from the thermodynamic data (2.8 kcal/mole) is in excellent agreement with the calculations of Pitzer and Donath (6). The puckering amplitude calculated for tetrahydrofuran from the infrared data was q_o = 0.44 Å, nearly as large as that calculated for cyclopentane from thermodynamic (3,4,5) and infrared (9) data.

A reinvestigation (42) of the molecular structure of tetrahydrofuran by electron diffraction was undertaken to compare its conformational behavior with that of cyclopentane and to determine the puckering amplitude

---

* These authors used the experimentally observed barrier for methanol, 1.07 kcal/mole (39).

by a completely independent method.

EXPERIMENTAL

Reagent grade tetrahydrofuran of better than 99% purity was obtained from the J. T. Baker Chemical Co., Phillipsburg, New Jersey, and used without further purification. Diffraction patterns were recorded on 4 X 5 in. Kodak process plates at camera distances of 21, 11 and 6.5 cm using an electron diffraction apparatus (13) equipped with an r^3 rotating sector. The experimental conditions under which the diffraction patterns were recorded using 40 kV electrons are given in Table 2.1. Plates were developed at 20° C for 5 min. with Kodak D-11 developer.

Table 2.1 Experimental conditions under which C_4H_8O diffraction patterns were recorded.

Camera distance (cm)	21.048	11.115	6.585
Sample temperature (°C)	0	0	0
Vapor pressure (torr)	30	30	30
Exposure time (sec)	6	10-15	40-45
Beam current (μA)	0.46	0.46	0.47

Photographic densities, measured with an automatic recording microphotometer with digital output (14), were converted to absorbancies and corrected for the radial variation of plate sensitivity (15). Intensities were calculated from the corrected absorbancies using the relation

$$I = A(1 + 0.05A^2)$$

as recommended by Janzen (15).

Four plates at each camera distance were averaged and used in the structural analysis.

ANALYSIS OF DATA

Experimental intensities were corrected for sector imperfections and extraneous scattering prior to division by the theoretical atomic intensity. Experimental leveled intensity, $I_0(s)$, and background intensity, $I_B(s)$, functions (16) for the three camera distances are given in Appendix B. Indices of resolution (19) were 1.06_5, 1.08 and 1.02 for the 21, 11 and 6.5 cm camera distances respectively.

Experimental and calculated molecular intensities and radial distribution functions were computed as previously described (16,19,20) with the usual corrections applied (19,21,22,23). Radial distribution functions were calculated using a Degard damping factor [$\exp(-0.0015s^2)$]. The analytical elastic scattering factors of Strand and Bonham (17) and the inelastic scattering factors of Heisenberg and Bewilogua (18) were used in all phases of the analysis. The Born failure phase shifts used were the analytical expressions of Bonham and Ukaji (43). Anharmonicity constants (22) were estimated (26) to be 2.0 Å^{-1} for bonded distances and taken to be 1.0 Å^{-1} for nonbonded distances.

The anharmonic radial distribution function, the molecular intensity of each camera distance, and the composite molecular intensity were fitted with appropriate calculated expressions in least squares analyses (27).

Calculated standard errors took into account the effects of both random and systematic errors (28).*

*Also see PART I, p. 5.

Molecular Model

The experimental radial distribution function of tetrahydrofuran, Figure 2.1, shows the ring to be decidedly nonplanar as was found in the case of cyclopentane (PART I). In order to compare the conformational behavior of tetrahydrofuran with that of cyclopentane and to make possible a comparison with infrared (38) results, a pseudorotation model was adopted. The criterion followed in choosing the model, Figure 2.2, was that it should conform as closely as possible to the cyclopentane model, Figure 1.2, yet accomodate the lower symmetry.

As in the case of cyclopentane, the puckering displacements in tetrahydrofuran are described relative to the plane of the unpuckered configuration of the "heavy" atom skeleton. An origin is taken inside the "heavy" atom skeleton and a z-axis is defined to be perpendicular to the plane of the skeleton. The dotted lines are hypothetical spokes of length

$$S_o = (r_{CC}/2)\operatorname{cosec} \gamma$$

extending from the origin to the "heavy" atoms (1,...,5) in their reference positions, where the angle γ is to be defined. The vectors, $\vec{S}_j$, radiating from the origin, define the instantaneous atomic positions of the "heavy" atoms. In order to make the analysis tractable, the following simplifying assumptions were made:

1. The C-O bond lengths are equal,

$$O_1 - C_2 = O_1 - C_5 = r_{CO},$$

as are the C-C bond lengths,

$$C_2 - C_3 = C_3 - C_4 = C_4 - C_5 = r_{CC};$$

Figure 2.1 Experimental radial distribution function for C_4H_8O. $\Delta f(r) = f(r)_{exptl} - f(r)_{calc}$.

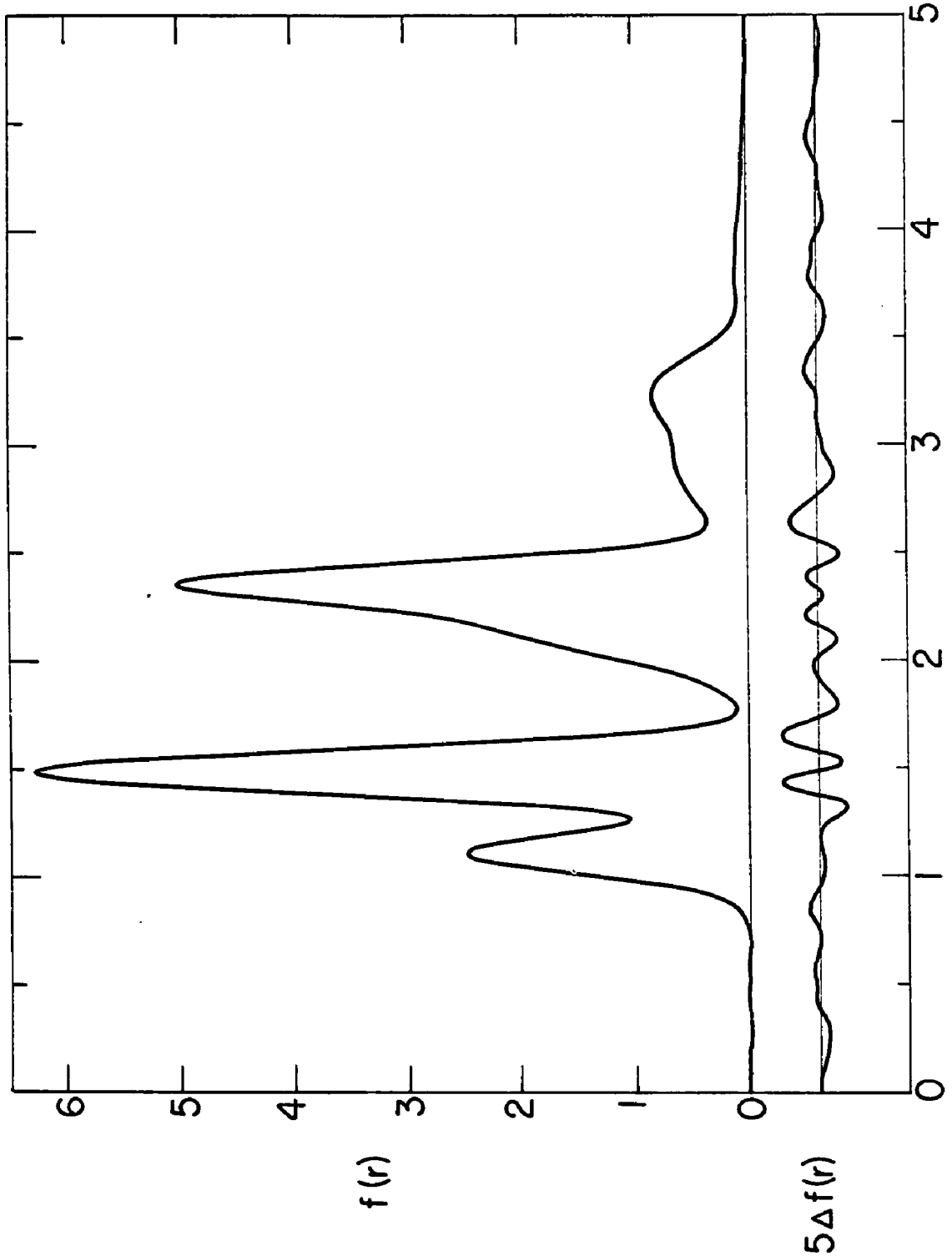


Figure 2.1

Figure 2.2 Pseudorotation model for C_4H_8O with the $\phi = 108°$ (C_s symmetry) conformation shown.

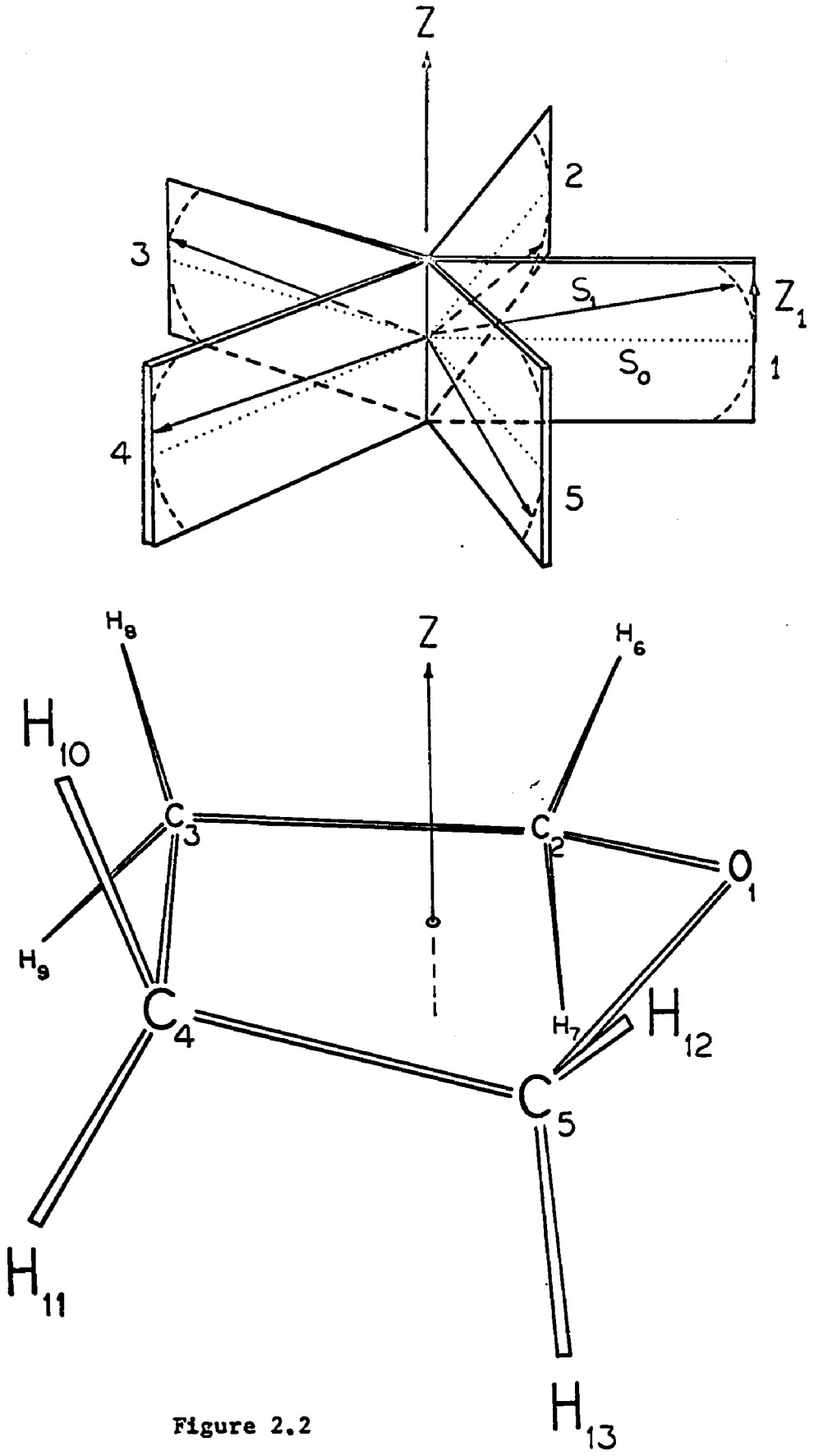


Figure 2.2

2. The angles between vertical planes 1-o-2 and 1-o-5 are equal,

$$\measuredangle 1o2 = \measuredangle 1o5 = \beta,$$

as are the angles between vertical planes 2-o-3, 3-o-4 and 4-o-5,

$$\measuredangle 2o3 = \measuredangle 3o4 = \measuredangle 4o5 = \gamma;$$

3. The spoke lengths, S_o, are all equal.

An angular displacement of the vector $\vec{S}_j$ from the horizontal reference plane is defined by

$$\alpha_j = \tan^{-1}(z_j/S_o) \qquad j = 1,\ldots,5$$

in which z_j corresponds to the hypothetical perpendicular displacement

$$z_j = \sqrt{2/5}\, q \cos[2(2\pi j/5 + \phi)].$$

Here again, as in the cyclopentane model, each vector $\vec{S}_j$ is constrained to move in its respective vertical plane. The individual α_j have now been specified for any given q and ϕ, as have the five angles between adjacent $\vec{S}_j$. These five angles together with the three simplifying assumptions give five simultaneous equations for the $|S_j|$ which must be satisfied if the individual r_{CO} and r_{CC} are to remain independent of q and ϕ.

Other features of the model which are equivalent to those in the cyclopentane model are:

1. The trajectories of the atoms, for a given q, are nearly parabolic instead of linear as in the model of Kilpatrick, et al., (3) and the actual distance traveled by atom j from the reference configuration is virtually identical to the perpendicular displacement z_j in the Kilpatrick, et al., model.

2. The hydrogen atoms (6,...,13), Figure 2.2, are constrained to follow the motion of the carbon atoms in order to preserve local C_{2v} sym-

metry at each methylene group.

3. All C-C-H valency angles are assumed to be equal.

Several other models have also been examined to determine the influence of model assumptions on derived molecular parameters, including particularly, the amplitude of puckering. Perhaps the most arbitrary of the three assumptions is 3; this assumption being equivalent to assigning values to β and γ, which determine the values of the derived C-O-C, C-C-O and C-C-C valency angles. Fortunately, even though the derived valency angles are strongly influenced, the distribution of nonbonded distances, and therefore the amplitude of puckering, is nearly insensitive to this assumption. Valency angles derived using this assumption are also reasonable, being comparable to those found in cyclopentane (Table 1.3) and dimethyl ether (44,45). An additional assumption of the model is that the atoms are displaced according to the model for cyclopentane (Figure 1.2), yet the vertical planes in which the "heavy" atoms move do not have an angular separation of $2\pi/5$ in the model. Here again, the derived puckering amplitude is insensitive to the assumption.

RESULTS

Structural parameters (excepting H...H distances) calculated by the pseudorotation model for a puckering amplitude of $q = 0.38$ Å at three phase angles are given in Table 2.2. Phase angles were chosen to divide the pseudorotation circuit, which encompasses all possible conformations of tetrahydrofuran, into three equal increments, $\Delta\phi$. Since all possible conformations are found in the range $\phi = 18°$ to $\phi = 63°$, the three phase angles chosen were $\phi = 18°$ (C_s conformation), $\phi = 40.5°$, and $\phi = 63°$

Table 2.2 Structural parameters[a] calculated by the C_4H_8O pseudorotation model for a puckering amplitude q = 0.38 Å.

Parameter	Pseudorotational Phase Angle		
	$\phi = 18^\circ$ (C_s symmetry)	$\phi = 40.5^\circ$	$\phi = 63^\circ$ (C_2 symmetry)
C-H	1.1140	1.1140	1.1140
C-O	1.4290	1.4290	1.4290
C-C	1.5380	1.5380	1.5380
O...H	2.1026	2.1026	2.1026
C...H	2.1980	2.1980	2.1980
$(O...H/C...H)_{ave}$	2.1740	2.1740	2.1740
$O_1...C_3$	2.3468	2.3367	2.3757
$O_1...C_4$	2.3468	2.3800	2.3757
$C_2...C_4$	2.4276	2.3820	2.3833
$C_2...C_5$	2.2937	2.3240	2.3478
$C_3...C_5$	2.4276	2.4311	2.3833
$(C...O/C...C)_{ave}$	2.3685	2.3708	2.3732
$O_1...H_8, O_1...H_9$	3.2466,2.9299	3.2903,2.7775	3.2956,2.8824
$O_1...H_{10}, O_1...H_{11}$	3.2466,2.9299	3.1039,3.1750	2.8824,3.2956
$C_2...H_{10}, C_2...H_{11}$	3.1916,3.1916	2.9340,3.3099	2.8204,3.3480
$C_2...H_{12}, C_2...H_{13}$	2.7362,3.2597	2.9492,3.2125	3.1902,3.0311
$C_3...H_{12}, C_3...H_{13}$	3.0032,3.3353	3.2414,3.1666	3.3374,2.8998
$C_4...H_6, C_4...H_7$	3.0032,3.3353	2.8159,3.3567	2.8998,3.3374
$C_5...H_6, C_5...H_7$	2.7362,3.2597	2.7918,3.2730	3.0311,3.1902
$C_5...H_8, C_5...H_9$	3.1916,3.1916	3.3422,2.9688	3.3480,2.8204

Table 2.2 (Continued)

Parameter	Pseudorotational Phase Angle		
	$\phi = 18^\circ$ (C_s symmetry)	$\phi = 40.5^\circ$	$\phi = 63^\circ$ (C_2 symmetry)
$\angle$ C-C-H	110.950	110.950	110.950
$\angle C_5-O_1-C_2$	106.748	108.813	110.468
$\angle O_1-C_2-C_3$	104.495	103.855	106.339
$\angle O_1-C_5-C_4$	104.495	106.618	106.339
$\angle C_2-C_3-C_4$	104.221	101.497	101.576
$\angle C_3-C_4-C_5$	104.221	104.433	101.576
$\angle C_2-(O_1-C_5)-C_4$	39.366	19.633	11.927
$\angle C_5-(O_1-C_2)-C_3$	39.366	36.472	11.927
$\angle O_1-(C_2-C_3)-C_4$	22.977	37.593	30.435
$\angle O_1-(C_5-C_4)-C_3$	22.977	5.173	30.435
$\angle C_2-(C_3-C_4)-C_5$	0.0	25.497	36.001

[a]Distances are in Å and angles in degrees, with the absolute values of the torsional angles reported. The maximum torsional angle is 41.15°.

(C_2 conformation). Experimental and calculated intensities, sM(s), are compared in Figure 2.3. The calculated intensity was constructed from the distances given in Table 2.2 (but including H...H distances), giving each conformation equal weight. The experimental radial distribution function is shown in Figure 2.1 and is compared with a calculated distribution function constructed from the parameters in Table 2.2, with each conformation given equal weight. Results of least squares analyses of the composite molecular intensity made on each pseudorotation isomer, as well as different isomeric concentrations of pseudorotation isomers, are shown in Table 2.3. The long O...H (e.g., $O_1...H_8$) and C...H (e.g., $C_2...H_{10}$) nonbonded distances were taken from Table 2.2 under their respective conformations and were not varied in the analysis.

The experimental diffraction intensities are very sensitive to the amplitude of puckering, as evidenced by the narrow distribution of C...O and C...C nonbonded distances under the third peak in the radial distribution function. Although this is a composite peak containing the short O...H (e.g., $O_1...H_6$) and C...H (e.g., $C_2...H_8$) distances also, its steep trailing edge shows that the spread in O...C and C...C distances is small. This is confirmed by the least squares analyses, which show the derived mean (O...C,C...C) nonbonded amplitude to be small and nearly independent of the phase angle of puckering assumed. Inspection of Table 2.2 discloses that the average (O...C,C...C) nonbonded distance calculated by the pseudorotation model is nearly independent of the phase angle of puckering.

Consideration of the standard deviations in Table 2.3 shows the fit for the $\phi = 18°$ conformation is significantly better than that for the $\phi = 63°$ conformation, while the fit for the $\phi = 40.5°$ conformation is significantly better than for either of these conformations. The differ-

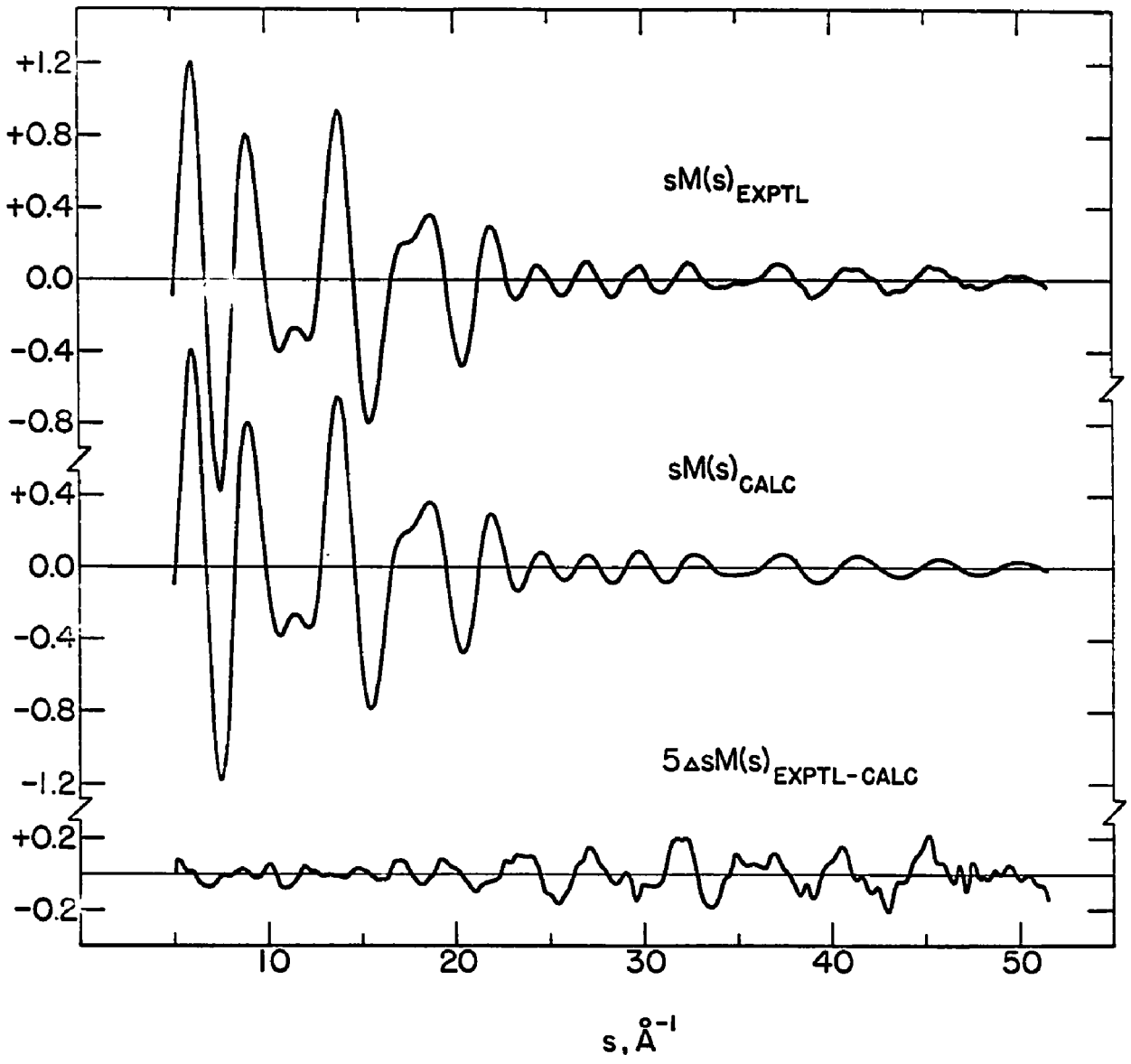


Figure 2.3 Comparison of experimental and calculated molecular intensity functions for C_4H_8O.
$\Delta sM(s) = sM(s)_{exptl} - sM(s)_{calc}$.

Table 2.3 Results of least squares analyses of the composite molecular intensity for C_4H_8O.

Parameter[a]		Isomeric Concentration				
Pseudorotation Isomer	ϕ = 18°	100.0			50.0	33.3
	ϕ = 40.5°		100.0			33.4
	ϕ = 63°			100.0	50.0	33.3
$\sigma(I)/I$[b]		0.81	0.58	1.04	0.65	0.59
C-H	r_g	1.113_9	1.113_9	1.113_9	1.113_9	1.113_9
	ℓ_g	0.080	0.080	0.080	0.080	0.080
C-O[c]	r_g	1.429	1.429	1.429	1.429	1.429
	ℓ_g	0.052_5	0.052_5	0.052_5	0.052_5	0.052_5
C-C[c]	r_g	1.538	1.538	1.538	1.538	1.538
	ℓ_g	0.052_5	0.052_5	0.052_5	0.052_5	0.052_5
short(O...H,C...H) mean	r_g	2.171_5	2.174	2.176_5	2.174_5	2.174_5
	ℓ_g	0.112	0.112	0.111_5	0.111_5	0.112_5
(O...C,C...C) mean	r_g	2.369_2	2.370_3	2.37_1	2.370_5	2.370_5
	ℓ_g	0.072_7	0.073_1	0.073_2	0.073_4	0.073_3
long(O...H,C...H)[d]						
	ℓ_g[e]	0.138	0.118_4	0.141	0.117	0.115_5

[a] Distances and amplitudes in Å.

[b] Standard deviation in ppt.

[c] ℓ(C-O) and ℓ(C-C) were constrained to be equal.

[d] These O...H and C...H nonbonded distances were taken from Table 2.2 for the respective isomers and their values were not varied in the least squares analyses.

[e] Amplitude given each O...H,C..,H distance.

ence in standard deviation for each of the conformations is almost entirely due to the misfit in the broad peak centered at 3 Å representing the spectrum of long O...H and C...H nonbonded distances. These distances were computed by the pseudorotation model with q = 0.38 Å, Table 2.2, and were not allowed to vary in the least squares analyses. A least squares fit in which the ϕ = 18° and ϕ = 63° conformations are given equal weights shows that the spectrum of long O...H and C...H nonbonded distan Table 2.2, for these conformations complement each other, giving a fit comparable to that for the ϕ = 40.5° conformation. This effect is illustrated in Figure 2.4, which shows a comparison between experimental and calculated radial distribution functions for the ϕ = 18°, ϕ = 63°, 50% ϕ = 18° + 50% ϕ = 63°, and ϕ = 40.5° conformers in the r = 2.5 Å to r = 4.0 Å region of the distribution function. The difference in fit between the ϕ = 40.5° and 50% ϕ = 18° + 50% ϕ = 63° forms is of little statistical significance, since this region of the radial distribution function is moderately sensitive to changes in the intensity background function at small scattering angles where it is least reliably known. That the electron diffraction results are consistent with free pseudorotation as found by thermodynamic and infrared studies is shown by the excellent least squares fit for the case that all three isomers are given equal weights.

Structural parameters and their estimated standard errors are given in Table 2.4. The C-C-H valency angle was derived from the mean (O...H, C...H) nonbonded distance at 2.2 Å.

A matrix of correlation coefficients, based on the least squares fit of the composite molecular intensity using a diagonal weight matrix

$$W(s) = 1 - \exp[-0.00828(s - 2.827)^2],$$

Figure 2.4 Experimental (solid curves) and calculated (dashed curves) radial distribution functions for the $\phi = 18°$ (C_s conformation), $\phi = 63°$ (C_2 conformation), 50% $\phi = 18°$ + 50% $\phi = 63°$ and $\phi = 40.5°$ pseudorotation conformers of C_4H_8O.

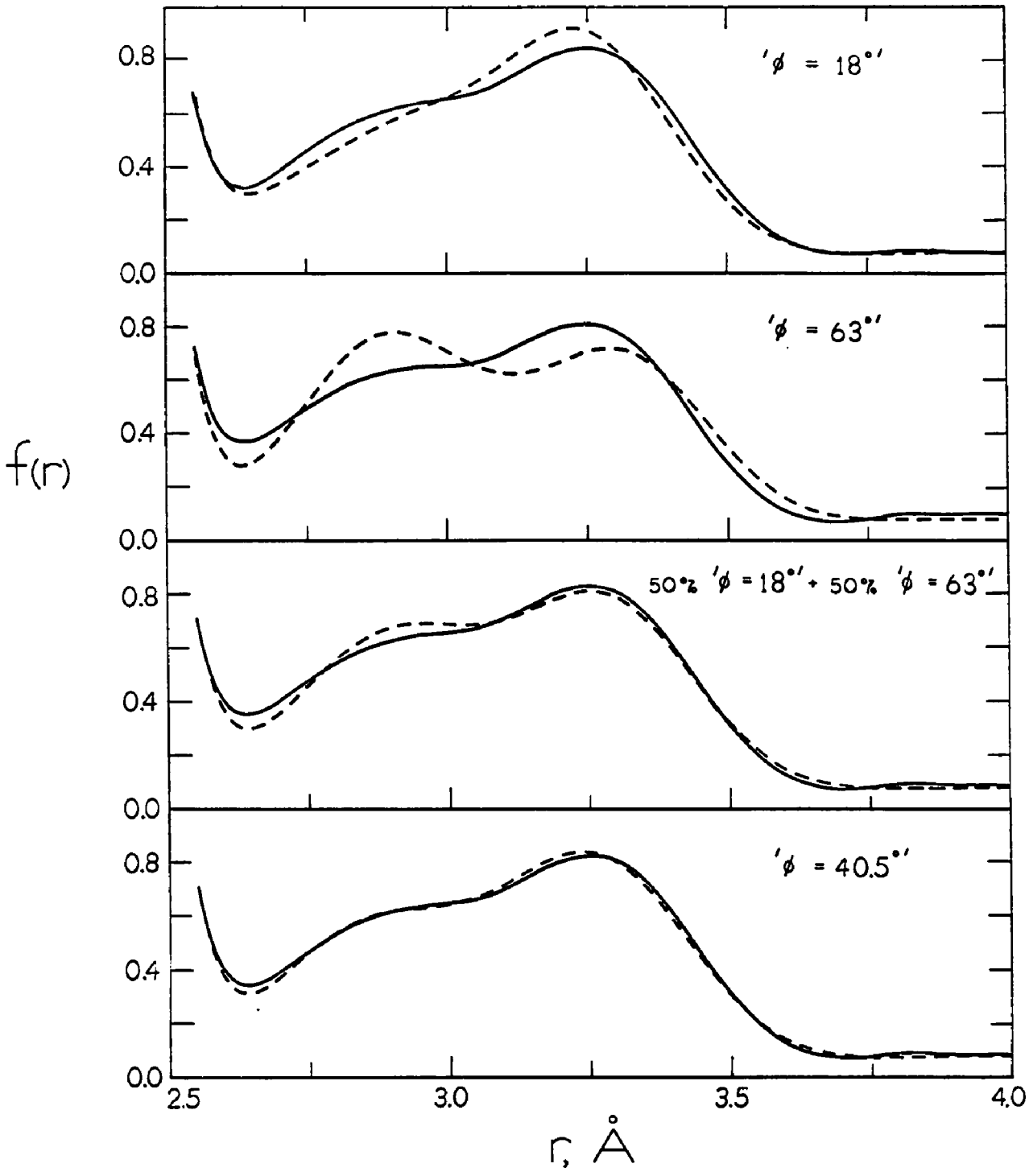


Figure 2.4

Table 2.4 Structural parameters[a] and estimated standard errors[b] for C_4H_8O.

Parameter	r_g	ℓ_g	∠
C-H	$1.114 \pm 0.001_3$	0.080 ± 0.002	
C-O[c]	$1.429 \pm 0.001_2$	$0.052_5 \pm 0.001_3$	
C-C[c]	$1.538 \pm 0.001_2$	$0.052_5 \pm 0.001_3$	
short(O...H,C...H)$_{mean}$	$2.174 \pm 0.002_1$	$0.112 \pm 0.002_7$	
(C...O,C...C)$_{mean}$	$2.370_5 \pm 0.001_7$	$0.073_3 \pm 0.001_5$	
long(O...H,C...H)[d]		$0.115_5 \pm 0.003_5$	
q_g	0.38 ± 0.02		
C-C-H			$110.9_5 \pm 0.2$

[a] Distances and amplitudes in Å, angle in degrees.

[b] The effects of both random and systematic errors (28) were included in calculated standard errors.

[c] ℓ(C-O) and ℓ(C-C) were constrained to be equal.

[d] Constrained to be the same as those in Table 2.2.

is given in Table 2.5.

DISCUSSION

The C-H and C-O bond lengths found in this study are not significantly different from those normally found. The C-C bond length is slightly longer than that found in n-alkanes (33), but the difference is of little statistical significance. Observed mean amplitudes of vibration are in excellent agreement with those found for cyclopentane (Table 1.4).

The excellent least squares fit obtained for the $\phi = 40.5°$ conformation, with a very reasonable calculated amplitude of vibration for the long O...H and C...H nonbonded distances, shows that it is not possible to distinguish by electron diffraction whether tetrahydrofuran is freely pseudorotating or exists in a single static conformation. However, a recent microwave study (44) which was in progress during the course of this investigation has confirmed that tetrahydrofuran does undergo nearly free pseudorotation. The microwave results establish the C_2 conformer to be only about 20 cal/mole more stable than the C_s form, but provide no measure of q. The excellent least squares fit for the case that all three isomers were assigned equal isomeric concentrations shows that the electron diffraction results are consistent with free pseudorotation and that the pseudorotation model adopted is a satisfactory model for describing the structure of tetrahydrofuran. The model indicates how the time average over pseudorotation conformers gives rise to the observed diffraction intensities.

The amplitude of puckering found by electron diffraction, $q_g = 0.38 \pm 0.02$ Å, is 0.06 Å smaller than found by infrared spectroscopy, $q_o = 0.44$ Å (38). This difference in puckering is nearly the same as that

Table 2.5 Matrix of correlation coefficients[a] for C_4H_8O.

	r(C-H)	r(C-O)	r(C-C)	r(O...H/C...H)[b]	r(C...O/C...C)	ℓ(C-H)
r(C-H)	1.0	0.16	0.15	-0.05	-0.04	0.01
r(C-O)		1.0	-0.20	-0.09	-0.07	0.19
r(C-C)			1.0	-0.20	-0.11	0.16
r(O...H/C...H)				1.0	0.45	-0.17
r(C...O/C...C)					1.0	-0.09
ℓ(C-H)						1.0
ℓ(C-O/C-C)						
ℓ(O...H/C...H)						
ℓ(C...O/C...C)						
ℓ(O...H/C...H)						
R						

[a]Based on 149 intensity values interpolated from 332 experimentally observed data points. Matrix elements are given by

$$\rho_{ij} = B_{ij}^{-1}/(B_{ii}^{-1}\ B_{jj}^{-1})^{1/2}$$

where the notation corresponds to that of O. Bastiansen, L. Hedberg, and K. Hedberg, J. Chem. Phys. 27, 1311 (1957).

[b]Mean r(O...H/C...H) short nonbonded distance.

Table 2.5 (Continued)

	ℓ(C-O/C-C)	ℓ(O...H/C...H)[c]	ℓ(C...O/C...C)	ℓ(O...H/C...H)[d]	R
r(C-H)	-0.13	0.04	0.01	-0.02	0.01
r(C-O)	0.42	0.03	-0.01	-0.01	-0.01
r(C-C)	-0.39	0.13	0.10	0.01	0.19
r(O...H/C...H)	-0.35	-0.36	-0.17	-0.10	-0.62
r(C...O/C...C)	-0.13	-0.56	-0.29	-0.13	-0.25
ℓ(C-H)	0.08	0.17	0.10	0.01	0.18
ℓ(C-O/C-C)	1.0	0.25	0.30	0.05	0.57
ℓ(O...H/C...H)		1.0	0.66	-0.04	0.48
ℓ(C...O/C...C)			1.0	-0.08	0.54
ℓ(O...H/C...H)				1.0	0.08
R					1.0

[c] ℓ(O...H/C...H) for short nonbonded distances.

[d] ℓ(O...H/C...H) for long nonbonded distances.

found between electron diffraction and published infrared results for cyclopentane, 0.045 Å, indicating consistency in the experimental methods. Although a small part of the difference is due to different operational definitions of q (PART I, p. 24), a re-evaluation of the infrared results may be in order in light of the recent unpublished study of cyclopentane by Hirakawa, et al., (34).

The puckering amplitude found for tetrahydrofuran is about 0.05_5 Å smaller than in cyclopentane. This is understandable in terms of the larger force constants for C-O-C (47) and C-C-O (48) valency angle deformations and the different barrier (39,45) to internal rotation about C-O bonds. The barrier to rotation about C-O bonds has been found to be dependent on the molecule considered, with a barrier in methanol of 1.07 kcal/mole (39) and in dimethyl ether of 2.72 kcal/mole (45). The free pseudorotation of tetrahydrofuran suggests that the dimethyl ether barrier is more representative of the barrier in this molecule.

PART III

Molecular Structure of Iodine Heptafluoride

INTRODUCTION

Recent electron diffraction investigations of XeF_6 (49,50,51,52,53 54) have shown this molecule to be appreciably distorted from octahedral (O_h) symmetry. Among theoretical models commonly used to predict molecular structure, only the valence-shell-electron-pair-repulsion (VSEPR) model of Gillespie and Nyholm (55) gave an unequivocal prediction *a priori* that the molecule should be distorted from O_h symmetry. Although the VSEPR model is in satisfactory agreement with several features of the XeF_6 structure (52), the distortion is smaller than that predicted. Since the VSEPR model regards XeF_6 as being seven-coordinated, it was of interest to examine another seven-coordinated molecule of uncertain structure, iodine heptafluoride, for common structure characteristics.

In addition, because of the rare occurrence of seven-coordinated binary compounds* suitable for study as free molecules in the gas phase, iodine heptafluoride is of interest in its own right. In several models of directed valency (55,58,59) it has been proposed that the geometry of ligands surrounding the central atom of a molecule may be predicted by considering the equilibrium configuration of similar particles restricted to the surface of a sphere. The potential energy of repulsion between the particles is usually expressed as

$$E = \sum_{i \neq j} r_{ij}^{-n},$$

*Only two other binary heptafluorides are known, ReF_7 (56) and OsF_7 (57), with the latter stable only at low temperatures.

where r_{ij} is the distance between particles i and j, and n is an appropriately chosen constant. For six or fewer particles on a sphere the arrangement corresponding to a minimum energy of repulsion is independent of the value of n, so long as n is positive. Furthermore, the computed geometries are in good accord with observed geometries. However, in the case of seven particles, the geometry predicted is dependent on the force law assumed, i.e., the value of n adopted (58,60,61). The symmetry predicted by this model changes from D_{5h} to C_2 or (equally favorable) C_s to C_{2v} to C_{3v} as the value of n is increased, and the energy difference between all these forms is rather small until n becomes large (60,61). The determination of the gas phase structure of IF_7, interpreted according to this model should allow an assessment of the hardness of the repulsive forces acting between the ligand bonds or ligand atoms.

Numerous structural studies of IF_7 to this date have been carried out, but none have sufficed to establish the equilibrium structure. Since prior studies have been reviewed in detail in a recent publication (62), no discussion of their provisional conclusions will be given here. It has been quite generally reported by previous workers that IF_7 has nearly D_{5h} symmetry in the gas phase.

EXPERIMENTAL

Iodine heptafluoride of spectroscopic purity was provided by Argonne National Laboratory, Argonne, Illinois, in a Monel storage vessel. The sample introduction system for the diffraction unit, specifically constructed by Argonne National Laboratory for previous XeF_6 experiments (51), was made of seasoned Monel and nickel. All sample introduction surfaces were thoroughly seasoned before use with ClF_3 and IF_7. Diffraction pat-

terns were recorded on 4 X 5 in. Kodak process plates using a previously described electron diffraction apparatus (13). Data were recorded at camera distances of 21 cm using an r^2 rotating sector and at 21, 11 and 6.5 cm using an r^3 rotating sector. The experimental conditions under which the diffraction patterns were recorded using 40 kV electrons are given in Table 3.1. Plates were developed at 20° C for 5 min. with Kodak D-11 developer.

Table 3.1 Experimental conditions under which IF_7 diffraction patterns were recorded.

Camera distance (cm)	21.124[a]	21.113[b]	11.125	6.617
Sample temperature (°C)	-78.5	-16[c]	0[c]	+15[c]
Vapor pressure (torr)	2.4	265	620	1250
Exposure time (sec)	2.8-5.5	0.9-1.9	1.2	2.5
Beam current (μA)	0.17	0.17	0.56	0.65

[a] r^2 rotating sector.

[b] r^3 rotating sector.

[c] A 2 in. length of the 3/32 in. diameter diffraction line was filled with the sample at the indicated temperature for recording the individual diffraction patterns. The simultaneous opening of the line valve and the turning on of the electron beam allowed short exposure times and minimized extraneous scattering caused by pressure build-up of the difficultly condensible IF_7, while keeping sample losses to a minimum.

Photographic densities, measured with an automatic recording microphotometer with digital output (14), were converted to absorbancies and corrected for the radial variation of plate sensitivity (15). Intensities were obtained from the corrected absorbancies (13) according to

$$I = A(1 - 0.05A)$$

except for the 21 cm camera distance (r^3 sector) in which the intensities were taken to be proportional to the absorbancy. Four plates at each camera distance were averaged and used in the structural analysis.

ANALYSIS OF DATA

Experimental intensities were corrected for sector imperfections* and extraneous scattering before division by the theoretical atomic intensity. Experimental leveled intensity, $I_0(s)$, and background intensity, $I_B(s)$, functions for each camera distance are given in Appendix C. Indices of resolution (19) were 1.10 for the 21 cm (r^2 sector) camera distance and 1.03, 0.90 and 1.00 for the 21, 11 and 6.5 cm (r^3 sector) camera distances respectively.

Experimental and calculated molecular intensities and radial distribution functions were computed as previously described (16,19,20) with the usual corrections applied (19,21,22,23). Radial distribution functions were calculated using a Degard damping factor [$\exp(-0.0010s^2)$].

---

*In order to characterize the imperfections in the r^2 sector and, at the same time, to compensate for errors in scattering theory at small scattering angles, scattered intensities from both elemental neon and xenon were measured using the r^2 sector. A weighted average r^2 sector calibration was constructed from these sector calibrations according to

$$\Phi = \frac{I_I + 7I_F}{(I_I/\Phi_{Xe}) + 7(I_F/\Phi_{Ne})} .$$

The sector calibrations, $\Phi(r)$, are the ratio of intensity theoretically expected at the plate as modified by a perfect r^2 sector and the intensity actually measured at the plate. Atomic scattering factors used in the calculation of the theoretical atomic intensities for scattering from iodine (I_I) and fluorine (I_F) were the analytical elastic factors of Strand and Bonham (17) and the inelastic factors of Heisenberg and Bewilogua (18). The neon sector calibration was used to correct for imperfections in the r^3 sector.

Atomic scattering factors used in all phases of the analysis were the partial wave elastic factors of Cox and Bonham (24), and the inelastic factors of Tavard (25) for fluorine and Pohler and Hansen (63) for iodine. Anharmonicity constants (22) were estimated (26) to be 2.1 $Å^{-1}$ for the I-F bonded distance and were taken to be 1.0 $Å^{-1}$ for F...F nonbonded distances. Corrections for Bastiansen-Morino shrinkage effects (64), estimated roughly from calculations on octahedral fluorides (65), were 0.0005 Å for $(F_{eq}...F_{eq})_{short}$, 0.001 Å for $(F_{ax}...F_{eq})$, and 0.002 Å for $(F_{eq}...F_{eq})_{long}$ and $(F_{ax}...F_{ax})$. The difference in amplitude of vibration between the different I-F bond lengths was estimated roughly using an extension (66) of Badger's rule (67), which relates force constants to bond lengths, since it is not possible to establish independent values from the diffraction intensities.

Calculated standard errors took into account the effects of both random and systematic errors (28).*

Molecular parameters were derived from geometrically constrained least squares analyses of the molecular intensity for each camera distance and the composite molecular intensity. In final analyses the 21 cm (r^2 sector) data were not used in constructing the composite molecular intensity and experimental radial distribution function. The neglect of this data has little influence on the derived parameters, but a strong effect on the observed standard deviation between the experimental and calculated intensities. The effect of this data on the radial distribution function is to increase the magnitude of the "foot" at the leading edge of the I-F bonded peak.

---

*Also see PART I, p. 5.

RESULTS

A comparison between the experimental radial distribution function of iodine heptafluoride and a calculated distribution function for a D_{5h} symmetry model is shown in Figure 3.1. The molecular parameters used in constructing the calculated distribution function were derived from a least squares analysis of the composite molecular intensity and are given in Table 3.2. The overall correspondence between peak positions and peak areas in the experimental and calculated distribution functions indicates that the molecule has "nearly" D_{5h} symmetry (Figure 3.2). According to the misfit in the 2.1 Å to 2.7 Å region, departures from D_{5h} symmetry are comparable in magnitude to vibrational displacements. Least squares analyses also detected a difference between axial and equatorial bond lengths in the molecule, the two axial bonds being shorter than the five equatorial bonds. Evidence for this difference is provided by the breadth of the I-F bonded peak and the shape and position of the 3.5 Å peak. The conspicuous failure of the Born approximation (21), which results in the severe splitting of the I-F bonded peak into two unsymmetrical peaks, does make it more difficult to establish the precise distribution of I-F bond lengths. The composite peak at 3.5 Å is made up of the $F_{ax}\cdots F_{ax}$ ($F_6\cdots F_7$, Figure 3.2) and long $F_{eq}\cdots F_{eq}$ (e.g., $F_1\cdots F_3$) nonbonded distances. If all the bond lengths were equal to the mean bond length derived from the least squares fit, 1.836 Å, this peak would be skewed inward, since the five long $F_{eq}\cdots F_{eq}$ distances would be moved inward and the $F_{ax}\cdots F_{ax}$ distance moved outward. Additionally, the center of gravity of the peak would be moved inward.

The asymmetry and breadth of the experimental peak at 2.5 Å indicates that a majority of the $F_{ax}\cdots F_{eq}$ (e.g., $F_1\cdots F_6$) nonbonded distances have

Figure 3.1 Comparison of the IF_7 experimental radial distribution function (solid curve) with the calculated function (dashed curve) for a D_{5h} symmetry model.

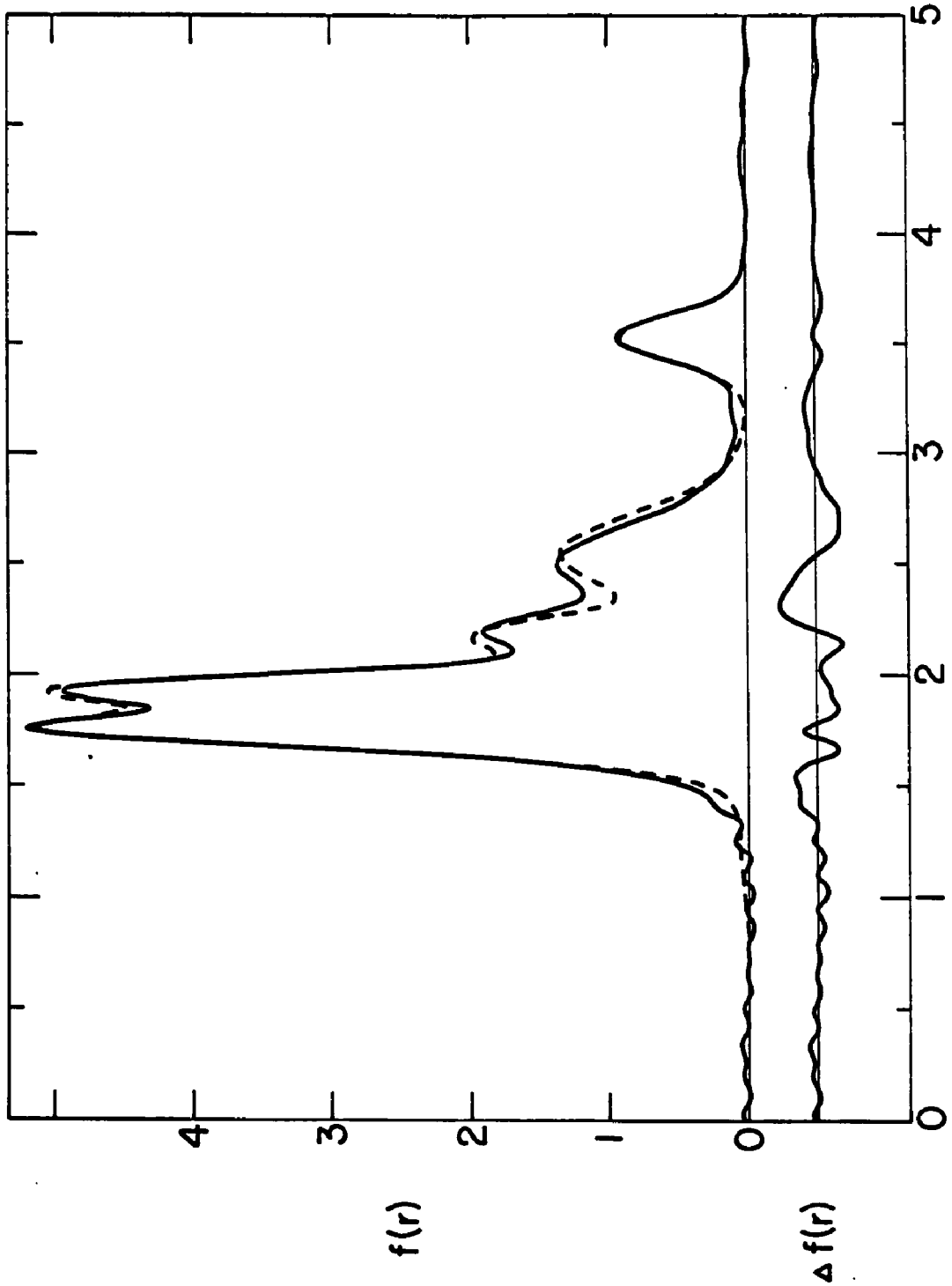


Figure 3.1

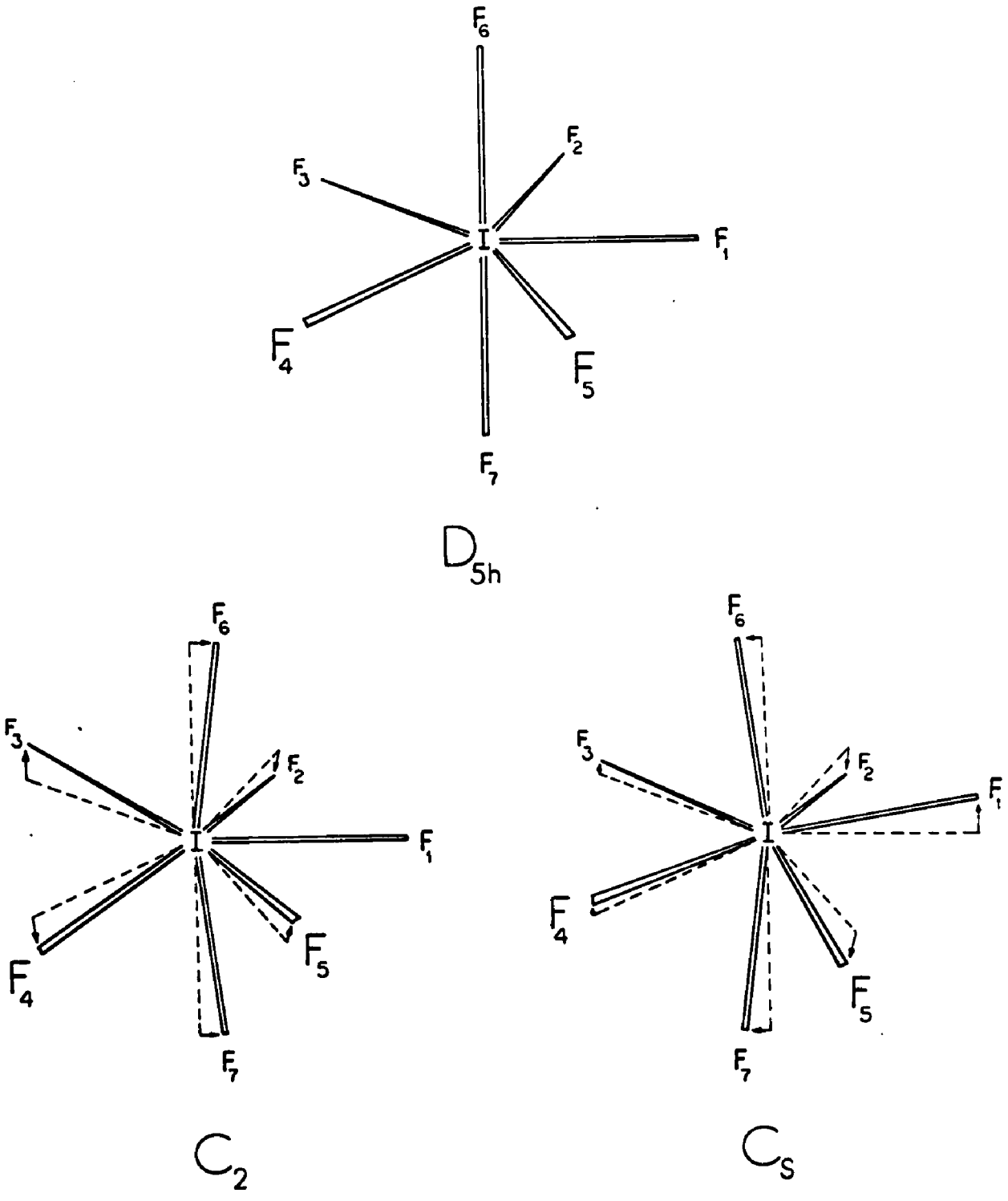


Figure 3.2 Molecular models of IF_7 having D_{5h}, C_2 and C_s symmetry.

been shortened while a few have been lengthened relative to the distribution in the D_{5h} model. It is evident that essentially harmonic vibrations of the atoms in independent modes of vibration will not displace the center of gravity of a D_{5h} distribution to a shorter distance (except for trivial shrinkage effects), nor result in the experimentally observed skewing.

In contrast to the 2.5 Å peak, the 2.2 Å peak, which corresponds to the short $F_{eq}...F_{eq}$ (e.g., $F_1...F_2$) nonbonded distances, has a very narrow breadth and its center of gravity has been displaced outward. The significance of the misfit in the 2.2 Å peak is not unequivocal. Poorly understood errors in scattering theory make uncertain the interpretation of details in the leading and trailing edges of peaks corresponding to scattering pairs of much different atomic number.

If the modes of vibration of IF_7 are considered to be uncorrelated, the appreciable discrepancy between experimental and D_{5h} distribution functions in the 2.2 Å to 2.7 Å region shows that the equilibrium structure cannot be of D_{5h} symmetry. The implications of this statement are discussed in greater detail below.

In all subsequent models discussed, it is assumed that the bonded distances can be grouped into two sets, corresponding to the axial and equatorial bond lengths of the D_{5h} model. This assumption should be valid since the displacements from D_{5h} are only the order of magnitude of vibrational displacements. In addition, mean amplitudes of vibration for the bonded and nonbonded distances are divided into four sets, a single amplitude being associated with the component distances under each peak in the radial distribution function.

Models of Static Deformation from D_{5h} Symmetry

The breadth of the 2.5 Å peak in the experimental radial distribution function shows that the fluorine atoms undergo moderately large displacements out of the equatorial plane and/or off the D_{5h} five-fold axis. Displacements away from the equatorial plane are suggested by the experimental nonbonded peak at 2.2 Å. These displacements along either C_2 or C_s symmetry coordinates have the effect of lengthening the short $F_{eq}\cdots F_{eq}$ nonbonded distances. An angular displacement, α_j, of the j^{th} fluorine atom along these symmetry coordinates may be defined in terms of two variables, α_{eq} and θ_{eq}, according to

$$\alpha_j = \alpha_{eq} \cos[2(2\pi j/5 + \theta_{eq})] \qquad j = 1,\ldots,5$$

where α_{eq} is a maximum out-of-plane angular displacement and θ_{eq} is a phase angle equal to 0 for C_s and $\pi/10$ for C_2 symmetry.

Although the puckering away from the equatorial plane significantly improves the fitting of the 2.2 Å peak, its effect in first order on the 2.5 Å peak is to increase its breadth symmetrically. In order to obtain an asymmetric distribution for the 2.5 Å peak, it is necessary to displace the axial atoms off the nominally five-fold axis (i.e., off the z-axis of the present coordinate system) in such a way as to shift the majority of the $F_{ax}\cdots F_{eq}$ distances inward while shifting a few outward relative to the D_{5h} symmetry model. Two conformations which satisfy this requirement and still preserve C_2 and C_s symmetry are shown in Figure 3.2. Results of least squares analyses of the composite molecular intensity for these two cases are given in Table 3.2 under their respective headings. The experimental data are fitted equally well by either of the models, with a very significant improvement in the fit compared to that for the D_{5h} model. The derived molecular parameters are nearly

Table 3.2 Results[a] of least squares analyses of the composite molecular intensity for IF_7.

Parameter	Molecular Model			
	D_{5h}	C_2	C_s	50% C_2 + 50% C_s
$\sigma(I)/I$[b]	1.792	1.345	1.350	1.347
$r_g(I-F)_{mean}$	1.836	1.837	1.837	1.837
$r_g(I-F_{eq}) - r_g(I-F_{ax})$	0.076	0.072	0.072	0.072
$r_g(I-F_{ax})$	1.781	1.786	1.786	1.786
$r_g(I-F_{eq})$	1.857	1.858	1.858	1.858
α_{eq}[c]		7.61	7.55	7.51
α_{ax}[d]		4.49	4.21	4.55
$\ell_g(I-F_{eq})$[e]	0.044	0.045	0.045	0.045
$\ell_g(F_{eq}\cdots F_{eq})_{short}$	0.061	0.060_5	0.061	0.061
$\ell_g(F_{ax}\cdots F_{eq})$	0.169	0.104	0.107	0.106
$\ell_g(F_{ax}\cdots F_{ax}),(F_{eq}\cdots F_{eq})_{long}$	0.093	0.091	0.091	0.091

[a] Distances and amplitudes in Å, angles in degrees.

[b] Standard deviation in the composite molecular intensity in ppt.

[c] Equatorial amplitude of puckering. See text for further details.

[d] Axial amplitude of bending. See text for further details.

[e] $\ell(I-F_{ax})$ constrained to be $\ell(I-F_{eq})$ - 0.002 Å.

independent of the assumed symmetry with the equatorial puckering amplitudes, α_{eq}, nearly identical in both these models. Similarly, for the C_2 and C_s structures, the axial bending amplitudes, α_{ax}, which correspond to the angular displacement away from the z-axis, are also in good agreement.

A least squares fit assuming equal concentrations of the C_2 and C_s models gave the same standard deviation as that for the C_2 and C_s fits. Comparisons between the experimental and calculated composite molecular intensities, sM(s), and radial distribution functions, using the parameters derived in this analysis are made in Figures 3.3 and 3.4 respectively (note that the difference curves have been multiplied by a factor of 2). A matrix of correlation coefficients based on this least squares fit of the composite molecular intensity using a diagonal weight matrix proportional to the scattering variable s is given in Table 3.3.

Rotation, $\Delta\theta_{ax}$, of the displaced axial atoms about the z-axis has little effect on the standard deviation until $\Delta\theta_{ax}$ deviates from its value in the C_2 (or C_s) symmetry model by more than 40°. Symmetry breaking displacements greater than this lead to rapidly increasing standard deviations. This is understandable since the effect of this operation is ultimately to reverse the direction of skew of the 2.5 Å peak.

A number of least squares analyses were also made assuming various isomeric concentrations of C_2, C_s and D_{5h} symmetry molecules. No improvement in standard deviation was found by adding various concentrations of molecules with D_{5h} symmetry. Quite to the contrary, there was a rapid increase in standard deviation for concentrations of D_{5h} molecules in excess of 20 %. Many other types of deformations and combinations of deformations were also tested, however, these were not able to impart the observed skew in the 2.5 Å peak.

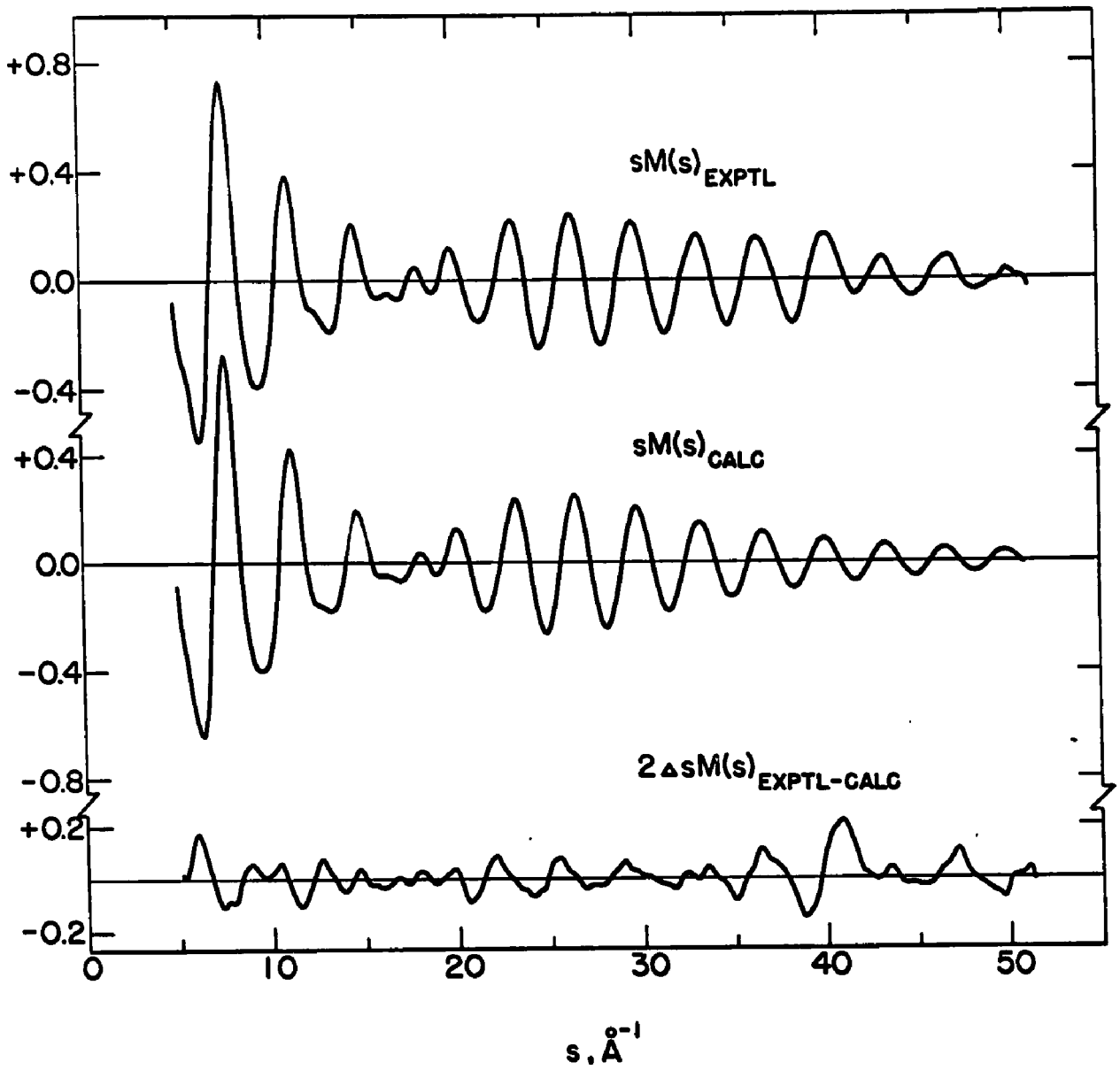


Figure 3.3 Comparison of experimental and calculated molecular intensity functions for IF_7. $\Delta sM(s) = sM(s)_{exptl} - sM(s)_{calc}$.

Figure 3.4 Experimental radial distribution function for IF_7. $\Delta f(r) = f(r)_{exptl} - f(r)_{calc}$.

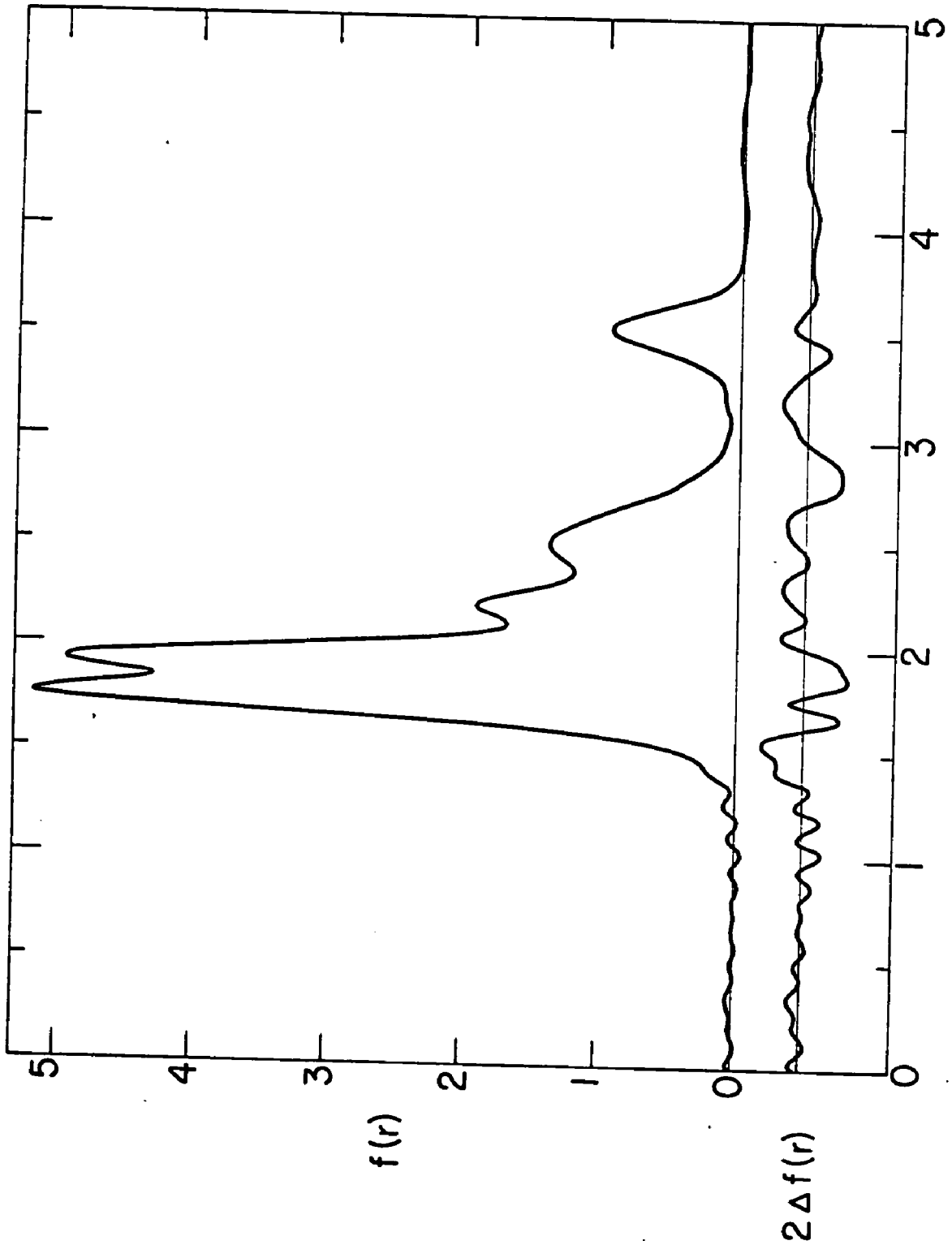


Figure 3.4

Table 3.3 Matrix of correlation coefficients[a] for IF_7.

	$r(I-F)_{mean}$	$\Delta r(I-F)$[b]	α_{eq}[c]	α_{ax}[d]	$\ell(I-F_{eq})$[e]
$r(I-F)_{mean}$	1.0	-0.51	0.34	-0.27	0.35
$\Delta r(I-F)$		1.0	-0.38	0.28	-0.60
α_{eq}			1.0	-0.90	0.28
α_{ax}				1.0	-0.18
$\ell(I-F_{eq})$					1.0
$\ell(F_{eq}\cdots F_{eq})_{short}$					
$\ell(F_{ax}\cdots F_{eq})$					
$\ell[F_{ax}\cdots F_{ax}),(F_{eq}\cdots F_{eq})_{long}]$					
R					

[a] Based on 148 intensity values interpolated from 341 experimentally observed data points. Matrix elements are given by

$$\rho_{ij} = B^{-1}_{ij}/(B^{-1}_{ii}\ B^{-1}_{jj})^{1/2}$$

where the notation corresponds to that of O. Bastiansen, L. Hedberg and K. Hedberg, J. Chem. Phys. 27, 1311 (1957).

[b] $\Delta r(I-F) = r(I-F_{eq}) - r(I-F_{ax})$.

[c] Equatorial amplitude of puckering. See text for further details.

[d] Axial amplitude of bending. See text for further details.

Table 3.3 (Continued)

	$\ell(F_{eq}\cdots F_{eq})_{short}$	$\ell(F_{ax}\cdots F_{eq})$	$\ell[(F_{ax}\cdots F_{ax}),(F_{eq}\cdots F_{eq})_{long}]$	R
$r(I\text{-}F)_{mean}$	-0.29	-0.36	-0.06	-0.07
$\Delta r(I\text{-}F)$	0.18	0.24	0.10	0.12
α_{eq}	-0.31	-0.19	-0.09	-0.08
α_{ax}	0.26	0.05	0.09	0.18
$\ell(I\text{-}F_{eq})$	-0.16	-0.17	0.01	0.32
$\ell(F_{eq}\cdots F_{eq})_{short}$	1.0	0.48	0.02	-0.03
$\ell(F_{ax}\cdots F_{eq})$		1.0	0.01	0.06
$\ell[(F_{ax}\cdots F_{ax}),(F_{eq}\cdots F_{eq})_{long}]$			1.0	0.46
R				1.0

[e] $\ell(I\text{-}F_{ax})$ constrained to be $\ell(I\text{-}F_{eq})$ - 0.002 Å.

Model of Dynamic Pseudorotation

The equivalent fits of the diffraction intensities and excellent agreement between the derived parameters for the C_2 and C_s symmetry models suggest the possibility of dynamic motions in iodine heptafluoride similar to those in five-membered ring molecules.* The description of such a pseudorotation model is given in terms of the same variables α_{eq}, θ_{eq}, α_{ax}, and θ_{ax} that were defined in the foregoing.

Although the pseudorotation of the equatorial atoms allows the 2.2 Å peak to be fitted, only a symmetric broadening of the 2.5 Å peak will result unless the motion of the axial atoms is correlated with that of the equatorial atoms, i.e., unless normal modes of vibration of different symmetry are coupled. Consideration of the static deformation models of the previous section indicates that the obvious modes to couple with the e_2'' symmetry modes are the doubly degenerate axial bending modes (e_1' symmetry).

Akin to the treatment of the e_2'' symmetry coordinates, the doubly degenerate e_1' symmetry coordinates of IF_7 are transformed into the polar coordinates α_{ax} and θ_{ax}, which are orthogonal to α_{eq} and θ_{eq}, where α_{ax} is the angular amplitude of bending off the z-axis of the present coordinate system and θ_{ax} is the phase angle of the axial amplitude. All that is required to correlate the motions of the axial and equatorial atoms is a phase relation between θ_{eq} and θ_{ax}. The required phase relationship implied by the static deformation models is

$$\theta_{ax} = 4\theta_{eq} + 6\pi/10.$$

Described in terms of the present coordinate system, the displacements of

---

*See PART I and PART II of this thesis.

the axial atoms are

$$\alpha_6 = \alpha_{ax}$$

$$\alpha_7 = \pi - \alpha_{ax}$$

$$\theta_j = \theta_{ax} = 4\theta_{eq} + 6\pi/10 \qquad j = 6,7.$$

The polar coordinates corresponding to four different pseudorotational phase angles, θ_{eq}, for an equatorial amplitude of puckering, $\alpha_{eq} = 7.5°$, and axial amplitude of bending, $\alpha_{ax} = 4.5°$, are given in Table 3.4. The spectrum of nonbonded distances generated for these same four pseudorotational phase angles are given in Table 3.5. Examination of the nonbonded distances indicates that although the individual values vary, the envelope of the distribution function is invariant. It follows that the electron diffraction intensities are independent of the phase angle of puckering and it cannot be distinguished if the molecule is pseudorotating or exists in a single static conformation. However, the diffraction intensities are sensitive to the magnitude of the displacement from D_{5h} symmetry, i.e., the equatorial puckering amplitude and axial bending amplitude. The derived structural parameters and their estimated standard errors are given in Table 3.6.

Coupling of e_1' and e_2'' Modes

In the treatments of the static and dynamic deformation models it has been shown that a correlation in phase between deformations along e_2'' and e_1' symmetry coordinates is necessary to impart the observed skew to the 2.5 Å peak. Correlations of this type may arise when bending modes have such large amplitudes of vibration that cubic and higher order terms

Table 3.4 Atomic coordinates[a] of IF_7 for $\alpha_{eq} = 7.55°$ and $\alpha_{ax} = 4.5°$.

Pseudorotational Phase Angle	Coordinate	Atom							
		I	F_1	F_2	F_3	F_4	F_5	F_6	F_7
63° (C_2 symmetry)	r	0.0	1.858	1.858	1.858	1.858	1.858	1.786	1.786
	ϕ	0.0	0.0	72.0	144.0	216.0	288.0	0.0	0.0
	θ	0.0	90.0	85.56	97.18	82.82	94.44	4.5	175.5
66°	r	0.0	1.858	1.858	1.858	1.858	1.858	1.786	1.786
	ϕ	0.0	0.0	72.0	144.0	216.0	288.0	12.0	12.0
	θ	0.0	89.21	86.22	96.90	82.61	95.05	4.5	175.5
69°	r	0.0	1.858	1.858	1.858	1.858	1.858	1.786	1.786
	ϕ	0.0	0.0	72.0	144.0	216.0	288.0	24.0	24.0
	θ	0.0	88.43	86.93	96.54	82.49	95.61	4.5	175.5
72° (C_s symmetry)	r	0.0	1.858	1.858	1.858	1.858	1.858	1.786	1.786
	ϕ	0.0	0.0	72.0	144.0	216.0	288.0	36.0	36.0
	θ	0.0	87.67	87.67	96.11	82.45	96.11	4.5	175.5

[a]Coordinates are polar coordinates in which 0 is the coaltitude.

Table 3.5 Molecular distances (in Å units) calculated by the IF_7 pseudorotation model for an equatorial angular amplitude $\alpha_{eq} = 7.55°$, and an axial bending amplitude, $\alpha_{ax} = 4.5°$.

Parameter	Pseudorotational Phase Angle			
θ_{eq}	63° (C_2 symmetry)	66°	69°	72° (C_s symmetry)
θ_{ax}	0°	12°	24°	36°
$(I-F)_{ax}$	1.786	1.786	1.786	1.786
$(I-F)_{eq}$	1.858	1.858	1.858	1.858
$F_3 \ldots F_4$	2.1857	2.1839	2.1828	2.1824
$F_3 \ldots F_7$	2.1857	2.1881	2.1910	2.1942
$F_4 \ldots F_5$	2.2047	2.2012	2.1977	2.1942
$F_5 \ldots F_6$	2.2163	2.2159	2.2149	2.2131
$F_6 \ldots F_7$	2.2047	2.2079	2.2107	2.2131
$(F \ldots F)_{ave}$	2.1995	2.1995	2.1995	2.1995
$F_3 \ldots F_8$	2.4741	2.4580	2.4465	2.4396
$F_3 \ldots F_9$	2.4741	2.4948	2.5195	2.5476
$F_4 \ldots F_8$	2.4433	2.4386	2.4371	2.4396
$F_4 \ldots F_9$	2.6445	2.6111	2.5785	2.5476
$F_5 \ldots F_8$	2.8084	2.7897	2.7666	2.7397
$F_5 \ldots F_9$	2.4966	2.4886	2.4794	2.4694
$F_6 \ldots F_8$	2.4966	2.5027	2.5065	2.5078
$F_6 \ldots F_9$	2.8084	2.8221	2.8305	2.8333
$F_7 \ldots F_8$	2.6445	2.6778	2.7098	2.7397
$F_7 \ldots F_9$	2.4433	2.4505	2.4595	2.4694

Table 3.5 (Continued)

Parameter	Pseudorotational Phase Angle			
θ_{eq}	63° (C_2 symmetry)	66°	69°	72° (C_s symmetry)
θ_{ax}	0°	12°	24°	36°
$F_3 \ldots F_5$	3.5279	3.5299	3.5317	3.5332
$F_3 \ldots F_6$	3.5279	3.5258	3.5235	3.5214
$F_4 \ldots F_6$	3.5161	3.5176	3.5194	3.5214
$F_4 \ldots F_7$	3.5352	3.5350	3.5343	3.5332
$F_5 \ldots F_7$	3.5161	3.5150	3.5143	3.5141
$F_8 \ldots F_9$	3.5610	3.5610	3.5610	3.5610
$(F \ldots F)_{ave}$	3.5307	3.5307	3.5307	3.5307

Table 3.6 Structural parameters[a] and estimated standard errors[b] for IF_7.

Parameter	r_g	ℓ_g	χ
$(I-F)_{mean}$	1.837 ± 0.002		
$(I-F_{eq}) - (I-F_{ax})$	0.07_2 ± 0.010		
$I-F_{ax}$ [c]	1.786 ± 0.007	0.043 ± 0.003	
$I-F_{eq}$	1.858 ± 0.004	0.045 ± 0.003	
α_{eq} [d]			7.5 ± 1
α_{ax} [e]			4.5 ± 1
$(F_{eq}\cdots F_{eq})_{short}$		0.061 ± 0.005	
$(F_{ax}\cdots F_{eq})$		0.106 ± 0.008	
$[(F_{ax}\cdots F_{ax}),(F_{eq}\cdots F_{eq})_{long}]$		0.091 ± 0.006	

[a] Distances and mean amplitudes of vibration in Å, angles in degrees.

[b] Calculated standard errors include the effects of both random and systematic errors (28). Standard errors do not include possible effects of errors in electron scattering theory.

[c] $\ell(I-F_{ax})$ constrained to be $\ell(I-F_{eq})$ - 0.002 Å.

[d] Equatorial amplitude of puckering. See text for further details.

[e] Axial amplitude of bending. See text for further details.

in the potential energy function which connect coordinates of different symmetry become important. The most important terms coupling the bending modes in the potential function should be simple cubic terms of the type

$$F_{ij}(S_i)^2(S_j)$$

where S_i and S_j are the symmetry coordinates involved and F_{ij} is the cubic constant connecting these coordinates. The symmetry allowed cubic terms of this type for a D_{5h} molecule (68) are

$$(e_2'')^2(e_1')$$

$$(e_1')^2(e_2')$$

$$(e_1'')^2(e_2').$$

It can be shown of these symmetry allowed cubic terms that the $(e_2'')^2(e_1')_{ax\ bend}$ term is unique in that it is the only term which is capable of giving the observed skew in the 2.5 Å peak.

DISCUSSION

Electron diffraction intensities of gaseous iodine heptafluoride may be accounted for in terms of molecular models with C_2 or C_s symmetry or in terms of a dynamic pseudorotation model. In either interpretation the deformations from D_{5h} symmetry are small, and characterized by a correlation in phase of displacements along e_2'' and e_1' symmetry coordinates. Unfortunately, the one-dimensional structural information implicit in the diffraction intensities does not distinguish between the case of molecules actually undergoing dynamic pseudorotation and the case of molecules existing in one of a large number of static conformations. Both cases account very well for the diffraction data. Physical arguments, however,

favor the dynamic pseudorotation model. The atomic displacements required to take the molecule from one C_2 configuration to an equivalent one via a C_s intermediate are so small that it is difficult to envision a potential barrier high enough to inhibit pseudorotation. Moreover, there is a striking similarity in geometry and in the magnitude of the displacements involved between the ring of fluorine atoms in the equatorial plane of IF_7 and the rings in various cyclic organic compounds which have been found to pseudorotate.*

The possibility of a unique relation between the phase of the equatorial puckering and the direction of axial bending was not totally unexpected. Theoretical calculations by Thompson and Bartell (60) treated bond-bond repulsions in XY_7 molecules as repulsions between points-on-a-sphere and obtained a simple relation between e_2'' and e_1' displacements. It was found that, as the hardness of the bond-bond repulsive potential is increased, the C_2 and C_s conformations ultimately become more stable than the D_{5h} conformations. For r^{-n} potential functions, the deformation from D_{5h} becomes spontaneous when n exceeds 2.5, and the C_2 and C_s configurations remain equivalent in energy. The model predicts that as n increases, the first deformation is an e_2'' buckling of the equatorial ring. As n is increased further the axial atoms experience an e_1' displacement from the five-fold reference axis, and the axial bend is proportional to the square of the ring pucker. The direction of the bend is just that required to fit the diffraction intensities. Although the calculated magnitude of the axial bending is somewhat smaller than that found (for the observed amplitude of ring pucker), the points-on-a-sphere model shows a pleasing qualitative agreement with experiments for a value of n = 3.5. This result reinforces Gillespie's VSEPR (55) interpretation that the geometry

*See PART I and PART II of this thesis.

of many molecules is determined by repulsions between occupied bond orbitals imposed by the exclusion principle. If the repulsions causing the deformation from D_{5h} symmetry had been ligand-ligand steric forces between atoms instead of bond-bond repulsions, a much harder repulsion (n = 12) would have been expected.

Although the diffraction intensities are not able to distinguish whether the molecule is pseudorotating, they are sufficiently sensitive to allow a determination of the equatorial puckering and axial bending displacements. The displacements found are α_{eq} = 7.5 ± 1° and α_{ax} = 4.5 ± 1°, respectively.

The I-F bond lengths in the molecule are describable in terms of axial and equatorial bonds. As predicted qualitatively by Gillespie's VSEPR model (58), the less crowded axial I-F bonds are 0.07_2 ± 0.01 Å shorter than the equatorial bonds. The mean I-F bond length, 1.837 ± 0.002 Å, is shorter than that observed in IF_5 (69), 1.860 ± 0.003 Å, a trend found in a large number of inorganic fluorine compounds as fluorine substitution is increased. This effect has been attributed (55) to an increase in the effective electronegativity of the central halogen with increased fluorine substitution.

The results of the present electron diffraction structural analysis are consistent with a large body of information concerning the structure available from other experimental techniques.

The infrared and Raman spectra of IF_7 vapor (62,70) have been interpreted in terms of D_{5h} symmetry. This is in accord with the present study since the displacements from D_{5h} symmetry found are only the order of magnitude of vibrational amplitudes. It has also been predicted on the basis of infrared and Raman analyses (62) that IF_7 is a relatively rigid

molecule compared to ReF_7, a prediction that is consistent with electron diffraction analyses of IF_7 and ReF_7 (71).

Considerable controversy has arisen over the interpretation of IF_7 x-ray diffraction data (72). The debate arose over the statistical significance of the observed deformations from D_{5h} symmetry in the orthorhombic crystal phase. This problem of interpretation arose mainly because of apparent disorder in the crystal (72). Since crystal packing forces may exercise a strongly inhibiting influence on free pseudorotation, the present diffraction data provide a basis for understanding the previous difficulty in interpreting the x-ray diffraction data. Neighbor-neighbor interactions might tend to freeze in the configurations of the various pseudorotation conformers. A disordered "freezing" could account for the observed results.

Additional observations of interest were derived from electrostatic-focusing molecular-beam experiments at -60° C (74). These show the molecules to have a measurable dipole moment, whereas at room temperature (75) there is no measurable dipole moment. Whether the dipole moment detected at low temperature is static or dynamic has not been established. The correspondence between the molecular beam and the electron diffraction results is that the e_1' deformation found in the structure determination is a polar deformation. An additional consequence of this polarity induced by the infrared inactive e_2'' mode is that the first overtone of the e_2'' mode should be appreciably infrared active.

In conclusion, it is seen that significant features of the molecular structure of IF_7 are in accord with the predictions of the VSEPR model (55), of which the points-on-a-sphere model is a representation (58). The seemingly small correspondence between the geometry of IF_7 and XeF_6

certainly should not be interpreted as strong evidence against Gillespie's interpretation of XeF_6 as a seven coordinated molecule. It does point out the difficulty in predicting geometries of molecules having seven electron pairs in the valence shell when the electron pairs are not all equivalent. The apparent nonrigidity of both XeF_6 and IF_7 is in conformity with the seven points-on-a-sphere model and provides some justification for treating XeF_6 as a seven-coordinated molecule in the spirit of the VSEPR model.

PART IV

Molecular Structure of Cyclobutanecarboxylic Acid Chloride

INTRODUCTION

Despite encouraging progress in ab-initio calculations, restricted rotation about single bonds remains poorly understood. Several years ago, the conformational equilibria of isopropyl and cyclopropyl carbonyl derivatives of the form $(CH_3)_2CH-CXO$ and $(CH_2)_2CH-CXO$ were investigated (76,77,78). Isopropyl carboxaldehyde displayed normal trans and gauche conformers with all bonds staggered. In the cyclopropyl derivatives an unexpected effect occurred. Trans conformers were present, but cis forms were found instead of gauche. Cis conformers are remarkable in that they eclipse the bonds at the ends of the bond in question, thereby not conforming to Pauling's rationalization (79) of restricted rotation. The effect must be attributed to the electronic interactions accompanying the closing down of the C-C-C angle adjacent to the bond of interest in going from isopropyl (~112°) to cyclopropyl (~60°). It therefore seemed worthwhile to study the intermediate case (~89°) of the cyclobutyl derivatives to establish whether gauche or cis conformers are found. Crude EHMO calculations predict (80) that gauche is more stable than cis.

EXPERIMENTAL

Cyclobutanecarboxylic acid chloride, obtained from the Aldrich Chemical Co., Milwaukee, Wisconsin, was vacuum distilled prior to use. Diffraction patterns were recorded on 4 X 5 in. Kodak process plates using a previously described electron diffraction apparatus (13). In order

that exposure times would not be excessively long, the sparingly volatile sample was introduced into the diffraction chamber through a heated nozzle assembly.* The nozzle was maintained at a temperature of approximately 100° C while the temperature of the sample flask was regulated independently of the nozzle temperature to provide the desired sample vapor pressure. Data were recorded at camera distances of 21 cm using the r^2 rotating sector and at 21, 11 and 6.5 cm using the r^3 rotating sector. The experimental conditions under which the diffraction patterns of the 40 kV electrons were recorded are given in Table 4.1. Plates were developed at 20° C for 5 min. with Kodak D-11 developer.

Table 4.1 Experimental conditions under which C_4H_7CClO diffraction patterns were recorded.

Camera distance (cm)	21.428 (r^2 sector)	21.290 (r^3 sector)	10.641_5	6.77_6
Sample temperature (°C)	22	46	52	52
Vapor pressure (torr)	7.5	25	34	34
Exposure time (sec)	2	7	20-25	45-55
Beam current (μA)	0.47	0.42	0.46	0.42

Photographic densities, measured with an automatic recording microphotometer with digital output (14), were converted to absorbancies and corrected for the radial variation of plate sensitivity (15). Intensities were calculated from the corrected absorbancies according to

$$I = A(1 + 0.05A^2)$$

*For a more detailed description of the heated nozzle assembly, see PART V, p. 114.

as recommended by Janzen (15). Six plates at each camera distance were averaged and included in the structural analysis.

ANALYSIS OF DATA

Experimental intensities were corrected for sector imperfections and extraneous scattering before division by the theoretical atomic intensity. The atomic scattering factors used to obtain leveled intensity curves were the analytical elastic factors of Strand and Bonham (17) and the inelastic factors of Heisenberg and Bewilogua (18). Experimental leveled intensity, $I_0(s)$, and intensity background, $I_B(s)$, functions (16) for each camera distance are given in Appendix D. Indices of resolution (19) were 1.00 for the 21 cm camera distance (r^2 sector) and 1.02_5, 1.07 and 1.07 for the 21, 11 and 6.5 cm camera distances (r^3 sector).

Experimental and calculated molecular intensities and radial distribution functions were computed as previously described (16,19,20), with the usual corrections applied (19,21,22,23). Radial distribution functions were calculated using a Degard damping factor, $[\exp(-0.0015s^2)]$, and calculated intensities grafted onto the experimental intensities inside $s = 3.5$ Å^{-1}. This makes the experimental distribution function moderately sensitive, in its broader peaks, to the assumed structure parameters. Therefore, in all comparisons of experimental and calculated radial distribution functions the structure parameters incorporated in the small angle contributions to the experimental function were carefully made consistent with the structure parameters in the calculated function. Atomic scattering factors used in all phases of the analysis after leveling of experimental intensities were the partial wave elastic factors of Cox and Bonham (24) and the inelastic factors of Tavard (25). Anharmonic-

ity constants (22) were estimated (26) to be 2.0 $Å^{-1}$, 2.0 $Å^{-1}$, 1.5 $Å^{-1}$ and 1.6 $Å^{-1}$ for the C-H, C-C, C=O and C-Cl bonded distances respectively, and taken to be 1.0 $Å^{-1}$ for all nonbonded distances.

Preliminary values of the bonded parameters were obtained from a least squares analysis of the anharmonic radial distribution function (27) in the interval r = 0.0 Å to r = 1.95 Å and were thereafter treated as constants until the final stages of the conformational analysis. The conformational analysis was achieved primarily through geometrically constrained (27) least squares analyses of the composite molecular intensity. In order to facilitate the analyses and to limit variable parameters to a reasonable number, the following simplifying assumptions concerning the molecular model, Figure 4.1, were made:

1. All C-H bonds have the same length;

2. All angles γ are equal, with the H-C-H or C_5-C_4-H plane perpendicular to the ring C-C-C plane;

3. All C-C-C valency angles in the ring are equal for a given dihedral angle, β;

4. All bond lengths and the angles α, γ, $\angle$ CCO and $\angle$ CCCl are independent of the angle of internal rotation, θ, and dihedral angle of the cyclobutane ring, β;

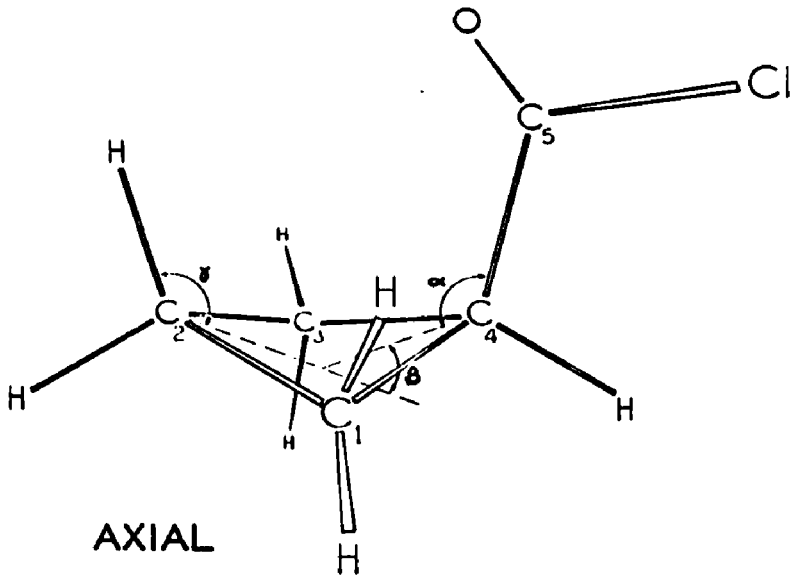
5. The C...C, C...O and C...Cl nonbonded distances are each assigned a single skeletal amplitude of vibration, independent of the nonbonded distance;

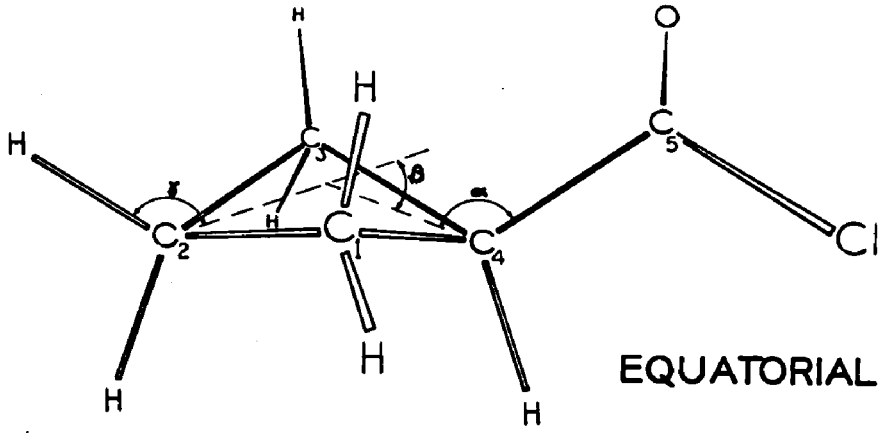
6. All C...H, O...H and Cl...H nonbonded distances are assigned

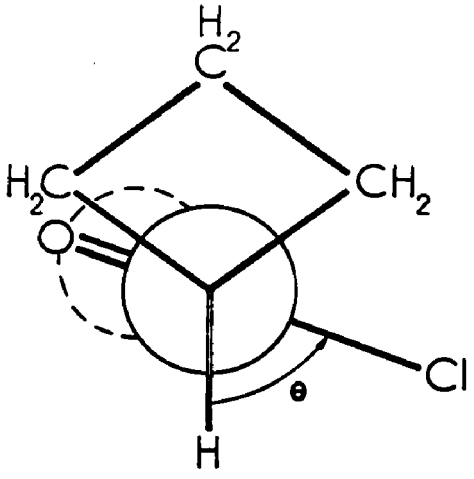
Figure 4.1 Axial and equatorial conformations of C_4H_7CClO.*

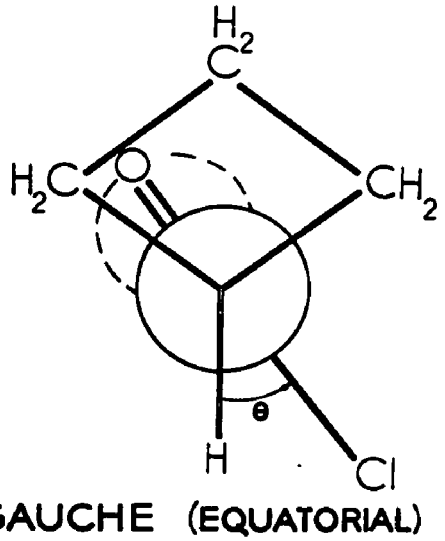
*The lower two figures are Newman diagrams representing the view along the C_4-C_5 bond and show the relative orientations of the ring and $-CClO$ group for the gauche conformation. The dashed lines in the Newman diagrams indicate the projections of the double bonds to the oxygen atoms if they are regarded as two bent single bonds.

Figure 4.1


O
Cl
C5
H
H
H
H
C2
C3
C4
C1
H
H
H
H
AXIAL


H
H
O
H
C5
C3
H
C2
C1
C4
Cl
H
H
H
EQUATORIAL


H2
C
H2C
CH2
O
Cl
θ
H
GAUCHE (AXIAL)


H2
C
H2C
O
CH2
θ
H
Cl
GAUCHE (EQUATORIAL)

the same skeletal amplitude of vibration;

7. The isomeric distribution in the angle of internal rotation and puckered ring conformations is represented by a small set of discrete conformers having maximum increments in internuclear distance of 0.1 Å to 0.2 Å between conformers. Although the valency angles α, γ, $\angle$ CCO and $\angle$ CCCl were assumed to be independent of the angle of internal rotation and dihedral angle of the ring, these parameters were found to be somewhat dependent* on the assumed distribution among conformations.

Calculated standard errors took into account the effects of both random and systematic errors (28).†

RESULTS

Internal Rotation and Ring Puckering

The distribution among rotational isomers in cyclobutanecarboxylic acid chloride can be inferred from the relative areas and positions of the peaks in the radial distribution function beyond 2.8 Å. Internal rotation dependent distances associated with the stronger scattering pairs (i.e., $C_2 \ldots Cl$ and $C_2 \ldots O$ nonbonded distances) are at distances greater than this value. Experimental and calculated radial distribution functions for the <u>cis</u> ($\theta = 0°$), <u>gauche</u> ($\theta = 60°$), <u>antigauche</u> ($\theta = 120°$) and <u>trans</u> ($\theta = 180°$) rotational isomers are compared in

---

* The effects of these assumptions on the reported parameters are believed to be less than the reported uncertainties.

† Also see PART I, p. 5.

Figure 4.2. The calculated functions used parameters derived from geometrically constrained least squares analyses of the composite intensity with the assumption that the cyclobutane ring is planar, since the major features of the distribution function are only moderately sensitive to ring puckering. The major scattering pairs contributing to the calculated distribution function are shown beneath their respective peaks. They are represented by the vertical lines that have heights proportional to their scattering power.

Only internal rotation isomers near the gauche conformation are present in appreciable concentrations. The cis and antigauche isomers may be immediately ruled out as being present in significant concentrations, since they have major peaks at positions of minima in the experimental distribution function. The antigauche conformation also contributes to the misfit of the 2.6 Å peak not shown in Figure 4.2, in addition to giving an unreasonably short H...Cl nonbonded distance of 2.25 Å. The major failing of the trans isomer is that too many of the distances have been shifted inward under the broad area ranging from 3.0 Å to 3.7 Å.

The predominance of the gauche and gauche-like isomers is suggested by radial distribution function (a), Figure 4.3. In the model corresponding to this figure, the cyclobutane ring was constrained to be planar and a distribution of three gauche-like isomers was assumed, with three torsional angles allowed to vary in the constrained least squares analysis. The minimum in the standard deviation occurred at isomeric concentrations and torsional angles of 27.5% θ = 43°, 27.5% θ = 51.6° and 45% θ = 73.9°.

Discrepancies between this calculated distribution function and the

Figure 4.2 Experimental (solid curves) and calculated (dashed curves) radial distribution functions of C_4H_7CClO for different internal rotation angles assuming a planar cyclobutane ring.*

*The major scattering pairs contributing to the calculated distribution function are shown beneath their respective peaks as vertical lines, each line having a height proportional to the scattering power of the pair.

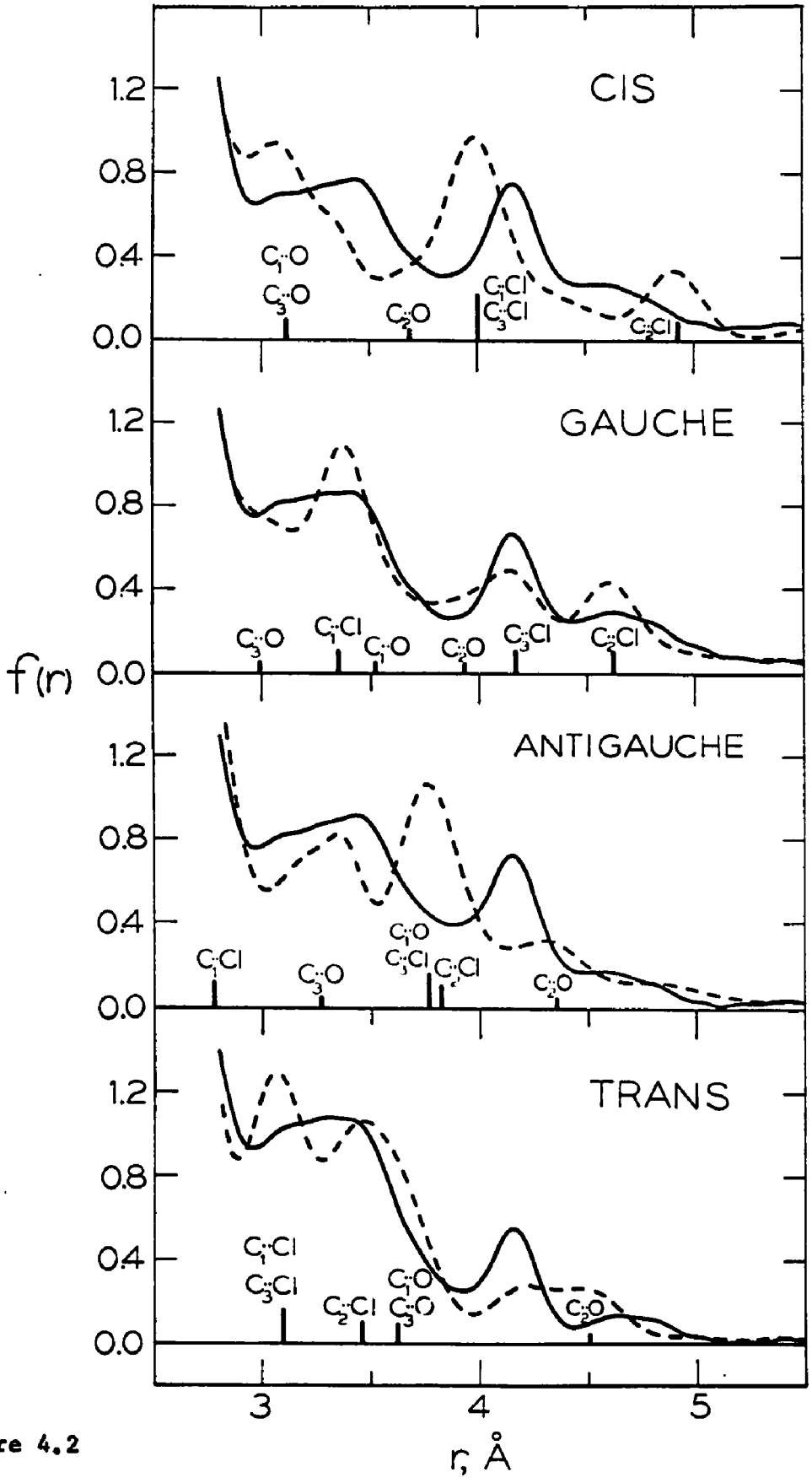

CIS
GAUCHE
ANTIGAUCHE
TRANS
f(r)
r, Å
1.2
0.8
0.4
0.0
3
4
5
C1·O
C3·O
C2·O
C1·Cl
C3·Cl
C2·Cl

Figure 4.2

Figure 4.3 Experimental (solid curves) and calculated (dashed curves) radial distribution functions showing the results of least squares minimization with respect to three internal rotation isomers for various assumed isomeric concentrations and ring conformations.*

* The calculated radial distribution functions of analyses (a) through (f) were computed using the parameters given in Table 4.2.

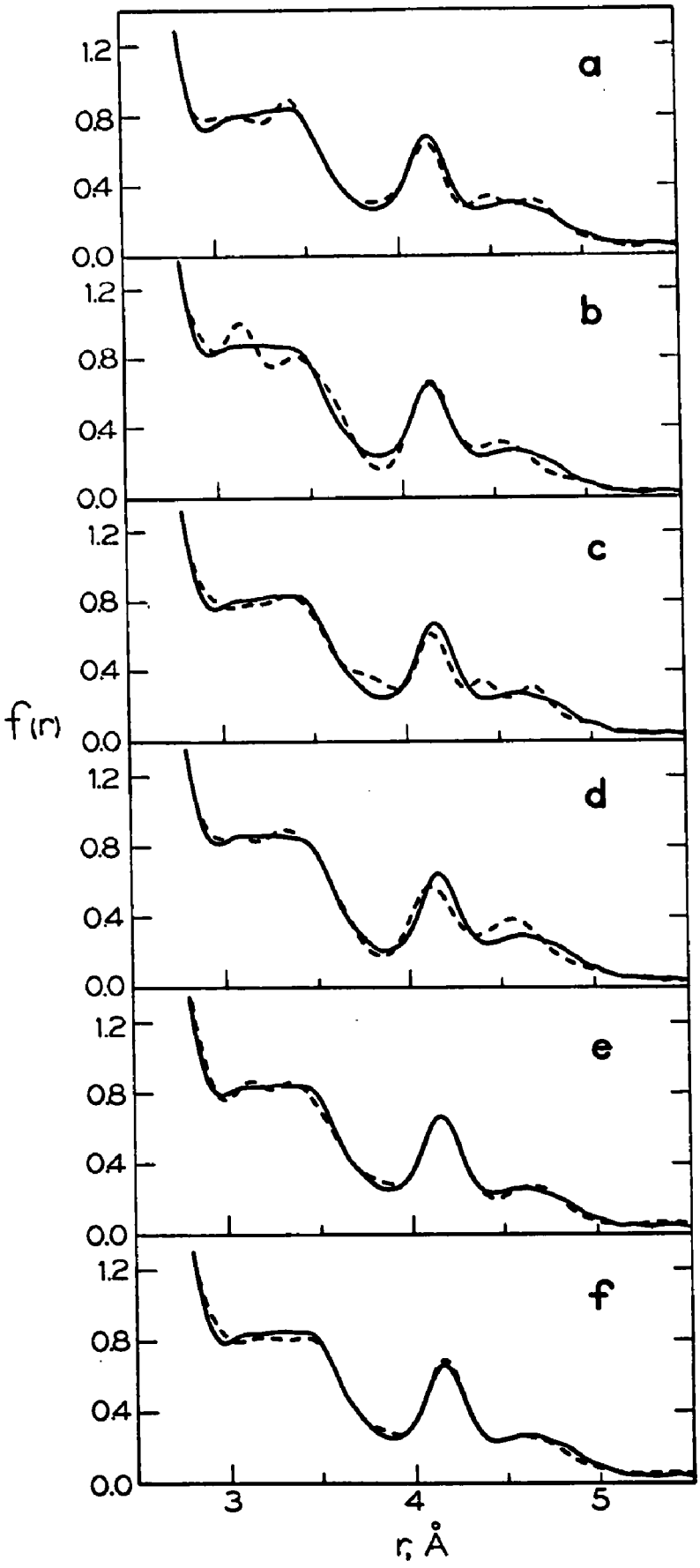


Figure 4.3

experimental function, indicate the presence of ring puckering in addition to torsional displacements from the gauche form. The effects of ring puckering are reflected in the radial distribution function at distances greater than 3.6 Å, where the major scattering pairs, $C_2...O$ and $C_2...Cl$, dependent on ring puckering appear. The results of an analysis of the effects of both small displacements from the gauche conformation and ring puckering are given in Table 4.2, with the corresponding radial distribution functions constructed from the derived parameters shown in Figure 4.3. In these analyses, a distribution of three gauche-like isomers was assumed, with the torsional angles allowed to vary in the constrained least squares analysis of the composite molecular intensity. The magnitude of the ring dihedral angle, β, was constrained to be the same for the axial and equatorial conformations in order to make the analysis tractable. In a number of analyses the latter constraint was relaxed and was determined to have no influence on the principal conclusions. The results indicate a correlation between internal rotation angle and ring conformation, with internal rotation angles less than or equal to the gauche angle predominating for the equatorial conformation and angles greater than the gauche angle predominating for the axial conformation. This effect is illustrated in the Newman projections of Figure 3.1. Approximately 55-60% of the molecules appear to exist in the equatorial conformation with the remainder in the axial conformation. The uncertainty in the isomeric concentration of the axial form is approximately ± 15%.

Whether the equilibrium configuration of the ring belongs to a puckered ring (static nonplanarity) or to a planar ring with a large out-of-plane bending amplitude (dynamic nonplanarity) in which the displacements

Table 4.2 Distribution in angle of internal rotation and ring puckering for C_4H_7CClO.[a] Results of least squares minimization with respect to three internal rotation isomers for various assumed isomeric concentrations and ring conformations.

Analysis	Assumed Isomer Concentration	Assumed Ring Conformation	θ[b]	α	β[c]	γ	∠CCO	∠CCCl	σ(I)/I[d]	σ[f(r)][e]
	27.5	p	42.9		0.0					
(a)	27.5	p	51.6	126.4	0.0	128.0	127.0	111.8	1.628	0.047
	45.0	p	73.9		0.0					
	30.0	a	30.8[f]		18.6					
(b)	30.0	a	48.8[f]	124.2	18.6	128.9	127.0	110.0	1.602	0.045
	40.0	a	70.1		18.6					

[a] Concentrations in percent and angles in degrees.

[b] p = planar conformation; a = axial conformation; e = equatorial conformation.

[c] The magnitude of β was constrained to be the same in axial and equatorial conformations, $|\beta_{ax}| = |\beta_{eq}|$. The absolute value of β is given.

[d] Standard deviation in ppt of the composite molecular intensity.

[e] Standard deviation between experimental and calculated radial distribution functions from 2.0 Å to 6.0 Å using a constant weighting function.

[f] These internal rotation angles constrained to have an angular difference of $\Delta\theta = 18°$.

Table 4.2 (Continued)

Analysis	Assumed Isomer Concentration	Assumed Ring Conformation	θ[b]	α	β[c]	γ	∠CCO	∠CCCl	σ(I)/I[d]	σ[f(r)][e]
	27.5	e	38.7		12.6					
(c)	27.5	e	50.0	129.1	12.6	134.2	128.9	111.3	1.495	0.039
	45.0	e	73.2		12.6					
	27.5	a	35.4		23.6[g]					
(d)	27.5	p	43.6	124.6	0.0	130.1	126.4	110.7	1.674	0.043
	45.0	e	74.2		23.6[g]					
	30.0	e[g]	42.1[h]		17.7					
(e)	30.0	e[g]	59.1[h]	122.0	17.7	130.2	126.5	111.3	1.451	0.030
	40.0	a	72.0		17.7					

[g] Not varied in the least squares analysis.

[h] These internal rotation angles constrained to have an angular difference of $\Delta\theta = 17°$.

Table 4.2 (Continued)

Analysis	Assumed Isomer Concentration	Assumed Ring Conformation	θ[b]	α	β[c]	γ	∠CCO	∠CCCl	σ(I)/I[d]	σ[f(r)][e]
	27.5	e	43.7		23.6					
(f)	27.5	p	56.2	124.6	0.0	129.8	127.3	110.6	1.435	0.026
	45.0	a	68.7		23.6					

in internal rotation angle are correlated with ring bending cannot be determined. The impossibility of ruling out the latter behavior is suggested by the excellent least squares fit in analysis (f), in which 27.5% of the molecules are in the equatorial form, 27.5% are in the planar form and 45% are in the axial form with the angle of internal rotation correlated with ring puckering. It is interesting that in this model the closest approach of the oxygen and the methylene hydrogen of the ring is 2.53 ± 0.03 Å for the three internal rotation angles. Here again the uncertainty in the isomeric concentration of the axial form is approximately ±15%. The latter interpretation of the data suggests a distinctly non-Gaussian distribution in internal rotation angle and ring puckering. An alternative, perhaps more reasonable interpretation of the data, is that the dihedral angle in the equatorial conformer has a smaller magnitude than that of the axial isomer. This effect was indicated since, when the constraint that $|\beta_{axial}| = |\beta_{equatorial}|$ was relaxed, the least squares program always indicated $|\beta_{axial}| > |\beta_{equatorial}|$.

Least squares analyses were also made in which various isomeric concentrations of a fourth isomer, the <u>trans</u> isomer, were assumed. No evidence for a significant concentration of molecules having a <u>trans</u> conformation was found (to within an estimated uncertainty in concentration of +15%).

The breadth of the distribution in θ is roughly 12°–15° and should allow a crude estimate of the barrier to internal rotation. If the potential energy of internal rotation about the C_4-C_5 bond is considered to be of the form

$$V(\theta) = V_o(1 - \cos 3\theta)$$

in the vicinity of the stable conformation in which θ is reckoned from

the gauche reference angle, it is possible to estimate the barrier height, V_o. Assuming a classical distribution in θ,

$$P(\theta) = N[\exp(-V(\theta)/RT)],$$

which may be further simplified for small displacements to

$$P(\theta) = N[\exp(-9V_o\theta^2/4RT)] = N[\exp(\theta^2/2\theta_{rms}^2)]$$

where θ_{rms} is the root-mean-square angular displacement from the gauche conformation. For an estimated θ_{rms} of 12°— 15°, V_o is roughly 2.5 to 4.0 kcal/mole. The temperature of the sample was arbitrarily taken to be 383° K, assuming a temperature drop of the sample upon free expansion from the nozzle of 15° C.

Molecular Parameters

The values of the bonded parameters were determined by least squares analyses of the 0.0 Å to 1.95 Å region of the anharmonic radial distribution, and by least squares analyses of the composite molecular intensity in the final stages of the conformational analysis. These parameters and the more important bond angles are reported in Table 4.3. In initial analyses of the anharmonic radial distribution function all C-C bonds in the molecule were assumed equal. On the basis of this assumption, the mean square amplitude of vibration of the C-C bond was found to be nearly as large as that of the ring C...C nonbonded distance. At this juncture a difference was assumed between the C-C bonds of the ring and the C-C bond adjacent the double bond, since single bonds adjacent to double bonds have been found to be shorter (81,82). A small improvement in standard deviation resulted for a difference between these bonds of 0.05 Å, however, error analyses indicate this figure has no statistical significance. The severe overlap of the bonded peaks has greatly limited

Table 4.3 Structural parameters[a] and estimated standard errors[b] for C_4H_7CClO.

Parameter	r_g	ℓ_g	∠
C-H	1.128 ± 0.014	0.076 ± 0.020	
C=O	1.195 ± 0.013	0.044 ± 0.008	
C-C	1.540 ± 0.003	0.058 ± 0.005	
C-Cl	1.793 ± 0.006	0.066 ± 0.006	
CCO			127.0 ± 1.5
CCCl			111.0 ± 2.0
α			123.5 ± 2.5
β			21. ± 5
γ			129. ± 4
θ_{ave}[c]			57. ± 5

[a] Distances and amplitudes in Å, angles in degrees. Angles were not corrected for shrinkage effects.

[b] Calculated standard errors took into account the effects of both random and systematic errors (28). The effects of uncertainties in isomeric concentrations were also included.

[c] $\theta_{rms} \approx 12°$ to $15°$.

the precision in the determination of the bond lengths. The results of this analysis are compared with parameters determined for related molecules in Table 4.4.

Experimental and calculated molecular intensities, sM(s), and radial distribution functions are compared in Figures 4.4 and 4.5 respectively. In each of these comparisons the calculated functions were constructed using the bonded parameters reported in Table 4.3 and the bond angles and internal rotation angles reported in Table 4.2, analysis (e).

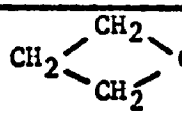
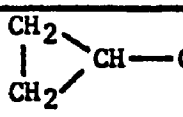
A matrix of correlation coefficients based on the least squares fit of the composite molecular intensity using a diagonal weight matrix proportional to the scattering variable s is given in Table 4.5.

DISCUSSION

The rotational isomerization about the C-CClO bond in this moderately strained cyclobutyl compound is found to be similar to that in unstrained alkyl carboxaldehydes (76,81,90), exhibiting gauche-like isomerization with no evidence for cis isomerization as observed in highly strained cyclopropyl compounds (76,78). This shows that the three-fold term of the torsional potential energy is dominant in cyclobutyl carbonyl compounds, in contrast to the dominance of the two-fold term in cyclopropyl carbonyl compounds.

The observed gauche-like conformations can be rationalized in terms of Pauling's staggered-bond scheme (79), which regards double bonds as two bent single bonds (see Figure 3.1). According to this point of view, the bonds are staggered in the present molecule. The absence of cis isomerization in C_4H_7CClO is consistent with the predictions of Walsh's π-electron model (91), which accounts for cis C_3H_5CXO. According to the

Table 4.4 Comparison of parameters[a] for C_4H_7CClO and related molecules.

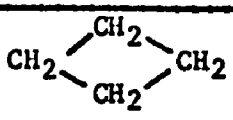
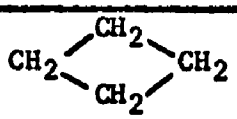
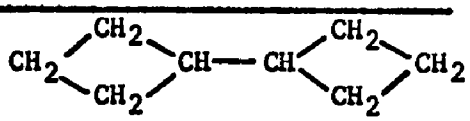
Molecule			$CH_3—CClO$
C-H	1.128 ± 0.014	1.105 ± 0.06	1.083 ± 0.005
C=O	1.195 ± 0.013	1.197 ± 0.025	1.192 ± 0.01
C-C	1.540 ± 0.003	1.506 ± 0.002	1.499 ± 0.01
C-Cl	1.793 ± 0.006	1.797 ± 0.009	1.789 ± 0.005
∠CCH	116.6 ± 3.0	120.7 ± 4	110.35 ± 0.17
∠CCO	127.0 ± 1.5	127.6 ± 3	127.08 ± 0.17
∠CCCl	111.0 ± 2.0	111. ± 2.5	112.65 ± 0.5
α	123.5 ± 2.5		
β	21.0 ± 5		
Method	SMED[b]	SMED	MW[c]
Reference	Present study	(78)	(83)

[a] Distances in Å, angles in degrees.

[b] Sector-microphotometer method of electron diffraction. Parameters are r_g values.

[c] Microwave method.

Table 4.4 (Continued)

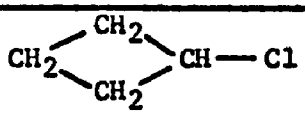
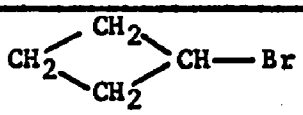
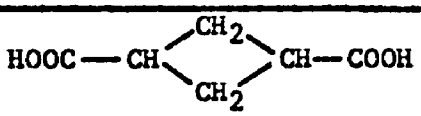
Molecule			
C-H	1.096 ± 0.04	1.092 ± 0.01	1.104 ± 0.01
C=O			
C-C	1.568 ± 0.02	1.548 ± 0.003	1.548 ± 0.004 (ring) 1.536 ± 0.016 (exo-ring)
C-Cl			
∠CCH	112.8 ± 4	(no value reported)	114.5 ± 2
∠CCO			
∠CCCl			
α			128.4 ± 2
β	$20 \pm \frac{10}{20}$	35[d]	33 ± 2.0
Method	VED[e]	SMED[f]	SMED[f]
Reference	(84)	(85)	(86)

[d] O. Bastiansen and P. N. Skancke, unpublished work (private communication from S. Cyvin quoted in R. C. Lord and I. Nakagawa, J. Chem. Phys. 39, 2951 (1963)).

[e] Visual method of electron diffraction.

[f] Sector-microphotometer method of electron diffraction. Parameters are r_a values.

Table 4.4 (Continued)

Molecule			
C-H		1.096[g]	
C=O			1.238 ± 0.005
C-C	1.538 ± 0.005	1.544 ± 0.003	1.560 ± 0.006 (ring) 1.494 ± 0.006 (exo-ring)
C-Cl	1.775 ± 0.005		
∠CCH	114.04 ± 0.5	114.4	
∠CCO			124.1 ± 0.3
∠CCCl	120.6 ± 0.5		
α	135 ± 1	131.0 ± 0.14	124.8 ± 0.4
β	20 ± 1[h]	29.4 ± 0.15	0.0
Method	MW	MW	X-ray[i]
Reference	(87)	(88)	(89)

[g] Assumed to be the same as that found for methyl bromide (J. P. Friend, R. F. Schneider and B. P. Dailey, J. Chem. Phys. 23, 1557 (1955)).

[h] In higher vibrational states these molecules are reported to become nearly planar (W. G. Rothschild, J. Chem. Phys. 45, 1215 (1966)).

[i] X-ray diffraction method.

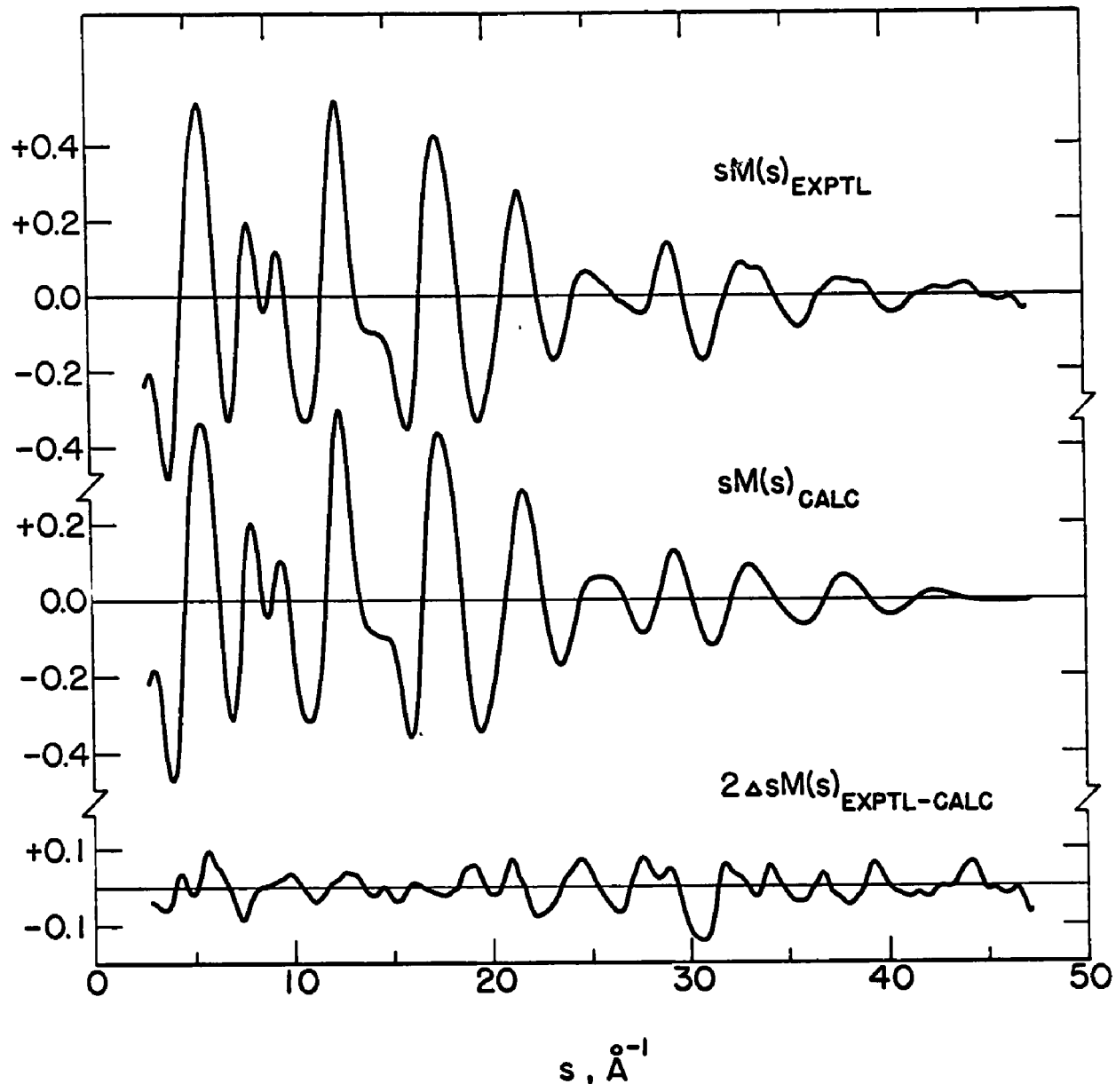


Figure 4.4 Experimental and calculated molecular intensity functions for C_4H_7CCl0. $\Delta sM(s) = sM(s)_{exptl} - sM(s)_{calc}$.

Figure 4.5 Experimental radial distribution function for C_4H_7CCl0. $\Delta f(r) = f(r)_{exptl} - f(r)_{calc}$.

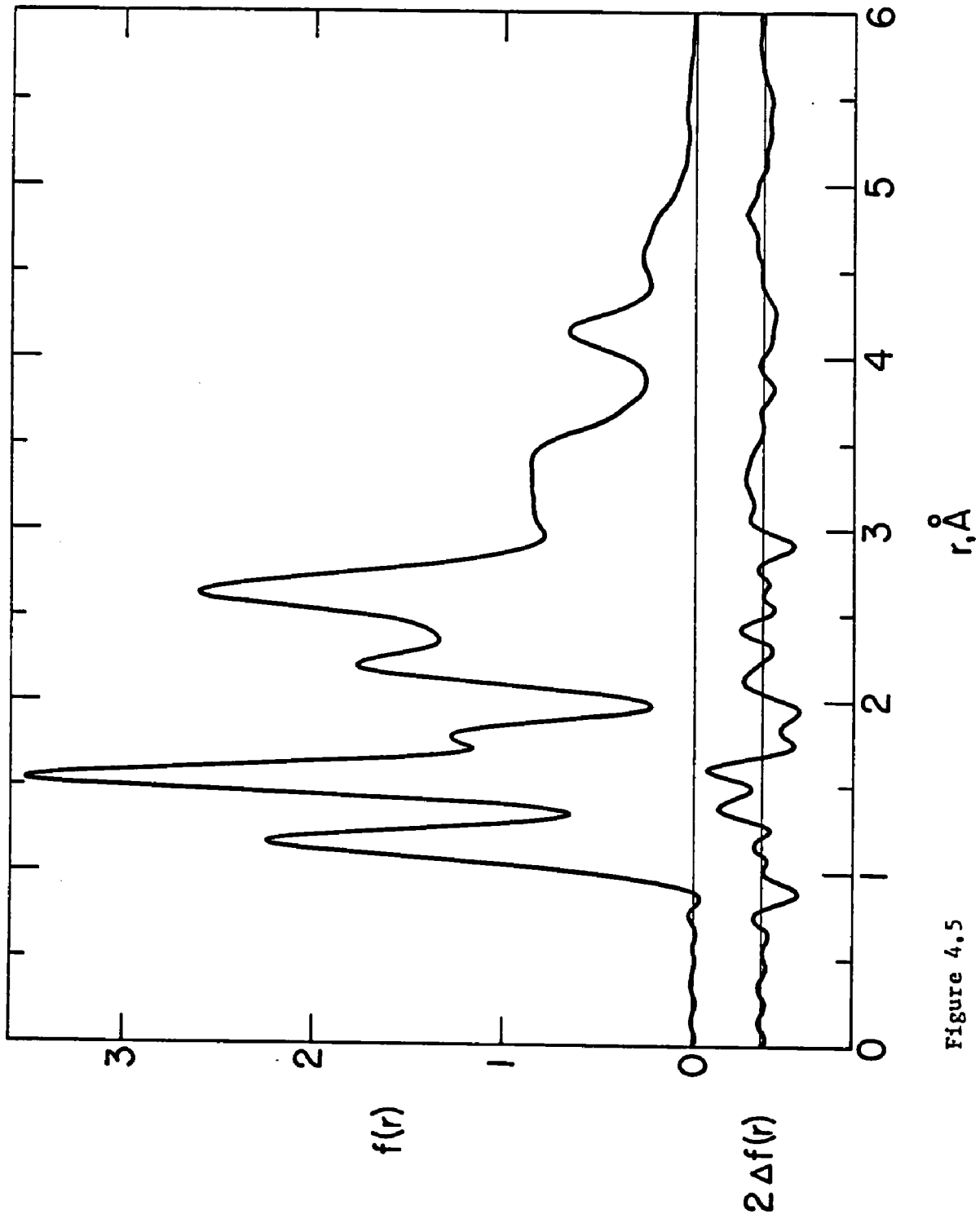


Figure 4.5

Table 4.5 Matrix of correlation coefficients[a] for C_4H_7CCl0.

	r_{C-H}	$r_{C=O}$	r_{C-C}[b]	Δr[c]	r_{C-Cl}	$\angle CCO$	$\angle CCCl$
r_{C-H}	1.0	-.65	.11	-.26	.17	-.02	-.31
$r_{C=O}$		1.0	.00	.28	-.12	.05	.39
r_{C-C}			1.0	.23	.20	.06	-.08
Δr				1.0	-.12	-.40	.40
r_{C-Cl}					1.0	.49	-.22
$\angle CCO$						1.0	-.48
$\angle CCCl$							1.0
α							
β							
γ							
θ							
l_{C-H}							
$l_{C=O}$							
l_{C-C}							
l_{C-Cl}							
$l_{C\ldots C}$							
$l_{O\ldots Cl}$							
$l_{C\ldots O}$							
$l_{C\ldots Cl}$							
$l_{X\ldots H}$							

[a] Based on 144 intensity values interpolated from 380 experimentally observed data points. Matrix elements are given by

$$\rho_{ij} = B_{ij}^{-1}/(B_{ii}^{-1} B_{jj}^{-1})^{1/2}$$

where the notation corresponds to that of O. Bastiansen, L. Hedberg and K. Hedberg, J. Chem. Phys. 27, 1311 (1957).

[b] $r(C-C)_{mean}$

[c] $\Delta r = r(C-C)_{ring} - r(C-C)_{exo-ring}$.

Table 4.5 (Continued)

	α	β	γ	θ	ℓ_{C-H}	$\ell_{C=O}$	ℓ_{C-C}
r_{C-H}	-.05	-.01	-.17	-.05	.51	.54	.22
$r_{C=O}$	-.03	.01	.18	.04	-.83	-.37	-.25
r_{C-C}	-.05	.03	.07	-.04	.02	.07	-.19
Δr	.68	.32	.32	.21	-.25	-.16	-.87
r_{C-Cl}	-.29	-.03	.10	-.16	.12	.10	.15
$\angle CCO$	-.25	.07	.04	-.57	-.02	.01	.37
$\angle CCCl$	.17	-.02	.08	.64	-.33	-.18	-.36
α	1.0	.33	.18	.15	.01	-.04	-.61
β		1.0	.46	-.25	-.02	-.02	-.28
γ			1.0	-.12	-.09	-.10	-.26
θ				1.0	-.04	-.03	-.19
ℓ_{C-H}					1.0	.28	.21
$\ell_{C=O}$						1.0	.14
ℓ_{C-C}							1.0
ℓ_{C-Cl}							
$\ell_{C...C}$							
$\ell_{O...Cl}$							
$\ell_{C...O}$							
$\ell_{C...Cl}$							
$\ell_{X...H}$							

Table 4.5 (Continued)

	ℓ_{C-Cl}	$\ell_{C\ldots C}$	$\ell_{O\ldots Cl}$	$\ell_{C\ldots O}$	$\ell_{C\ldots Cl}$	$\ell_{X\ldots H}$[d]
r_{C-H}	-.02	-.04	.14	-.06	.05	.01
$r_{C=O}$	.01	-.02	-.25	.07	.00	-.06
r_{C-C}	-.10	-.08	.04	.02	.11	.00
Δr	-.03	-.26	.23	.22	.11	.38
r_{C-Cl}	-.04	-.09	-.23	.01	.00	-.20
$\measuredangle CCO$	.01	.24	.09	-.09	-.32	-.62
$\measuredangle CCCl$	.01	.01	-.44	.15	-.25	.27
α	.01	-.14	.64	.05	-.06	.28
β	-.02	-.06	.24	.32	.12	-.33
γ	.05	-.32	-.01	.42	-.05	-.17
θ	-.01	-.08	-.27	-.12	-.04	.42
ℓ_{C-H}	-.01	.02	.20	-.06	.00	.04
$\ell_{C=O}$	-.02	.00	.07	-.04	.03	-.01
ℓ_{C-C}	.01	.22	-.22	-.19	-.10	.35
ℓ_{C-Cl}	1.0	-.02	.00	.00	-.03	-.04
$\ell_{C\ldots C}$		1.0	.01	.24	.05	-.18
$\ell_{O\ldots Cl}$			1.0	.03	.10	.07
$\ell_{C\ldots O}$				1.0	.27	.06
$\ell_{C\ldots Cl}$					1.0	.20
$\ell_{X\ldots H}$						1.0

[d] $\ell_{X\ldots H} = \ell_{C\ldots H} = \ell_{O\ldots H} = \ell_{Cl\ldots H}$.

π-electron model, conjugative stabilization would be expected to be much less important in the case of cyclobutyl carbonyl compounds than in cyclopropyl carbonyl compounds, since this would require four-center unsaturation in the cyclobutyl group as compared to three-center unsaturation in the cyclopropyl group.

The fact that only gauche-like isomers were detected in this molecule is in accord with a number of previous findings. In this and other examples, the carbonyl oxygen exhibits a propensity to eclipse a methyl or methylene group in preference to a hydrogen atom. Other examples include isopropyl carboxaldehyde (76), propionaldehyde (92), pivaldehyde (93), 2-methylcyclohexanone (94) and trans 1-3-cyclobutane dicarboxylic acid (89).*

Bond lengths, angles and amplitudes of vibration in C_4H_7CClO are in reasonable agreement with those determined for related molecules. The C-H bond length is close to the average values found in cyclopropyl methyl ketone (78) and isopropyl carboxaldehyde (76). It may be noted that the mean of the C-C bond length found by Bastiansen, et al., (85) in cyclobutane and the C-C bond length in acetyl chloride (83) is approximately 1.540 Å, in excellent agreement with that found for cyclobutanecarboxylic acid chloride. No statistically significant difference between the ring and exo-ring C-C bond lengths was provided by the diffraction intensities. However, the C-C amplitude seems larger than might have been expected from comparisons with amplitudes of other

---

* Crystal packing forces may influence the preferred conformation in this molecule.

cyclic molecules (78).* If the peak is considered to have two non-equivalent components, one corresponding to the ring C-C bonds and the second corresponding to the exo-ring C-C bond, with a difference of 0.005 Å between components, the derived amplitude (ℓ_g = 0.053 Å) is closer to that expected.

One of the interesting aspects of the study is the apparent correlation between the ring bending and internal rotation angle implied by the diffraction data. Although the evidence for such a correlation is marginal, the correlation would be consistent with the principal finding of this research, namely, that the carbonyl oxygen experiences an attraction for the methylene groups of the ring. If the methylene hydrogen closest to the oxygen tended to follow the oxygen as the -CClO group librated, the result would be the observed coupling between the ring pucker and -CClO internal rotation. Steric interactions between the chlorine and ring could not cause the coupling because they act in the wrong sense. Despite the evidence that carbonyl oxygens interact attractively with alkyl groups in conformational equilibria, it must not be assumed that the O...H interactions involved are closely related to normal hydrogen bonds. The present O...H distances of 2.5 Å are much longer than those associated with ordinary hydrogen bonds.

---

*Also see PART I and PART II of this thesis.

PART V

Molecular Structure of Phosphorus Pentachloride

INTRODUCTION

The Group Va pentahalides studied to date in the gas phase are trigonal bipyramids with axial bonds longer than equatorial bonds (95,96). Many theoretical models account qualitatively for these structural characteristics. One of the simplest of these models, the valence-shell-electron-pair-repulsion (VSEPR) model of Gillespie and Nyholm (55,97), also predicts that the difference between the axial and equatorial bonds should increase as the ligand electronegativity decreases. A comparison of PF_5 (95) and PCl_5 (98,99,100) seems to bear this out, but there are appreciable differences in the bond lengths reported for the latter molecule. A redetermination of the structure of gaseous PCl_5 is therefore of some interest. An additional reason for studying the molecule by electron diffraction is to establish the mean amplitudes of vibration, since these have not previously been reported. An experimental measurement of the mean amplitudes should provide enough additional information to resolve the existing ambiguity in the assignments for the e' frequencies.

EXPERIMENTAL

Reagent grade phosphorus pentachloride was purchased from the J. T. Baker Chemical Co., Phillipsburg, New Jersey. Care was taken to prevent decomposition of the sample by transfering it from the shipping container to a suitable sample flask in a dry nitrogen atmosphere. The sample was

sublimed to the walls of the sample flask with volatile impurities periodically removed by flashing off numerous vapor pressure heads during the refinement. In addition, residual volatile impurities were flashed off prior to recording each set of diffraction patterns.

An early vapor pressure study of phosphorus pentachloride (101) indicated that slight association occurs at temperatures below 100° C while at temperatures above 110° C dissociation to phosphorus trichloride and chlorine becomes important. A recent mass spectral study (102) has given supporting evidence for association ($P_2Cl_{10}^+$ observed) at room temperature. To reduce these complicating effects and to keep exposure times from being excessively long, the sample was introduced into the diffraction chamber through a heated nozzle assembly. The nozzle assembly consisted of a jacketed nozzle that allowed heating fluid to be passed through the annular region between the inlet tubing and outer jacket, and a sample flask which was connected to the nozzle by an o-ring joint and was entirely enclosed in a low temperature furnace. The inlet tubing and valves of the nozzle were of Monel metal with Teflon gaskets at all joints except the o-ring joint. The nozzle tip was constructed of nickel with a throat 0.29 mm in diameter and 0.70 mm in length. The 1-liter sample flask, fitted with a Teflon needle valve, was of Pyrex. Steam was passed through the nozzle jacket to ensure a temperature of approximately 100° C. The temperature of the sample flask was regulated independently of the nozzle temperature. Diffraction patterns were recorded on 4 X 5 in. Kodak process plates at camera distances of 21, 11 and 6.5 cm using an electron diffraction apparatus (13) equipped with an r^3 sector. The experimental conditions under which the diffraction patterns were recorded using 40 kV electrons are given in Table 5.1. Plates

were developed at 20° C for 5 min. with Kodak D-11 developer.

Photographic densities, measured with an automatic recording microphotometer with digital output (14), were converted to absorbancies, and corrected for the radial variation of plate sensitivity (15). Intensities were calculated from the corrected absorbancies according to

$$I = A(1 + 0.05A^2),$$

as recommended by Janzen (15). Six plates at each camera distance were averaged and used in the structural analysis.

Table 5.1 Experimental conditions under which PCl_5 diffraction patterns were recorded.

Camera distance (cm)	21.290	10.641_5	6.776
Sample temperature (°C)	80	90	90
Vapor pressure (torr)	7.8	16	16
Exposure time (sec)	7-8	30-35	75
Beam current (μA)	0.42	0.46	0.42

ANALYSIS OF DATA

Experimental intensities were corrected for sector imperfections and extraneous scattering prior to division by the theoretical atomic intensity. Atomic scattering factors used were the analytical elastic factors of Strand and Bonham (17) and the inelastic factors of Heisenberg and Bewilogua (18). Experimental leveled intensity, $I_0(s)$, and background intensity, $I_B(s)$, functions (16) for each of the three camera distances are given in Appendix E. Indices of resolution (19) were 1.07, 1.06 and

1.03 for the 21, 11 and 6.5 cm camera distances respectively.

Experimental and calculated molecular intensities and radial distribution functions were computed as previously described (16,19,20) with the usual corrections applied (19,21,22,23). Radial distribution functions were calculated using a Degard damping factor [$\exp(-0.0015s^2)$]. Atomic scattering factors used in all phases of the analysis after leveling of experimental intensities were the partial wave elastic factors of Cox and Bonham (24) and the inelastic factors of Tavard (25). Anharmonicity constants (22) were estimated (26) to be 1.6 $Å^{-1}$ for the P-Cl bonded distance and were taken to be 1.0 $Å^{-1}$ for the Cl...Cl nonbonded distances.

Soon after the structural analysis began it became apparent that an impurity had been present in the sample. The diffraction data disclosed the presence of a broad impurity peak in the radial distribution function at 1.4 Å. Infrared spectral analysis of the vapors issuing from the nozzle of the diffraction apparatus showed these impurities to be phosphoryl chloride and hydrogen chloride. The P-O and H-Cl distances account for the appearance of a peak in the radial distribution function at 1.4 Å. These impurities were apparently formed during the diffraction experiments by hydrolysis of PCl_5. Estimates of the $POCl_3$ present at each camera distance were 15, 8 and 8 mole percent at the 21, 11 and 6.5 cm camera distances as inferred from the diffraction and infrared data. The mole ratio of $POCl_3$ to HCl was taken as 1 to 2.

Corrections for the impurities were made by subtracting the intensity contribution due to these impurities from the experimental leveled intensities using appropriate theoretical expressions and the known molecular structures of $POCl_3$ (103,104) and HCl (105). The corrected experimental leveled intensity and background intensity functions are given in

Appendix F.

The anharmonic radial distribution function, the molecular intensity of each camera distance, and the composite molecular intensity were fitted with the appropriate calculated expressions in least squares analyses (27) of both the corrected and uncorrected data. Small corrections were made for Bastiansen-Morino shrinkage effects (64) in geometrically constrained least squares analyses. These shrinkage corrections, taken from the calculations of Brunvoll (106), were 0.0007 Å for $Cl_{ax}...Cl_{eq}$, 0.007 Å for $Cl_{eq}...Cl_{eq}$, and 0.0025 Å for $Cl_{ax}...Cl_{ax}$. The computed shrinkages are consistent with a vibrational assignment of the $P(Cl_{eq})_3$ equatorial bending frequency lower than the $P(Cl_{ax})_2$ axial bend.

The difference between the mean amplitudes of vibration for the axial and equatorial P-Cl bond lengths, $\Delta\ell$, was taken from Brunvoll (106) and included as a constraint in the analysis since it was not possible to establish independent values from the diffraction intensities. The value of $\Delta\ell$ calculated by Brunvoll is approximately twice the value estimated using a rough extension (66) of Badger's rule (67) which relates variations in force constants to variations in bond lengths.

Calculated standard errors took into account the effects of both random and systematic errors (28).*

RESULTS

Experimental and calculated molecular intensities, sM(s), are compared in Figure 5.1. The experimental radial distribution function is shown in Figure 5.2 and is compared with the calculated distribution

---

*Also see PART I, p. 5.

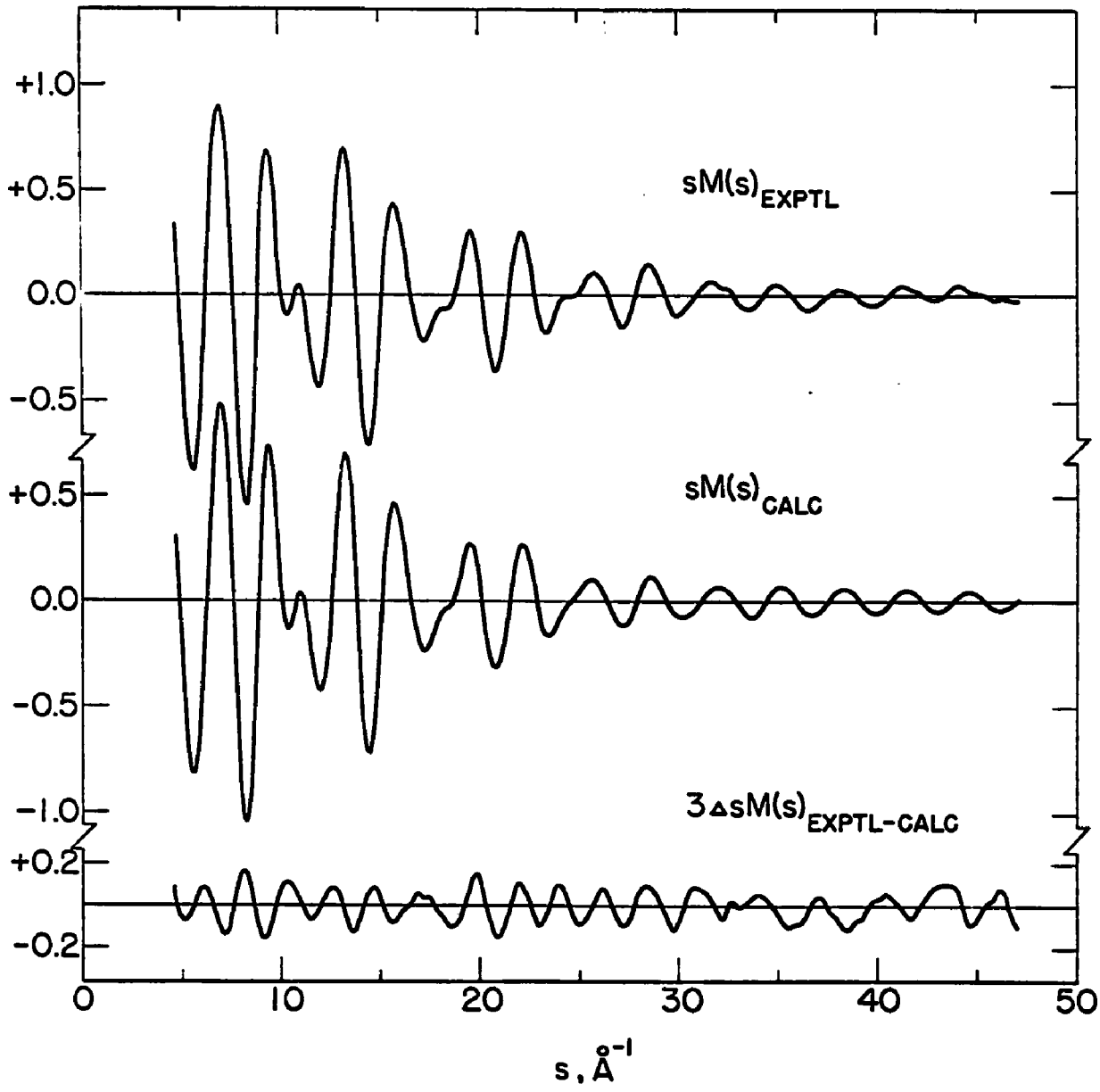


Figure 5.1 Comparison of experimental and calculated molecular intensity functions for PCl_5. $\Delta sM(s) = sM(s)_{exptl} - sM(s)_{calc}$.

Figure 5.2 Experimental radial distribution function for PCl_5. $\Delta f(r) = f(r)_{exptl} - f(r)_{calc}$.

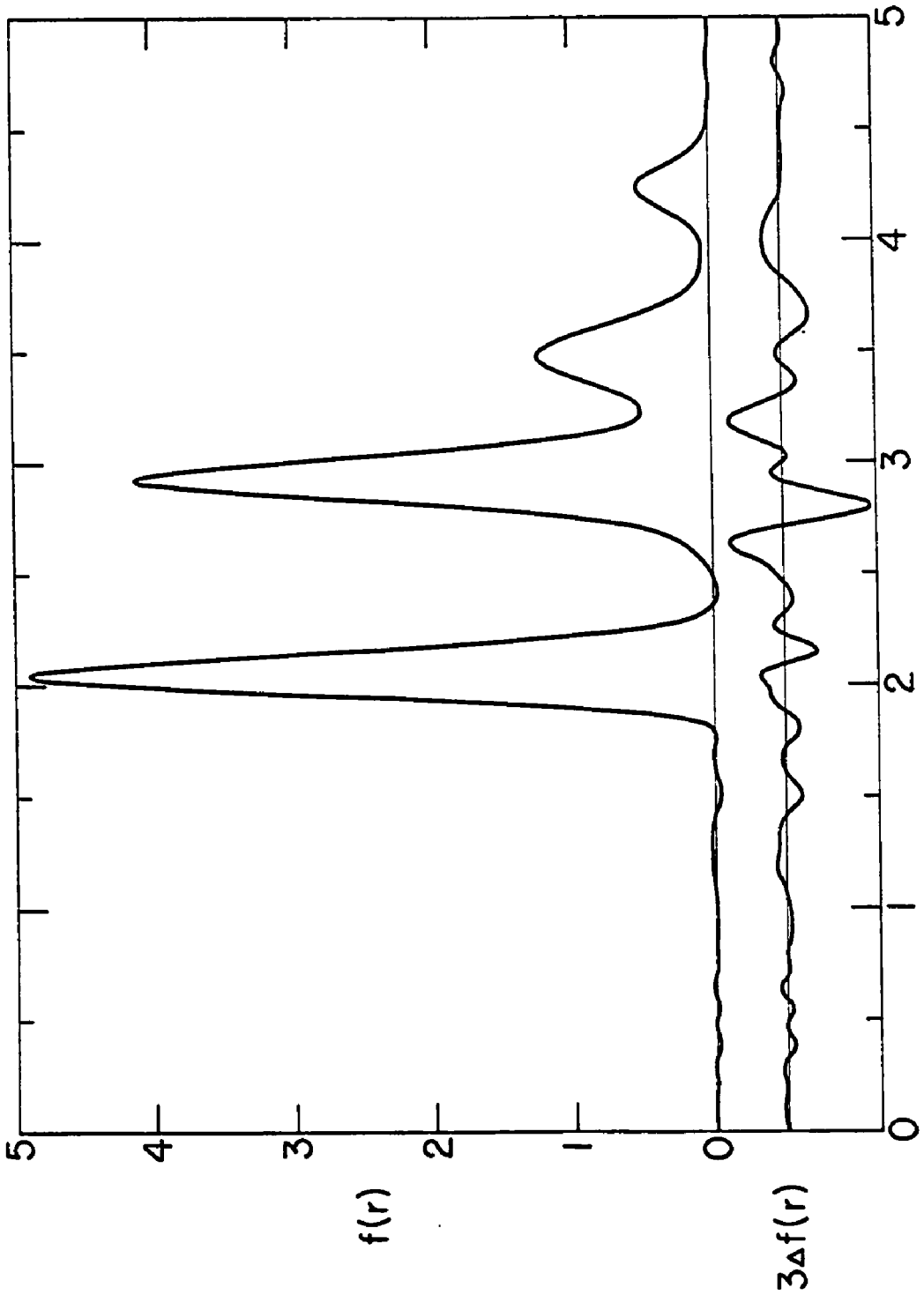


Figure 5.2

function. The positions and areas of the four well resolved peaks in the experimental radial distribution function are in agreement with a trigonal bipyramidal structure except for small discrepancies in the 2.9 Å region. This discrepancy arises from scattered intensities at small scattering angles. Intensities from scattering angles beyond $s \approx 12$ Å^{-1} contribute virtually nothing to the anomalous area.

Results of constrained least squares analyses made on both the corrected and uncorrected molecular intensity for each camera distance are summarized in Figure 5.3. These results show that the mean bond length, $(P\text{-}Cl)_{mean}$, is relatively insensitive to the $POCl_3$ and HCl impurities present in the vapor, while the difference between axial and equatorial bond lengths, $\Delta(P\text{-}Cl)$, is moderately sensitive.

Structural parameters and estimated standard errors derived from least squares analyses are given in Table 5.2. The mean amplitudes of vibration are compared with those calculated by Brunvoll (106) for a temperature of 298° K. Estimated amplitudes at 383° K are also listed. They were calculated roughly from Brunvoll's 298° K values by assuming that mean square amplitudes vary as $\coth(h\nu_{eff}/2kT)$, where ν_{eff} is the average frequency of the modes contributing most heavily to the particular amplitude. The temperature 383° K was adopted arbitrarily, assuming the temperature drop of the sample upon free expansion was 15°. The actual drop appropriate for vibrational relaxation is unknown and may be very different from this figure. Results of the present study are compared with those of previous electron diffraction studies in Table 5.3.

A matrix of correlation coefficients, based on a least squares fit of the composite molecular intensity using a diagonal weight matrix with elements proportional to the scattering variable s, is given in

Figure 5.3 Summary of results of least squares analyses on corrected and uncorrected 21 cm (————————), 11 cm (——·——·——) and 6.5 cm (— — — —→) camera distance intensities. $\Delta(P\text{-}Cl) = (P\text{-}Cl_{ax}) - (P\text{-}Cl_{eq})$.

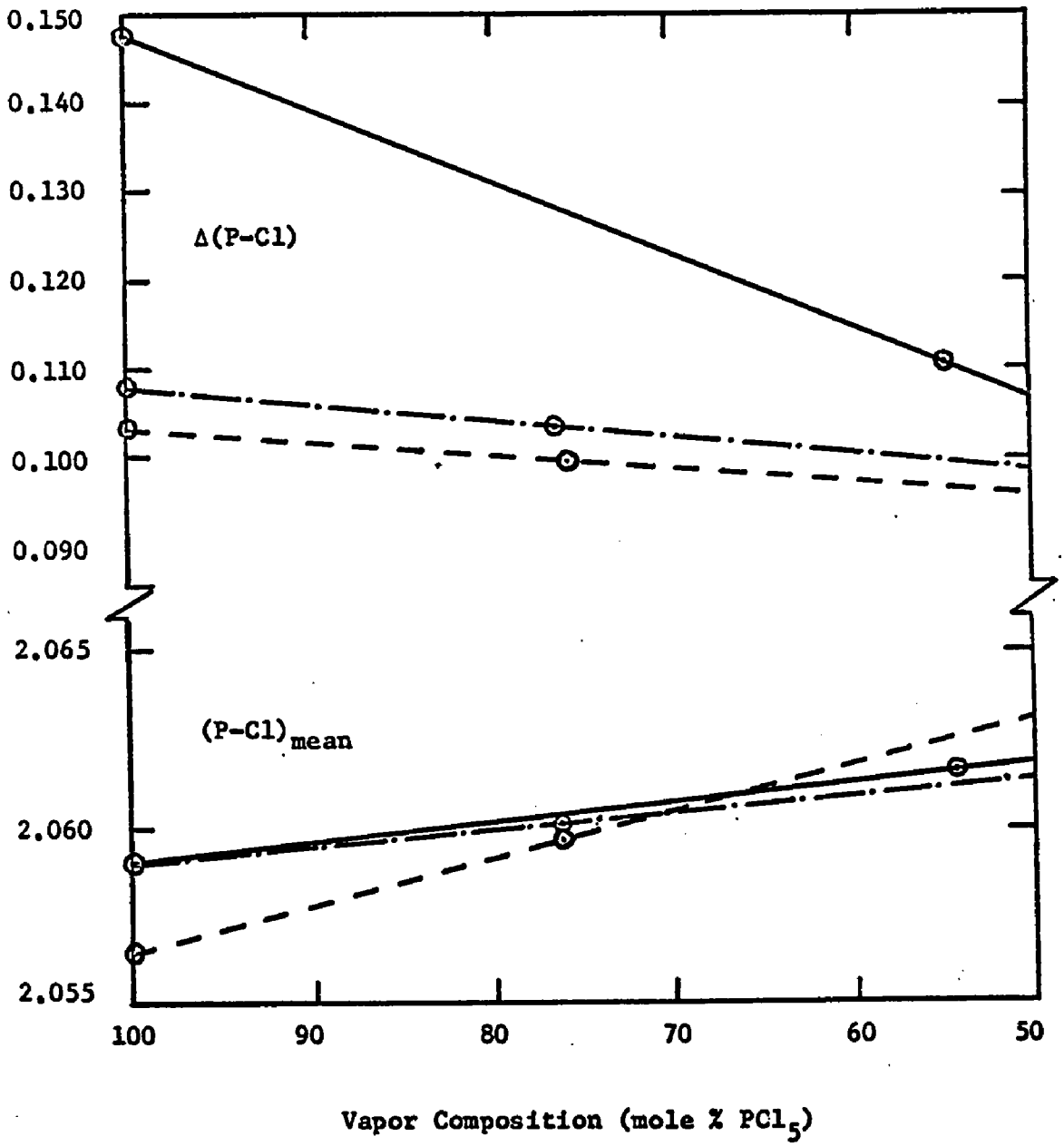


Table 5.2 Structural parameters (in Å) and estimated standard errors[a] for PCl_5.

Parameter	r_g	ℓ_g, exptl	ℓ_g, calc[b] 298° K	383° K[c]
$(P-Cl)_{mean}$	2.061 ± 0.002			
$(P-Cl_{ax}) - (P-Cl_{eq})$	0.104 ± 0.01			
$(P-Cl_{eq})$	$2.019_5 \pm 0.007$	0.047 ± 0.005	0.050 (0.052)	0.053 (0.056)
$(P-Cl_{ax})$[d]	$2.123_5 \pm 0.009$	0.055 ± 0.005	0.058 (0.058)	0.062 (0.062)
$Cl_{ax}...Cl_{eq}$	$2.93_0 \pm 0.012$	0.091 ± 0.004	0.073 (0.102)	0.080 (0.116)
$Cl_{eq}...Cl_{eq}$	$3.49_1 \pm 0.010$	0.146 ± 0.007	0.126 (0.068)	0.142 (0.075)
$Cl_{ax}...Cl_{ax}$	$4.24_{45} \pm 0.010$	0.081 ± 0.006	0.060 (0.060)	0.066 (0.066)

[a] The effects of both random and systematic errors (28) were taken into account in computing standard errors. The effects of uncertainties in the concentration were also included.

[b] See reference (106). Values in parentheses are consistent with a vibrational assignment of the equatorial bending frequency greater than the axial bending frequency; the other values are based on the opposite assumption.

[c] Computed assuming mean square amplitudes vary as $\coth(h\nu_{eff}/2kT)$; see text.

[d] $\ell_g(P-Cl_{ax}) - \ell_g(P-Cl_{eq})$ was constrained to be 0.008 Å in the analysis as taken from reference (106).

Table 5.3 Comparison of electron diffraction studies of PCl_5.

Study	Parameter (Å)			
	$(P-Cl)_{mean}$	$\Delta(P-Cl)$[d]	$P-Cl_{eq}$	$P-Cl_{ax}$
Rouault, VED[a] (98)	2.10	0.15	2.04 ± 0.06	2.19 ± 0.02
Schomaker and Sargent, VED (99)	2.066	0.09	2.03	2.12
Romanov and Spiridonov, SMED[b] (100)	2.06	0.12	2.02 ± 0.01	2.14 ± 0.01
Present work, SMED[c]	2.061 ± 0.002	0.104 ± 0.01	2.019_5 ± 0.007	2.123_5 ± 0.009

[a] Visual method of electron diffraction.

[b] Sector microphotometer method of electron diffraction. Parameters are r_a values.

[c] Sector microphotometer method of electron diffraction. Parameters are r_g (0) values.

[d] $\Delta(P-Cl) = (P-Cl_{ax}) - (P-Cl_{eq})$.

Table 5.4.

DISCUSSION

The observed mean bond length, 2.061 ± 0.002 Å, is in excellent agreement with that found recently by Romanov and Spiridonov (100). This mean bond length is 0.019 Å longer than that found in PCl_3 (107), whereas, in the analogous fluoride compounds, the mean bond length in PF_5 (95) is 0.019 Å shorter than that found in PF_3 (108).

The difference between axial and equatorial bond lengths, 0.104 ± 0.01 Å, is found to be in reasonable agreement with the results of Schomaker and Sargent (99) and Romanov and Spiridonov (100), being nearly the average of these two results. This difference is approximately twice the difference found in PF_5, 0.043 ± 0.008 Å (95) , and AsF_5, 0.055 ± 0.010 Å (96). Gillespie's VSEPR model (55,97) qualitatively predicts this increase on going from the fluorine to the chlorine compound, attributing the increase to the greater size of the bonding electron pairs in PCl_5 because of the lower electronegativity of chlorine.

Mean amplitudes of vibration for PCl_5 are of interest since insufficient information is available from the vibrational spectrum to make an unambiguous assignment for this and related molecules. Some spectroscopists (109) have assigned the lower of the two e' frequencies to the in-plane equatorial bend, while others have assigned it to the axial bend. The experimental mean amplitudes are found to differ from the calculated values by approximately 10%, except for the $Cl_{eq}...Cl_{eq}$ amplitude. Notwithstanding this minor disagreement, there can be no doubt that the vibrational assignment in which the in-plane equatorial bending frequency is lower than the axial bending is the one which fits the pattern of

Table 5.4 Matrix of correlation coefficients[a] for PCl_5.

	$r(P\text{-}Cl)_{mean}$	$\Delta r(P\text{-}Cl)$[b]	$\ell(P\text{-}Cl_{eq})$[c]	$\ell(Cl_{ax}\ldots Cl_{eq})$	$\ell(Cl_{eq}\ldots Cl_{eq})$	$\ell(Cl_{ax}\ldots Cl_{ax})$	R
$r(P\text{-}Cl)_{mean}$	1.0	0.12	-0.02	0.03	-0.10	0.01	0.06
$\Delta r(P\text{-}Cl)$		1.0	-0.40	0.05	-0.04	0.03	0.15
$\ell(P\text{-}Cl_{eq})$			1.0	0.26	0.03	0.04	0.46
$\ell(Cl_{ax}\ldots Cl_{eq})$				1.0	-0.04	0.06	0.55
$\ell(Cl_{eq}\ldots Cl_{eq})$					1.0	-0.02	0.01
$\ell(Cl_{ax}\ldots Cl_{ax})$						1.0	0.10
R							1.0

[a]Based on 136 intensity values interpolated from 331 experimentally observed data points. Matrix elements are given by

$$\rho_{ij} = B_{ij}^{-1}/(B_{ii}^{-1}\ B_{jj}^{-1})^{1/2}$$

where the notation corresponds to that of O. Bastiansen, L. Hedberg, and K. Hedberg, J. Chem. Phys. 27, 1311 (1957).

[b]$\Delta r(P\text{-}Cl) = r(P\text{-}Cl_{ax}) - r(P\text{-}Cl_{eq})$.

[c]$\ell(P\text{-}Cl_{ax}) - \ell(P\text{-}Cl_{eq})$ was constrained to be 0.008 Å.

amplitudes determined by electron diffraction. Analogous assignments in the cases of PF_5 (95) and AsF_5 (96) also seem called for by the electron diffraction studies of the compounds.

REFERENCES

(1) J. G. Aston, S. C. Schumann, H. L. Fink and P. M. Doty, J. Am. Chem. Soc. 63, 2029 (1941); J. G. Aston, M. L. Fink and S. C. Schumann, J. Am. Chem. Soc. 65, 341 (1943).

(2) K. S. Pitzer, Science 101, 672 (1945).

(3) J. E. Kilpatrick, K. S. Pitzer and R. S. Spitzer, J. Am. Chem. Soc. 69, 2483 (1947).

(4) R. S. Spitzer and H. M. Huffmann, J. Am. Chem. Soc. 69, 211 (1947).

(5) J. P. McCullough, J. Chem. Phys. 29, 966 (1958); J. P. McCullough, R. E. Pennington, J. C. Smith, I. A. Hossenlopp and G. Waddington, J. Am. Chem. Soc. 81, 5880 (1959).

(6) K. S. Pitzer and W. E. Donath, J. Am. Chem. Soc. 81, 3213 (1959).

(7) J. B. Hendrickson, J. Am. Chem. Soc. 83, 4537 (1961); J. B. Hendrickson, J. Am. Chem. Soc. 85, 4059 (1963).

(8) S. Lifson and A. Warshel, J. Chem. Phys. 49, 5116 (1968).

(9) J. R. Durig and D. W. Wertz, J. Chem. Phys. 49, 2118 (1968).

(10) H. J. Geise, W. J. Adams and L. S. Bartell, Tetrahedron (in press); and PART II of this thesis.

(11) O. Hassell and H. Viervoll, Tidsskr. Bergv. 6, 31 (1946); O. Hassell and H. Viervoll, Acta Chem. Scand. 1, 149 (1947).

(12) A. Almenningen, O. Bastiansen and P. N. Skancke, Acta Chem. Scand. 15, 711 (1961).

(13) L. S. Bartell, K. Kuchitsu and R. J. de Neui, J. Chem. Phys. 35, 1211 (1961); L. S. Bartell in Physical Methods in Chemistry, A. Weissberger and B. W. Rossiter, Ed., 4th Ed., Interscience Publishers, New York (in press).

(14) L. S. Bartell and H. W. Higginbotham, J. Chem. Phys. 42, 851 (1965).

(15) J. Janzen (unpublished Ph.D. thesis, Iowa State University, Ames, Iowa, 1968).

(16) R. A. Bonham and L. S. Bartell, J. Chem. Phys. 31, 703 (1959).

(17) T. S. Strand and R. A. Bonham, J. Chem. Phys. 48, 1688 (1964).

(18) W. Heisenberg, Physik Z. 32, 737 (1931); L. Bewilogua, Physik Z. 32, 740 (1931).

(19) L. S. Bartell, L. O. Brockway and R. H. Schwendeman, J. Chem. Phys. 23, 1854 (1955).

(20) R. M. Gavin, Jr. and L. S. Bartell, J. Chem. Phys. 48, 2460 (1968).

(21) V. Schomaker and R. G. Glauber, Nature 170, 290 (1952); R. G. Glauber and V. Schomaker, Phys. Rev. 89, 667 (1953); J. A. Ibers and J. A. Hoerni, Acta Cryst. 7, 405 (1954).

(22) L. S. Bartell, J. Chem. Phys. 23, 1219 (1955); K. Kuchitsu and L. S. Bartell, J. Chem. Phys. 35, 1945 (1961).

(23) L. S. Bartell and L. O. Brockway, J. Chem. Phys. 32, 512 (1960).

(24) H. L. Cox, Jr. and R. A. Bonham, J. Chem. Phys. 47, 2599 (1967).

(25) C. Tavard, D. Nicolas and M. Rouault, J. Chem. Phys. 64, 540 (1967).

(26) D. R. Herschbach and V. W. Laurie, J. Chem. Phys. 35, 458 (1961); E. R. Lippincott and R. Schroeder, J. Chem. Phys. 23, 1131 (1955).

(27) L. S. Bartell, D. A. Kohl, B. L. Carroll and R. M. Gavin, Jr., J. Chem. Phys. 42, 3079 (1965); T. L. Boates and L. S. Bartell, to be published.

(28) L. S. Bartell in Physical Methods in Chemistry, A. Weissberger and B. W. Rossiter, Ed., 4th Ed., Interscience Publishers, New York (in press). The effects of systematic interactions implicit in Equation 27 of this reference were not taken into account.

(29) E. J. Jacob, H. B. Thompson and L. S. Bartell, J. Chem. Phys. 47, 3736 (1967).

(30) J. H. Schachtschneider and R. G. Snyder, Spectrochim. Acta 19, 117 (1963).

(31) L. S. Bartell, J. Chem. Phys. 32, 827 (1960).

(32) S. J. Cyvin, Molecular Vibrations and Mean Square Amplitudes, Elsevier Publishing Co., Amsterdam, 1968, p. 89.

(33) R. A. Bonham, L. S. Bartell and D. A. Kohl, J. Am. Chem. Soc. 81, 4765 (1959).

(34) A. Hirakawa and K. Kuchitsu, personal communication to L. S. Bartell, 1969.

(35) H. J. Geise, C. Altona and C. Romers, Tetrahedron Letters, 1383 (1967).

(36) C. Altona, H. J. Geise and C. Romers, Tetrahedron 24, 13 (1968).

(37) D. W. Scott, Symposium on Molecular Structure and Spectroscopy, Columbus, Ohio, June 1962.

(38) W. J. Lafferty, D. W. Robinson, R. V. St. Louis, J. W. Russell and H. L. Strauss, J. Chem. Phys. 50, 124 (1969).

(39) E. V. Iwash and D. M. Dennison, J. Chem. Phys. 21, 1804 (1953).

(40) J. P. McCullough, D. R. Douslin, W. H. Hubbard, S. S. Todd, J. F. Messerly, I. A. Hossenlopp, F. R. Frow, J. P. Dawson and G. Waddington, J. Am. Chem. Soc. 81, 5884 (1959); D. L. Hildenbrand, G. C. Sinke, R. A. McDonald, W. R. Kramer and D. R. Stull, J. Chem. Phys. 31, 650 (1959); J. C. Evans and J. C. Wahr, J. Chem. Phys. 31, 655 (1959).

(41) W. N. Hubbard, H. L. Fink, D. W. Scott, J. P. McCullough, K. Katz, M. E. Gross, J. F. Messerly, R. E. Pennington and G. Waddington, J. Am. Chem. Soc. 74, 6025 (1952).

(42) J. Y. Beach, J. Chem. Phys. 9, 54 (1941).

(43) R. A. Bonham and T. Ukaji, J. Chem. Phys. 36, 72 (1962).

(44) K. Kimura and M. Kubo, J. Chem. Phys. 30, 151 (1959).

(45) P. A. Kasai and R. J. Meyers, J. Chem. Phys. 30, 1096 (1959); P. A. Kasai and R. J. Meyers, J. Chem. Phys. 38, 2753 (1963).

(46) G. G. Engerholm, A. C. Luntz, W. D. Gwinn and D. O. Harris, J. Chem. Phys. 50, 2446 (1969).

(47) E. L. Eliel, N. L. Allinger, S. J. Angyal and G. A. Morrison, Conformational Analysis, Interscience Publishers, New York, 1965.

(48) I. S. Chan, J. Zinn and W. D. Gwinn, J. Chem. Phys. 34, 1319 (1961); P. Zabarbe, M. T. Forel and G. Bessis, Spectrochim. Acta 24A, 2165 (1968).

(49) L. S. Bartell, R. M. Gavin, Jr., H. B. Thompson and C. L. Chernick, J. Chem. Phys. 43, 2547 (1965).

(50) L. S. Bartell, J. Chem. Phys. 46, 4530 (1967).

(51) R. M. Gavin, Jr., and L. S. Bartell, J. Chem. Phys. 48, 2460 (1968).

(52) L. S. Bartell and R. M. Gavin, Jr., J. Chem. Phys. 48, 2466 (1968).

(53) K. Hedberg, S. H. Peterson and R. R. Ryan, J. Chem. Phys. 44, 1726 (1966).

(54) W. Harshbarber, B. K. Bohn and S. H. Bauer, J. Am. Chem. Soc. 89, 6466 (1967).

(55) R. J. Gillespie and R. S. Nyholm, Quart. Rev. (London) 11, 339 (1957); R. H. Gillespie, Noble Gas Compounds, University of Chicago Press, Chicago, 1963, p. 333.

(56) J. G. Malm, H. Selig and S. Fried, Quart. Rev. (London) 82, 1510 (1960).

(57) O. Glemser, H. W. Roesky, K. H. Hellberg and H. V. Werther, Chem. Ber. 99, 2652 (1966).

(58) R. J. Gillespie, Can. J. Chem. 38, 818 (1960).

(59) B. F. Gray and H. O. Pritchard, J. Chem. Phys. 25, 779 (1956).

(60) H. B. Thompson and L. S. Bartell, Inorg. Chem. 7, 488 (1968).

(61) T. A. Claxton and G. C. Benson, Can. J. Chem. 44, 157 (1966).

(62) H. H. Claassen, E. L. Gasner and H. Selig, J. Chem. Phys. 49, 1803 (1968).

(63) R. F. Pohler and H. P. Hansen, J. Chem. Phys. 42, 2347 (1965).

(64) O. Bastiansen and M. Traetteberg, Acta Cryst. 13, 1108 (1960); Y. Morino, Acta Cryst. 13, 1107 (1960); Y. Morino, S. J. Cyvin, K. Kuchitsu and T. Iijima, J. Chem. Phys. 36, 1109 (1962).

(65) E. Meisingseth and S. J. Cyvin, Acta Chem. Scand. 16, 2452 (1962); G. Nagarajan and E. R. Lippincott, J. Chem. Phys. 42, 1809 (1965).

(66) L. S. Bartell and B. L. Carroll, J. Chem. Phys. 42, 1135 (1965).

(67) R. M. Badger, J. Chem. Phys. 2, 128 (1934).

(68) G. Herzberg, Infrared and Raman Spectra of Polyatomic Molecules, D. Van Nostrand Co., Inc., Princeton, N. J., 1945.

(69) A. G. Robiette, private communication to L. S. Bartell, 1969.

(70) R. C. Lord, M. A. Lynch, Jr., W. C. Schumb and E. J. Slowinski, Jr., J. Am Chem. Soc. 72, 522 (1950).

(71) E. J. Jacob and L. S. Bartell, to be published.

(72) R. D. Burbank and F. N. Bensey, Jr., J. Chem. Phys. 27, 981 (1957); R. D. Burbank, Acta Cryst. 15, 1207 (1962).

(73) J. Donohue, J. Chem. Phys. 30, 1618 (1959); L. L. Lohr and W. N. Lipscomb, J. Chem. Phys. 36, 2225 (1962); J. Donohue, Acta Cryst. 18, 1018 (1965).

(74) W. Klemperer, private communication to L. S. Bartell.

(75) W. E. Falconer, A. Büchler, J. L. Stauffer and W. Klemperer, J. Chem. Phys. 48, 312 (1968).

(76) J. P. Guillory and L. S. Bartell, J. Chem. Phys. 43, 654 (1965).

(77) L. S. Bartell and J. P. Guillory, J. Chem. Phys. 43, 647 (1965).

(78) L. S. Bartell, J. P. Guillory and A. T. Parks, J. Phys. Chem. 69, 3043 (1965).

(79) L. Pauling, Nature of the Chemical Bond, 3rd Ed., Cornell University Press, Ithaca, N. Y., 1960, p. 137.

(80) R. Hoffmann, Tetrahedron Letters 43, 3819 (1965).

(81) R. W. Kilb, C. C. Lin and E. B. Wilson, Jr., J. Chem. Phys. 26, 1695 (1957).

(82) L. S. Bartell and R. A. Bonham, J. Chem. Phys. 32, 824 (1960).

(83) K. M. Sinnot, J. Chem. Phys. 34, 851 (1961).

(84) J. D. Dunitz and V. Schomaker, J. Chem. Phys. 20, 1703 (1952).

(85) A. Almenningen, O. Bastiansen and P. N. Skancke, Acta Chem. Scand. 15, 711 (1961).

(86) A. DeMeijere, Acta Chem. Scand. 20, 1093 (1965).

(87) H. Kim and W. D. Gwinn, J. Chem. Phys. 44, 865 (1966).

(88) W. G. Rothschild and B. P. Dailey, J. Chem. Phys. 36, 2931 (1962).

(89) T. N. Margulis and M. S. Fischer, J. Am. Chem. Soc. 89, 223 (1967).

(90) C. C. Lin and J. D. Swalen, Rev. Mod. Phys. 31, 841 (1959).

(91) A. D. Walsh, Nature 159, 165, 712 (1947); A. D. Walsh, Trans. Faraday Soc. 45, 179 (1949).

(92) R. J. Abraham and J. A. Pople, Mol. Phys. 3, 609 (1960); S. S. Butcher and E. B. Wilson, Jr., J. Chem. Phys. 40, 1671 (1964).

(93) A. M. Ronn and R. C. Woods III, J. Chem. Phys. 45, 3831 (1966).

(94) N. L. Allinger and H. M. Blatter, J. Am. Chem. Soc. 83, 994 (1961).

(95) K. W. Hansen and L. S. Bartell, Inorg. Chem. 4, 1775 (1965).

(96) F. B. Clippard, Jr. and L. S. Bartell, to be published.

(97) R. J. Gillespie, J. Chem. Educ. 40, 295 (1963); R. J. Gillespie, J. Am. Chem. Soc. 85, 4672 (1963); R. J. Gillespie, Inorg. Chem. 5, 1634 (1966).

(98) M. Rouault, Ann. Phys. 14, 78 (1940).

(99) Unpublished determination by Schomaker and Sargent, quoted in D. P. Stevenson and D. M. Yost, J. Chem. Phys. 9, 403 (1941).

(100) G. V. Romanov and V. P. Spiridonov, Zh. Strukt. Khim. 8, 131 (1967).

(101) A. Smith and R. H. Lombard, J. Am. Chem. Soc. 37, 2055 (1915).

(102) T. Kennedy, D. S. Payne, R. I. Reed and W. Snedden, Proc. Chem. Soc. 133 (1959).

(103) L. O. Brockway and J. Y. Beach, J. Am. Chem. Soc. 60, 1836 (1938); Q. Williams, J. Sheridan and W. Gordy, J. Chem. Phys. 20, 164 (1952); G. R. Badgley and R. L. Livingston, J. Am. Chem. Soc. 76, 261 (1954).

(104) L. V. Vilkov, L. S. Khaĭkin, A. F. Vasilév and T. F. Tuliakov, Zh. Strukt. Khim. 9, 1071 (1968).

(105) R. A. Bonham and J. L. Peacher, J. Chem. Phys. 38, 2319 (1963).

(106) J. Brunvoll, Acta Chem. Scand. 21, 473 (1967).

(107) K. Hedberg and M. Iwasaki, J. Chem. Phys. 36, 589 (1962).

(108) Y. Morino, K. Kuchitsu and T. Moritani, Inorg. Chem. 8, 867 (1969).

(109) P. C. Van Der Voorn, K. F. Purcell and R. S. Drago, J. Chem. Phys. 43, 3456 (1965). (Also see earlier work cited therein).

APPENDICES

APPENDIX A

Experimental Leveled Intensity and Background Intensity Functions for C_5H_{10} *

---

* Only data points for which background intensities, $I_B(s)$, are given were used in the structural analysis.

21 cm Camera Distance (r^3 Sector)

S	$I_0(S)$	$I_B(S)$	S	$I_0(S)$	$I_B(S)$	S	$I_0(S)$	$I_B(S)$	S	$I_0(S)$	$I_B(S)$
3.782	1.4619		8.354	1.9475	1.7902	12.891	1.9220	1.7930	17.252	1.8644	1.8202
3.906	1.4711		8.477	1.9732	1.7898	13.013	1.9407	1.7935	17.373	1.8659	1.8211
4.030	1.4797		8.601	1.9877	1.7894	13.134	1.9539	1.7940	17.493	1.8686	1.8220
4.154	1.4847		8.724	1.9898	1.7891	13.256	1.9601	1.7945	17.613	1.8703	1.8230
4.278	1.4922		8.847	1.9827	1.7889	13.378	1.9589	1.7950	17.733	1.8717	1.8239
4.401	1.5169		8.970	1.9663	1.7886	13.500	1.9501	1.7955	17.853	1.8712	1.8248
4.525	1.5386		9.093	1.9429	1.7884	13.622	1.9335	1.7961	17.973	1.8714	1.8258
4.649	1.5836		9.216	1.9150	1.7882	13.743	1.9110	1.7967	18.093	1.8692	1.8268
4.773	1.6543		9.339	1.8821	1.7881	13.865	1.8836	1.7973	18.213	1.8662	1.8278
4.897	1.7225		9.462	1.8474	1.7880	13.987	1.8524	1.7979	18.333	1.8614	1.8289
5.020	1.8012	1.8080	9.585	1.8124	1.7879	14.108	1.8188	1.7986	18.453	1.8563	1.8300
5.144	1.8834	1.8176	9.708	1.7776	1.7879	14.230	1.7881	1.7992	18.572	1.8486	1.8311
5.268	1.9662	1.8265	9.830	1.7462	1.7879	14.351	1.7582	1.7999	18.692	1.8392	1.8322
5.391	2.0492	1.8344	9.953	1.7175	1.7880	14.473	1.7330	1.8006	18.812	1.8290	1.8334
5.515	2.1188	1.8411	10.076	1.6930	1.7880	14.594	1.7119	1.8013	18.931	1.8186	1.8346
5.639	2.1670	1.8463	10.199	1.6722	1.7880	14.715	1.6960	1.8021	19.051	1.8083	1.8359
5.762	2.1941	1.8483	10.321	1.6590	1.7880	14.837	1.6870	1.8028	19.170	1.7973	1.8372
5.886	2.2019	1.8484	10.444	1.6506	1.7880	14.958	1.6828	1.8036	19.289	1.7890	1.8385
6.010	2.1796	1.8470	10.567	1.6471	1.7880	15.079	1.6841	1.8044	19.409	1.7822	1.8399
6.133	2.1334	1.8444	10.689	1.6491	1.7880	15.200	1.6905	1.8052	19.528	1.7780	1.8413
6.257	2.0635	1.8407	10.812	1.6553	1.7880	15.321	1.7006	1.8061	19.647	1.7765	1.8427
6.380	1.9787	1.8357	10.935	1.6642	1.7880	15.442	1.7139	1.8070	19.766	1.7786	1.8442
6.504	1.8855	1.8300	11.057	1.6745	1.7881	15.563	1.7274	1.8079	19.886	1.7834	1.8457
6.627	1.7921	1.8239	11.180	1.6863	1.7882	15.684	1.7428	1.8087	20.005	1.7920	1.8472
6.751	1.7035	1.8177	11.302	1.6981	1.7883	15.805	1.7583	1.8096	20.124	1.8043	1.8487
6.874	1.6312	1.8118	11.424	1.7099	1.7885	15.926	1.7736	1.8104	20.242	1.8182	1.8503
6.998	1.5764	1.8074	11.547	1.7221	1.7888	16.047	1.7883	1.8112	20.361	1.8345	1.8519
7.121	1.5443	1.8039	11.669	1.7328	1.7890	16.168	1.8024	1.8120	20.480	1.8493	1.8536
7.245	1.5352	1.8010	11.792	1.7444	1.7894	16.288	1.8137	1.8129	20.599	1.8641	1.8552
7.368	1.5477	1.7985	11.914	1.7579	1.7897	16.409	1.8244	1.8138	20.718	1.8774	
7.491	1.5802	1.7965	12.036	1.7715	1.7901	16.530	1.8339	1.8147	20.836	1.8891	
7.615	1.6274	1.7949	12.158	1.7882	1.7905	16.650	1.8401	1.8156	20.955	1.8991	
7.738	1.6837	1.7936	12.280	1.8074	1.7909	16.771	1.8476	1.8166	21.073	1.9085	
7.861	1.7439	1.7926	12.403	1.8290	1.7913	16.891	1.8524	1.8175	21.192	1.9146	
7.985	1.8046	1.7918	12.525	1.8522	1.7917	17.012	1.8565	1.8185	21.310	1.9176	
8.108	1.8614	1.7912	12.647	1.8767	1.7922	17.132	1.8610	1.8193	21.428	1.9184	
8.231	1.9093	1.7907	12.769	1.9012	1.7926						

11 cm Camera Distance (r^3 Sector)

S	$I_0(S)$	$I_B(S)$	S	$I_0(S)$	$I_B(S)$	S	$I_0(S)$	$I_B(S)$	S	$I_0(S)$	$I_B(S)$
7.620	3.2714		15.952	3.3709	3.4405	24.060	3.4433	3.4897	31.847	3.5881	3.6049
7.854	3.4950		16.181	3.4197	3.4389	24.281	3.4548	3.4807	32.058	3.5961	3.6114
8.087	3.7002		16.409	3.4610	3.4375	24.501	3.4662	3.4698	32.268	3.6067	3.6180
8.320	3.8630		16.638	3.4896	3.4364	24.722	3.4767	3.4590	32.479	3.6175	3.6246
8.554	3.9238		16.866	3.5091	3.4354	24.942	3.4845	3.4545	32.689	3.6294	3.6313
8.787	3.9418		17.094	3.5222	3.4346	25.162	3.4959	3.4559	32.898	3.6437	3.6381
9.020	3.8497		17.322	3.5277	3.4339	25.382	3.5042	3.4591	33.108	3.6574	3.6449
9.253	3.7829		17.548	3.5331	3.4332	25.602	3.5101	3.4636	33.317	3.6684	3.6517
9.485	3.6481		17.777	3.5348	3.4325	25.821	3.5130	3.4681	33.526	3.6788	3.6586
9.718	3.5091		18.004	3.5282	3.4320	26.040	3.5115	3.4714	33.734	3.6867	3.6654
9.951	3.3853	3.5458	18.231	3.5146	3.4315	26.258	3.5024	3.4748	33.942	3.6934	3.6724
10.183	3.2898	3.5401	18.458	3.4881	3.4311	26.477	3.4898	3.4783	34.150	3.6949	3.6793
10.416	3.2391	3.5343	18.685	3.4521	3.4307	26.695	3.4708	3.4820	34.357	3.6976	3.6864
10.648	3.2369	3.5284	18.911	3.4075	3.4303	26.913	3.4555	3.4857	34.565	3.6999	3.6935
10.880	3.2483	3.5226	19.137	3.3619	3.4300	27.131	3.4395	3.4896	34.772	3.6984	3.7006
11.112	3.2835	3.5167	19.363	3.3247	3.4297	27.348	3.4341	3.4935	34.978	3.6999	
11.344	3.3266	3.5108	19.589	3.3054	3.4294	27.565	3.4349	3.4976	35.184	3.7033	
11.576	3.3688	3.5051	19.815	3.3075	3.4291	27.782	3.4449	3.5018	35.390	3.7072	
11.807	3.4092	3.4995	20.040	3.3343	3.4289	27.998	3.4628	3.5062	35.596	3.7148	
12.039	3.4558	3.4940	20.266	3.3763	3.4289	28.215	3.4856	3.5106	35.801	3.7241	
12.270	3.5176	3.4887	20.491	3.4294	3.4289	28.431	3.5102	3.5152	36.006	3.7336	
12.501	3.5997	3.4837	20.715	3.4797	3.4290	28.646	3.5326	3.5199	36.210	3.7477	
12.733	3.6850	3.4790	20.940	3.5154	3.4292	28.862	3.5553	3.5247	36.415	3.7593	
12.964	3.7594	3.4745	21.164	3.5358	3.4296	29.077	3.5679	3.5296	36.619	3.7705	
13.194	3.8024	3.4704	21.388	3.5316	3.4300	29.292	3.5777	3.5347	36.822	3.7828	
13.425	3.7970	3.4665	21.612	3.5108	3.4306	29.506	3.5793	3.5399	37.025	3.7934	
13.656	3.7321	3.4629	21.836	3.4775	3.4313	29.720	3.5793	3.5452	37.228	3.8049	
13.886	3.6251	3.4596	22.059	3.4435	3.4316	29.934	3.5752	3.5506	37.431	3.8162	
14.116	3.4948	3.4565	22.283	3.4069	3.4308	30.148	3.5700	3.5562	37.633	3.8280	
14.346	3.3743	3.4538	22.506	3.3857	3.4311	30.361	3.5675	3.5619	37.835	3.8385	
14.576	3.2756	3.4514	22.728	3.3728	3.4330	30.574	3.5647	3.5677	38.037	3.8483	
14.806	3.2204	3.4493	22.951	3.3708	3.4378	30.787	3.5633	3.5736	38.238	3.8562	
15.035	3.2018	3.4474	23.173	3.3791	3.4524	31.000	3.5656	3.5797	38.439	3.8632	
15.265	3.2153	3.4457	23.395	3.3939	3.4678	31.212	3.5687	3.5859	38.639	3.8698	
15.494	3.2620	3.4440	23.617	3.4094	3.4820	31.424	3.5734	3.5921	38.839	3.8779	
15.723	3.3172	3.4422	23.838	3.4276	3.4931	31.635	3.5774	3.5985	39.039	3.8886	

6.5 cm Camera Distance (r^3 Sector)

S	$I_0(S)$	$I_B(S)$	S	$I_0(S)$	$I_B(S)$	S	$I_0(S)$	$I_B(S)$	S	$I_0(S)$
20.232	4.5701		32.029	4.4289	4.4517	42.614	4.4413	4.4392	52.231	4.6775
20.612	4.6739		32.384	4.4339	4.4480	42.940	4.4403	4.4428	52.524	4.6917
20.991	4.7451		32.739	4.4441	4.4445	43.264	4.4419	4.4467	52.817	4.7047
21.369	4.7452		33.093	4.4526	4.4412	43.588	4.4450	4.4509	53.108	4.7153
21.747	4.6872		33.445	4.4626	4.4381	43.911	4.4498	4.4554	53.398	4.7278
22.124	4.5882	4.5845	33.797	4.4644	4.4352	44.233	4.4560	4.4601	53.687	4.7410
22.501	4.5224	4.5799	34.148	4.4553	4.4324	44.553	4.4626	4.4651	53.976	4.7554
22.876	4.4874	4.5750	34.498	4.4384	4.4299	44.873	4.4713	4.4704	54.263	4.7674
23.252	4.4972	4.5700	34.847	4.4226	4.4276	45.191	4.4803	4.4760	54.549	4.7804
23.626	4.5195	4.5648	35.196	4.4064	4.4255	45.509	4.4878	4.4819	54.834	4.7930
24.000	4.5469	4.5595	35.543	4.4003	4.4235	45.826	4.4930	4.4880	55.118	4.8085
24.373	4.5673	4.5541	35.889	4.4026	4.4218	46.141	4.5005	4.4944	55.401	4.8230
24.745	4.5748	4.5487	36.235	4.4098	4.4204	46.455	4.5063	4.5011	55.682	4.8374
25.117	4.5897	4.5432	36.579	4.4193	4.4191	46.769	4.5102	4.5081	55.963	4.8501
25.488	4.5946	4.5378	36.923	4.4264	4.4181	47.081	4.5144	4.5154	56.243	4.8652
25.858	4.5894	4.5324	37.265	4.4310	4.4173	47.393	4.5228	4.5229	56.522	4.8815
26.227	4.5646	4.5271	37.607	4.4314	4.4167	47.703	4.5292	4.5307	56.799	4.8976
26.596	4.5193	4.5217	37.948	4.4292	4.4164	48.012	4.5366	4.5387	57.076	4.9129
26.964	4.4696	4.5165	38.287	4.4236	4.4163	48.320	4.5448	4.5471	57.351	4.9290
27.331	4.4346	4.5113	38.626	4.4185	4.4165	48.627	4.5534	4.5557	57.626	4.9444
27.697	4.4278	4.5061	38.964	4.4112	4.4170	48.933	4.5641	4.5646	57.899	4.9602
28.063	4.4533	4.5010	39.301	4.4053	4.4177	49.239	4.5745	4.5739	58.172	4.9772
28.427	4.4925	4.4960	39.636	4.4048	4.4186	49.542	4.5863	4.5833	58.443	4.9928
28.791	4.5285	4.4911	39.971	4.4066	4.4199	49.845	4.5965	4.5930	58.713	5.0074
29.154	4.5426	4.4862	40.305	4.4128	4.4213	50.147	4.6038	4.6029	58.983	5.0231
29.517	4.5361	4.4814	40.638	4.4187	4.4231	50.448	4.6155	4.6128	59.251	5.0395
29.878	4.5154	4.4768	40.970	4.4262	4.4251	50.748	4.6242	4.6227	59.518	5.0556
30.239	4.4872	4.4722	41.301	4.4329	4.4274	51.047	4.6319	4.6329	59.784	5.0748
30.598	4.4628	4.4678	41.630	4.4377	4.4299	51.344	4.6422	4.6434	60.050	5.0963
30.957	4.4436	4.4636	41.959	4.4409	4.4328	51.641	4.6529	4.6542	60.314	5.1185
31.315	4.4326	4.4594	42.287	4.4417	4.4359	51.936	4.6657		60.577	5.1403
31.673	4.4274	4.4555								

APPENDIX B

Experimental Leveled Intensity and Background Intensity Functions for C_4H_8O*

*Only data points for which background intensities, $I_B(s)$, are given were used in the structural analysis.

21 cm Camera Distance (r^3 Sector)

S	$I_0(S)$	$I_B(S)$	S	$I_0(S)$	$I_B(S)$	S	$I_0(S)$	$I_B(S)$	S	$I_0(S)$	$I_B(S)$
3.472	1.3005		8.046	1.5417	1.6434	12.585	1.6149	1.6454	17.072	1.6882	1.6721
3.596	1.3119		8.169	1.5987	1.6433	12.709	1.6289	1.6457	17.192	1.6909	1.6732
3.720	1.3158		8.293	1.6531	1.6430	12.830	1.6454	1.6460	17.313	1.6928	1.6742
3.844	1.3201		8.416	1.7007	1.6428	12.952	1.6555	1.6464	17.433	1.6941	1.6753
3.968	1.3297		8.539	1.7408	1.6425	13.073	1.6588	1.6468	17.553	1.6947	1.6763
4.092	1.3405		8.662	1.7703	1.6423	13.195	1.7084	1.6470	17.673	1.6952	1.6774
4.216	1.3455		8.785	1.7893	1.6421	13.317	1.7289	1.6473	17.793	1.6958	1.6784
4.339	1.3619		8.907	1.7977	1.6420	13.439	1.7461	1.6485	17.913	1.6983	1.6794
4.463	1.3758		9.031	1.7964	1.6419	13.561	1.7592	1.6490	18.033	1.7001	1.6804
4.587	1.4137		9.154	1.7860	1.6418	13.682	1.7677	1.6499	18.153	1.7022	1.6814
4.711	1.4520		9.277	1.7700	1.6417	13.804	1.7707	1.6507	18.273	1.7065	1.6824
4.835	1.5131		9.400	1.7494	1.6417	13.926	1.7674	1.6513	18.393	1.7095	1.6834
4.959	1.5750		9.523	1.7250	1.6416	14.047	1.7577	1.6520	18.513	1.7121	1.6844
5.082	1.6443	1.6423	9.646	1.6991	1.6415	14.169	1.7431	1.6526	18.632	1.7132	1.6854
5.206	1.7200	1.6579	9.769	1.6737	1.6414	14.290	1.7253	1.6532	18.752	1.7147	1.6864
5.330	1.7975	1.6550	9.892	1.6506	1.6414	14.412	1.7031	1.6539	18.871	1.7155	1.6874
5.453	1.8678	1.6705	10.015	1.6324	1.6413	14.533	1.6802	1.6546	18.991	1.7137	1.6885
5.577	1.9376	1.6776	10.137	1.6111	1.6413	14.655	1.6657	1.6553	19.110	1.7114	1.6895
5.701	1.9977	1.6806	10.260	1.5960	1.6414	14.776	1.6337	1.6561	19.230	1.7072	1.6905
5.824	2.0237	1.6810	10.383	1.5868	1.6415	14.897	1.6131	1.6568	19.349	1.7011	1.6917
5.948	2.0405	1.6804	10.505	1.5784	1.6416	15.018	1.5967	1.6576	19.468	1.6942	1.6927
6.071	2.0314	1.6785	10.628	1.5765	1.6417	15.140	1.5838	1.6584	19.588	1.6868	1.6937
6.195	2.0009	1.6756	10.751	1.5775	1.6417	15.261	1.5757	1.6591	19.707	1.6795	1.6946
6.319	1.9477	1.6720	10.873	1.5815	1.6418	15.382	1.5717	1.6599	19.826	1.6720	1.6956
6.442	1.8772	1.6679	10.996	1.5854	1.6419	15.503	1.5711	1.6607	19.945	1.6650	1.6965
6.566	1.7958	1.6636	11.119	1.5903	1.6419	15.624	1.5745	1.6615	20.064	1.6600	1.6975
6.689	1.7068	1.6591	11.241	1.5951	1.6420	15.745	1.5820	1.6622	20.183	1.6576	1.6985
6.813	1.6181	1.6548	11.363	1.5990	1.6422	15.866	1.5918	1.6630	20.302	1.6575	1.6996
6.936	1.5360	1.6512	11.486	1.6011	1.6423	15.986	1.6034	1.6639	20.421	1.6591	1.7007
7.060	1.4690	1.6491	11.608	1.6018	1.6425	16.107	1.6161	1.6647	20.539	1.6617	1.7018
7.183	1.4152	1.6474	11.730	1.6015	1.6427	16.228	1.6288	1.6655	20.658	1.6650	1.7030
7.306	1.3715	1.6461	11.853	1.5997	1.6429	16.349	1.6400	1.6664	20.777	1.6714	
7.430	1.3536	1.6459	11.975	1.5976	1.6432	16.469	1.6536	1.6673	20.895	1.6795	
7.553	1.3761	1.6445	12.097	1.5956	1.6436	16.590	1.6639	1.6682	21.014	1.6892	
7.676	1.3997	1.6440	12.219	1.5955	1.6440	16.710	1.6718	1.6691	21.132	1.6999	
7.800	1.4390	1.6437	12.341	1.5987	1.6445	16.831	1.6785	1.6701	21.251	1.7096	
7.923	1.4966	1.6435	12.464	1.6055	1.6449	16.951	1.6848	1.6711	21.369	1.7198	

11 cm Camera Distance (r^3 Sector)

S	$I_0(S)$	$I_B(S)$	S	$I_0(S)$	$I_B(S)$	S	$I_0(S)$	$I_B(S)$	S	$I_0(S)$	$I_B(S)$
7.679	2.8734		16.009	3.1151	3.2295	24.115	3.2476	3.2426	31.899	3.3811	3.3722
7.912	3.0328		16.238	3.1572	3.2283	24.336	3.2549	3.2448	32.110	3.3999	3.3941
8.145	3.2159		16.466	3.1998	3.2272	24.557	3.2589	3.2472	32.321	3.3980	3.3992
8.379	3.4124		16.695	3.2335	3.2262	24.777	3.2585	3.2496	32.531	3.4024	3.3945
8.612	3.5190		16.923	3.2529	3.2254	24.997	3.2575	3.2521	32.741	3.4079	3.3999
8.845	3.6134		17.151	3.2635	3.2246	25.217	3.2523	3.2547	32.951	3.4089	3.4053
9.078	3.6019		17.379	3.2650	3.2239	25.437	3.2494	3.2574	33.160	3.4122	3.4107
9.311	3.5596		17.606	3.2650	3.2233	25.656	3.2480	3.2602	33.369	3.4156	3.4152
9.544	3.4705		17.834	3.2677	3.2227	25.876	3.2516	3.2630	33.578	3.4177	3.4217
9.776	3.3695	3.3126	18.061	3.2706	3.2223	26.095	3.2572	3.2660	33.786	3.4203	3.4273
10.009	3.2807	3.3078	18.288	3.2737	3.2219	26.313	3.2679	3.2690	33.994	3.4246	3.4329
10.241	3.2176	3.3032	18.515	3.2757	3.2216	26.532	3.2751	3.2722	34.202	3.4317	3.4375
10.474	3.1730	3.2987	18.741	3.2787	3.2214	26.750	3.2831	3.2754	34.409	3.4378	3.4442
10.706	3.1687	3.2943	18.968	3.2826	3.2212	26.967	3.2906	3.2787	34.616	3.4466	3.4499
10.938	3.1731	3.2899	19.194	3.2883	3.2211	27.185	3.2937	3.2820	34.823	3.4526	
11.170	3.1878	3.2858	19.420	3.2421	3.2210	27.402	3.2953	3.2855	35.030	3.4584	
11.402	3.1995	3.2817	19.646	3.2097	3.2210	27.619	3.2919	3.2891	35.236	3.4665	
11.634	3.2003	3.2779	19.871	3.1795	3.2211	27.836	3.2894	3.2927	35.442	3.4736	
11.865	3.1908	3.2741	20.097	3.1551	3.2213	28.053	3.2873	3.2965	35.647	3.4813	
12.097	3.1797	3.2704	20.322	3.1412	3.2216	28.269	3.2882	3.3003	35.852	3.4864	
12.328	3.1801	3.2669	20.547	3.1430	3.2219	28.485	3.2918	3.3043	36.057	3.4947	
12.559	3.2040	3.2635	20.772	3.1565	3.2224	28.700	3.2992	3.3083	36.262	3.5026	
12.790	3.2506	3.2603	20.996	3.1802	3.2230	28.916	3.3086	3.3125	36.466	3.5115	
13.021	3.3147	3.2572	21.220	3.2116	3.2237	29.131	3.3165	3.3167	36.670	3.5196	
13.252	3.3921	3.2542	21.444	3.2390	3.2244	29.345	3.3249	3.3211	36.873	3.5266	
13.483	3.4550	3.2514	21.668	3.2604	3.2253	29.560	3.3303	3.3255	37.076	3.5356	
13.713	3.4840	3.2487	21.892	3.2719	3.2263	29.774	3.3375	3.3300	37.279	3.5414	
13.944	3.4737	3.2461	22.115	3.2709	3.2274	29.988	3.3394	3.3346	37.482	3.5492	
14.174	3.4235	3.2437	22.338	3.2634	3.2287	30.201	3.3421	3.3392	37.684	3.5595	
14.404	3.3439	3.2415	22.561	3.2519	3.2300	30.415	3.3425	3.3439	37.885	3.5696	
14.634	3.2515	3.2394	22.784	3.2365	3.2315	30.628	3.3441	3.3487	38.087	3.5765	
14.863	3.1640	3.2374	23.006	3.2243	3.2331	30.840	3.3470	3.3536	38.288	3.5819	
15.093	3.0971	3.2355	23.229	3.2199	3.2348	31.053	3.3500	3.3585	38.489	3.5860	
15.322	3.0582	3.2338	23.451	3.2207	3.2366	31.265	3.3555	3.3635	38.689	3.5927	
15.551	3.0556	3.2322	23.672	3.2268	3.2385	31.477	3.3631	3.3686	38.890	3.6032	
15.780	3.0762	3.2308	23.894	3.2368	3.2405	31.688	3.3706	3.3736	39.089	3.6128	

6.5 cm Camera Distance (r^3 Sector)

S	$I_0(S)$	$I_B(S)$	S	$I_0(S)$	$I_B(S)$	S	$I_0(S)$	$I_B(S)$	S	$I_0(S)$
20.232	7.7527		32.029	7.5307	7.5977	42.614	7.4022	7.4055	52.231	7.6323
20.612	7.7333		32.384	7.5411	7.5157	42.940	7.3941	7.4075	52.524	7.6509
20.991	7.7973	7.8897	32.739	7.5299	7.5100	43.264	7.3990	7.4099	52.817	7.6631
21.369	7.8859	7.8734	33.093	7.5090	7.5016	43.588	7.4021	7.4127	53.108	7.6736
21.747	7.8617	7.8585	33.445	7.4910	7.4935	43.911	7.4053	7.4159	53.398	7.6899
22.124	7.8465	7.8441	33.797	7.4746	7.4857	44.233	7.4147	7.4195	53.688	7.7051
22.501	7.8940	7.8300	34.148	7.4599	7.4783	44.553	7.4242	7.4235	53.976	7.7193
22.877	7.8136	7.8163	34.498	7.4502	7.4712	44.873	7.4344	7.4280	54.263	7.7309
23.252	7.7988	7.8030	34.848	7.4501	7.4645	45.192	7.4458	7.4328	54.549	7.7440
23.626	7.7472	7.7900	35.196	7.4529	7.4583	45.509	7.4484	7.4381	54.834	7.7579
24.000	7.7584	7.7773	35.543	7.4471	7.4524	45.825	7.4543	7.4440	55.118	7.7692
24.373	7.7332	7.7649	35.889	7.4445	7.4469	46.141	7.4578	7.4502	55.401	7.7855
24.745	7.7649	7.7524	36.235	7.4421	7.4415	46.456	7.4586	7.4569	55.682	7.8007
25.117	7.7386	7.7402	36.579	7.4427	7.4364	46.769	7.4569	7.4640	55.963	7.8159
25.488	7.6984	7.7279	36.923	7.4480	7.4315	47.081	7.4549	7.4715	56.243	7.8320
25.858	7.6864	7.7157	37.265	7.4437	7.4271	47.393	7.4765	7.4793	56.522	7.8509
26.227	7.6876	7.7035	37.607	7.4378	7.4230	47.703	7.4907	7.4874	56.799	7.8700
26.596	7.7011	7.6914	37.949	7.4270	7.4191	48.012	7.4894	7.4959	57.076	7.8892
26.964	7.7082	7.6794	38.287	7.4122	7.4156	48.320	7.4985	7.5047	57.351	7.9044
27.331	7.6893	7.6674	38.626	7.4035	7.4125	48.628	7.5123	7.5138	57.626	7.9195
27.697	7.6583	7.6555	38.964	7.3907	7.4097	48.934	7.5222	7.5231	57.899	7.9390
28.063	7.6275	7.6437	39.301	7.3907	7.4073	49.239	7.5358	7.5327	58.172	7.9523
28.427	7.6047	7.6320	39.637	7.3934	7.4054	49.543	7.5474	7.5424	58.443	7.9691
28.791	7.6037	7.6205	39.971	7.3984	7.4039	49.846	7.5565	7.5524	58.714	7.9828
29.154	7.6147	7.6092	40.305	7.4058	7.4028	50.147	7.5659	7.5626	58.983	7.9994
29.517	7.6097	7.5981	40.638	7.4129	7.4021	50.448	7.5770	7.5730	59.251	8.0183
29.878	7.6083	7.5872	40.970	7.4127	7.4017	50.748	7.5848	7.5836	59.518	8.0367
30.239	7.5875	7.5767	41.301	7.4108	7.4017	51.047	7.5926	7.5943	59.785	8.0586
30.598	7.5601	7.5663	41.630	7.4136	7.4020	51.344	7.6016	7.6051	60.050	8.0833
30.957	7.5366	7.5563	41.959	7.4065	7.4029	51.641	7.6088	7.6161	60.314	8.1090
31.315	7.5328	7.5465	42.287	7.4050	7.4040	51.935	7.6282		60.577	8.1307
31.673	7.5359	7.5370								

APPENDIX C

Experimental Leveled Intensity and Background Intensity Functions for IF_7*

---

* Only data points for which background intensities, $I_B(s)$, are given were used in the structural analysis.

21 cm Camera Distance (r^2 Sector)

S	$I_0(S)$	$I_B(S)$	S	$I_0(S)$	$I_B(S)$	S	$I_0(S)$	$I_B(S)$	S	$I_0(S)$	$I_B(S)$
2.101	0.6094	0.9345	4.694	1.1390	1.0677	7.280	1.1915	1.1163	9.856	1.1146	1.1488
2.225	0.5704	0.9461	4.817	1.1034	1.0708	7.403	1.2175	1.1181	9.979	1.1215	1.1501
2.348	0.5641	0.9570	4.941	1.0777	1.0738	7.526	1.2335	1.1199	10.101	1.1315	1.1514
2.472	0.5788	0.9672	5.064	1.0554	1.0767	7.649	1.2403	1.1216	10.223	1.1422	1.1527
2.595	0.6133	0.9768	5.187	1.0417	1.0795	7.772	1.2384	1.1234	10.346	1.1566	1.1541
2.719	0.6647	0.9856	5.310	1.0304	1.0822	7.895	1.2295	1.1251	10.468	1.1702	1.1554
2.842	0.7291	0.9939	5.434	1.0229	1.0849	8.017	1.2140	1.1267	10.590	1.1852	1.1567
2.966	0.8044	1.0017	5.557	1.0165	1.0874	8.140	1.1963	1.1284	10.712	1.1971	
3.089	0.8864	1.0088	5.680	1.0099	1.0899	8.263	1.1746	1.1300	10.834	1.2069	
3.213	0.9715	1.0155	5.803	1.0014	1.0923	8.386	1.1553	1.1317	10.957	1.2130	
3.336	1.0557	1.0216	5.927	0.9933	1.0947	8.508	1.1378	1.1332	11.079	1.2161	
3.460	1.1333	1.0273	6.050	0.9854	1.0970	8.631	1.1241	1.1348	11.201	1.2145	
3.583	1.2008	1.0326	6.173	0.9826	1.0992	8.754	1.1141	1.1363	11.323	1.2104	
3.707	1.2538	1.0375	6.296	0.9838	1.1013	8.876	1.1074	1.1378	11.445	1.2025	
3.830	1.2869	1.0421	6.419	0.9894	1.1033	8.999	1.1029	1.1392	11.567	1.1955	
3.954	1.3041	1.0464	6.542	1.0053	1.1053	9.122	1.1011	1.1407	11.689	1.1851	
4.077	1.3016	1.0505	6.665	1.0277	1.1072	9.244	1.1012	1.1421	11.810	1.1785	
4.200	1.2844	1.0543	6.788	1.0564	1.1091	9.367	1.1012	1.1434	11.932	1.1693	
4.324	1.2543	1.0580	6.911	1.0899	1.1109	9.489	1.1017	1.1448	12.054	1.1640	
4.447	1.2173	1.0614	7.034	1.1258	1.1127	9.612	1.1043	1.1462	12.176	1.1602	
4.571	1.1773	1.0646	7.157	1.1618	1.1145	9.734	1.1082	1.1475	12.298	1.1567	

21 cm Camera Distance (r^3 Sector)

S	$I_0(S)$	$I_B(S)$	S	$I_0(S)$	$I_B(S)$	S	$I_0(S)$	$I_B(S)$	S	$I_0(S)$	$I_B(S)$
3.215	2.1013		7.776	2.7503	2.5182	12.304	2.5414	2.5657	16.780	2.5939	2.5997
3.339	2.2860		7.899	2.7279	2.5215	12.426	2.5412	2.5659	16.900	2.5940	2.6015
3.462	2.4379		8.022	2.6942	2.5246	12.547	2.5402	2.5661	17.020	2.5965	2.6033
3.586	2.5797		8.145	2.6568	2.5276	12.669	2.5390	2.5663	17.140	2.5988	2.6052
3.709	2.7018		8.267	2.6152	2.5304	12.791	2.5389	2.5666	17.260	2.6016	2.6071
3.833	2.7576		8.390	2.5704	2.5331	12.912	2.5359	2.5670	17.380	2.6051	2.6090
3.956	2.8413		8.513	2.5345	2.5357	13.034	2.5359	2.5673	17.500	2.6088	2.6110
4.080	2.8032		8.636	2.5018	2.5382	13.155	2.5330	2.5677	17.620	2.6135	2.6130
4.203	2.7326		8.758	2.4815	2.5405	13.277	2.5301	2.5681	17.739	2.6183	2.6151
4.326	2.6505		8.881	2.4620	2.5427	13.398	2.5296	2.5685	17.859	2.6231	2.6172
4.450	2.6022		9.004	2.4513	2.5448	13.520	2.5292	2.5690	17.979	2.6247	2.6194
4.573	2.5286		9.126	2.4475	2.5468	13.641	2.5338	2.5694	18.098	2.6296	2.6217
4.697	2.4783		9.249	2.4444	2.5486	13.762	2.5398	2.5700	18.218	2.6306	2.6239
4.820	2.4370		9.372	2.4436	2.5504	13.883	2.5497	2.5706	18.337	2.6304	2.6263
4.943	2.4091	2.4054	9.494	2.4440	2.5519	14.005	2.5608	2.5712	18.457	2.6296	2.6287
5.067	2.3556	2.4119	9.617	2.4491	2.5534	14.126	2.5727	2.5718	18.576	2.6277	2.6311
5.190	2.3115	2.4182	9.739	2.4547	2.5547	14.247	2.5854	2.5726	18.695	2.6273	2.6337
5.313	2.3053	2.4243	9.862	2.4660	2.5559	14.368	2.5980	2.5734	18.815	2.6280	2.6362
5.437	2.2762	2.4303	9.984	2.4794	2.5570	14.489	2.6066	2.5743	18.934	2.6298	2.6389
5.560	2.2995	2.4362	10.106	2.4991	2.5580	14.610	2.6114	2.5753	19.053	2.6327	2.6416
5.683	2.2742	2.4419	10.229	2.5210	2.5589	14.731	2.6148	2.5762	19.172	2.6369	2.6443
5.807	2.2607	2.4475	10.351	2.5478	2.5598	14.852	2.6130	2.5772	19.291	2.6437	2.6472
5.930	2.2520	2.4529	10.473	2.5742	2.5605	14.973	2.6111	2.5783	19.410	2.6499	
6.053	2.2389	2.4582	10.596	2.5981	2.5612	15.094	2.6023	2.5794	19.529	2.6588	
6.176	2.2301	2.4633	10.718	2.6221	2.5618	15.214	2.5987	2.5806	19.648	2.6632	
6.299	2.2319	2.4684	10.840	2.6398	2.5624	15.335	2.5925	2.5818	19.767	2.6700	
6.423	2.2456	2.4733	10.962	2.6511	2.5629	15.456	2.5868	2.5830	19.885	2.6771	
6.546	2.2792	2.4780	11.084	2.6562	2.5633	15.576	2.5819	2.5843	20.004	2.6803	
6.669	2.3220	2.4827	11.207	2.6530	2.5637	15.697	2.5796	2.5857	20.123	2.6828	
6.792	2.3858	2.4871	11.329	2.6439	2.5640	15.818	2.5779	2.5871	20.241	2.6874	
6.915	2.4581	2.4915	11.451	2.6293	2.5643	15.938	2.5800	2.5885	20.360	2.6889	
7.038	2.5337	2.4957	11.573	2.6126	2.5646	16.058	2.5817	2.5899	20.478	2.6887	
7.161	2.6036	2.4998	11.695	2.5950	2.5648	16.179	2.5845	2.5915	20.596	2.6873	
7.284	2.6683	2.5038	11.817	2.5777	2.5650	16.299	2.5853	2.5930	20.715	2.6876	
7.407	2.7158	2.5076	11.938	2.5647	2.5652	16.420	2.5889	2.5946	20.833	2.6883	
7.530	2.7518	2.5113	12.060	2.5533	2.5654	16.540	2.5906	2.5963	20.951	2.6894	
7.653	2.7616	2.5148	12.182	2.5454	2.5655	16.660	2.5923	2.5980	21.069	2.6923	

11 cm Camera Distance (r^3 Sector)

S	$I_0(S)$	$I_B(S)$	S	$I_0(S)$	$I_B(S)$	S	$I_0(S)$	$I_B(S)$	S	$I_0(S)$	$I_B(S)$
8.430	3.4714	3.5339	16.737	3.6769	3.6868	24.591	3.7165	3.7501	32.136	3.8834	3.8918
8.663	3.4388	3.5446	16.965	3.6751	3.6881	24.811	3.7206	3.7527	32.347	3.8984	3.8974
8.896	3.4263	3.5548	17.193	3.6754	3.6895	25.031	3.7278	3.7554	32.557	3.9093	3.9031
9.129	3.4212	3.5645	17.421	3.6836	3.6909	25.251	3.7398	3.7582	32.766	3.9201	3.9089
9.361	3.4261	3.5738	17.648	3.6937	3.6923	25.470	3.7554	3.7612	32.976	3.9297	3.9148
9.594	3.4417	3.5825	17.875	3.7009	3.6938	25.689	3.7693	3.7642	33.185	3.9383	3.9209
9.826	3.4640	3.5908	18.102	3.7047	3.6952	25.908	3.7855	3.7674	33.394	3.9429	3.9271
10.059	3.4905	3.5986	18.329	3.7028	3.6967	26.127	3.7976	3.7706	33.602	3.9445	3.9334
10.291	3.5740	3.6059	18.555	3.6967	3.6982	26.345	3.8053	3.7739	33.810	3.9435	3.9398
10.523	3.6391	3.6127	18.782	3.6932	3.6997	26.564	3.8073	3.7774	34.018	3.9451	3.9464
10.755	3.6918	3.6191	19.008	3.6941	3.7013	26.781	3.8051	3.7809	34.226	3.9463	3.9530
10.987	3.7290	3.6250	19.234	3.7000	3.7029	26.999	3.8016	3.7845	34.433	3.9471	3.9596
11.219	3.7351	3.6303	19.460	3.7097	3.7045	27.216	3.7931	3.7882	34.640	3.9490	3.9663
11.450	3.7211	3.6351	19.685	3.7214	3.7062	27.433	3.7845	3.7920	34.846	3.9533	3.9729
11.682	3.6898	3.6395	19.911	3.7287	3.7078	27.650	3.7764	3.7959	35.053	3.9616	3.9797
11.913	3.6603	3.6436	20.136	3.7277	3.7095	27.867	3.7728	3.7999	35.258	3.9705	3.9865
12.144	3.6421	3.6473	20.361	3.7220	3.7112	28.083	3.7761	3.8039	35.464	3.9830	3.9935
12.375	3.6332	3.6507	20.585	3.7141	3.7130	28.299	3.7807	3.8080	35.669	3.9977	4.0006
12.606	3.6328	3.6538	20.810	3.7068	3.7147	28.515	3.7920	3.8121	35.874	4.0110	4.0078
12.837	3.6287	3.6567	21.034	3.6991	3.7165	28.730	3.8094	3.8163	36.079	4.0228	4.0153
13.068	3.6250	3.6594	21.258	3.6959	3.7183	28.945	3.8249	3.8205	36.283	4.0331	4.0229
13.298	3.6223	3.6619	21.482	3.6978	3.7202	29.160	3.8366	3.8248	36.487	4.0434	4.0307
13.529	3.6250	3.6641	21.706	3.7016	3.7221	29.374	3.8491	3.8292	36.691	4.0506	4.0387
13.759	3.6337	3.6662	21.929	3.7090	3.7240	29.589	3.8583	3.8336	36.894	4.0569	4.0470
13.989	3.6569	3.6682	22.152	3.7188	3.7259	29.803	3.8624	3.8381	37.097	4.0620	4.0555
14.219	3.6850	3.6701	22.375	3.7294	3.7278	30.016	3.8656	3.8426	37.300	4.0670	4.0643
14.449	3.7092	3.6719	22.598	3.7421	3.7298	30.230	3.8648	3.8471	37.502	4.0734	4.0733
14.678	3.7213	3.6737	22.820	3.7564	3.7318	30.443	3.8622	3.8516	37.704	4.0803	
14.908	3.7151	3.6753	23.042	3.7627	3.7339	30.655	3.8576	3.8563	37.905	4.0918	
15.137	3.7007	3.6769	23.264	3.7676	3.7361	30.868	3.8526	3.8610	38.107	4.0974	
15.366	3.6875	3.6784	23.486	3.7664	3.7382	31.080	3.8498	3.8658	38.308	4.1060	
15.595	3.6759	3.6799	23.707	3.7574	3.7405	31.292	3.8523	3.8708	38.508	4.1155	
15.824	3.6688	3.6813	23.929	3.7444	3.7428	31.503	3.8535	3.8758	38.708	4.1273	
16.053	3.6697	3.6827	24.150	3.7329	3.7451	31.715	3.8610	3.8810	38.908	4.1443	
16.281	3.6730	3.6841	24.370	3.7208	3.7476	31.926	3.8715	3.8864	39.108	4.1612	
16.509	3.6762	3.6855									

6.5 cm Camera Distance (r^3 Sector)

S	$I_0(S)$	$I_B(S)$	S	$I_0(S)$	$I_B(S)$	S	$I_0(S)$	$I_B(S)$	S	$I_0(S)$
18.715	5.4115		30.907	5.3832	5.4000	41.862	5.4518	5.4592	51.803	5.6853
19.095	5.4165		31.263	5.3701	5.4000	42.189	5.4618	5.4657	52.097	5.6931
19.475	5.4492		31.619	5.3662	5.4002	42.514	5.4716	5.4717	52.389	5.7038
19.854	5.4742		31.974	5.3824	5.4006	42.839	5.4816	5.4767	52.681	5.7150
20.232	5.4720		32.328	5.4013	5.4011	43.162	5.4907	5.4816	52.971	5.7249
20.610	5.4480		32.681	5.4156	5.4016	43.485	5.4961	5.4864	53.261	5.7371
20.987	5.4193		33.033	5.4260	5.4023	43.806	5.4951	5.4913	53.549	5.7492
21.364	5.4047	5.4405	33.384	5.4296	5.4030	44.127	5.4942	5.4964	53.836	5.7583
21.740	5.4033	5.4378	33.734	5.4184	5.4038	44.446	5.4971	5.5018	54.122	5.7676
22.115	5.4112	5.4351	34.084	5.4042	5.4046	44.765	5.4991	5.5074	54.408	5.7771
22.490	5.4413	5.4325	34.432	5.3913	5.4056	45.082	5.5058	5.5132	54.692	5.7927
22.864	5.4672	5.4299	34.780	5.3811	5.4065	45.398	5.5135	5.5192	54.975	5.8029
23.237	5.4768	5.4274	35.127	5.3849	5.4075	45.714	5.5238	5.5256	55.257	5.8173
23.610	5.4543	5.4250	35.472	5.3988	5.4086	46.028	5.5370	5.5324	55.538	5.8333
23.982	5.4164	5.4227	35.817	5.4133	5.4098	46.341	5.5463	5.5394	55.818	5.8468
24.353	5.3762	5.4205	36.161	5.4297	5.4111	46.654	5.5560	5.5466	56.097	5.8626
24.724	5.3622	5.4184	36.504	5.4354	5.4126	46.965	5.5633	5.5540	56.375	5.8754
25.094	5.3744	5.4164	36.846	5.4330	5.4142	47.275	5.5684	5.5616	56.652	5.8911
25.463	5.4021	5.4145	37.188	5.4281	5.4160	47.584	5.5688	5.5695	56.927	5.9059
25.831	5.4320	5.4126	37.528	5.4187	5.4180	47.892	5.5740	5.5774	57.202	5.9208
26.199	5.4540	5.4109	37.867	5.4094	5.4204	48.200	5.5801	5.5856	57.476	5.9312
26.566	5.4562	5.4093	38.205	5.4039	5.4232	48.506	5.5889	5.5938	57.749	5.9456
26.932	5.4350	5.4078	38.543	5.4033	5.4261	48.811	5.5980	5.6022	58.020	5.9606
27.297	5.4018	5.4064	38.879	5.4124	5.4290	49.115	5.6083	5.6107	58.291	5.9721
27.662	5.3712	5.4051	39.214	5.4270	5.4318	49.418	5.6183	5.6192	58.561	5.9856
28.026	5.3577	5.4040	39.549	5.4422	5.4334	49.719	5.6275	5.6278	58.829	5.9979
28.389	5.3700	5.4030	39.882	5.4540	5.4347	50.020	5.6404	5.6365	59.097	6.0127
28.751	5.3884	5.4022	40.215	5.4584	5.4364	50.320	5.6476	5.6452	59.363	6.0304
29.112	5.4146	5.4015	40.546	5.4575	5.4385	50.619	5.6547	5.6539	59.629	6.0456
29.473	5.4342	5.4009	40.877	5.4544	5.4414	50.917	5.6625	5.6627	59.893	6.0647
29.833	5.4384	5.4005	41.206	5.4504	5.4468	51.213	5.6675	5.6715	60.157	6.0805
30.192	5.4266	5.4002	41.535	5.4490	5.4528	51.509	5.6759		60.419	6.0977
30.550	5.4042	5.4000								

APPENDIX D

Experimental Leveled Intensity and Background Intensity Functions for C_4H_7CClO*

---

* Only data points for which background intensities, $I_B(s)$, are given were used in the structural analysis.

21 cm Camera Distance (r^2 Sector)

S	$I_0(S)$	$I_B(S)$	S	$I_0(S)$	$I_B(S)$	S	$I_0(S)$	$I_B(S)$	S	$I_0(S)$	$I_B(S)$
2.068	4.2206	4.3314	4.624	4.1823	4.1886	7.174	3.7682	3.9171	9.714	3.8522	3.8185
2.190	3.8981	4.3266	4.746	4.2639	4.1788	7.295	3.7953	3.9054	9.835	3.8330	3.8201
2.312	3.8037	4.3215	4.868	4.3345	4.1686	7.417	3.8307	3.8945	9.956	3.8098	3.8221
2.434	3.7852	4.3163	4.989	4.3854	4.1580	7.538	3.8672	3.8843	10.076	3.7850	3.8246
2.555	3.8032	4.3109	5.111	4.4291	4.1470	7.659	3.9028	3.8747	10.197	3.7647	3.8276
2.677	3.8839	4.3054	5.232	4.4524	4.1356	7.780	3.9299	3.8660	10.317	3.7478	3.8310
2.799	3.9321	4.2997	5.354	4.4725	4.1237	7.901	3.9461	3.8581	10.438	3.7385	3.8348
2.921	3.9813	4.2941	5.475	4.4726	4.1111	8.022	3.9462	3.8512	10.559	3.7326	3.8392
3.043	4.0125	4.2884	5.597	4.4604	4.0981	8.143	3.9312	3.8450	10.679	3.7328	3.8439
3.164	3.9928	4.2825	5.718	4.4343	4.0847	8.264	3.9082	3.8396	10.799	3.7374	
3.286	3.9696	4.2764	5.840	4.3828	4.0710	8.385	3.8749	3.8348	10.920	3.7452	
3.408	3.8961	4.2700	5.961	4.3153	4.0569	8.506	3.8440	3.8306	11.040	3.7566	
3.529	3.8270	4.2632	6.082	4.2407	4.0424	8.627	3.8206	3.8269	11.160	3.7706	
3.651	3.7716	4.2560	6.204	4.1571	4.0276	8.748	3.8087	3.8239	11.281	3.7867	
3.773	3.7335	4.2485	6.325	4.0679	4.0128	8.869	3.8042	3.8214	11.401	3.8098	
3.895	3.7391	4.2408	6.447	3.9795	3.9981	8.990	3.8097	3.8194	11.521	3.8381	
4.016	3.7593	4.2327	6.568	3.8998	3.9835	9.111	3.8267	3.8180	11.641	3.8730	
4.138	3.8169	4.2244	6.689	3.8338	3.9693	9.231	3.8433	3.8171	11.762	3.9105	
4.260	3.8928	4.2159	6.810	3.7908	3.9556	9.352	3.8556	3.8167	11.882	3.9543	
4.381	3.9931	4.2071	6.932	3.7620	3.9422	9.473	3.8643	3.8168	12.002	3.9956	
4.503	4.0914	4.1980	7.053	3.7582	3.9294	9.594	3.8627	3.8174	12.122	4.0373	

21 cm Camera Distance (r^3 Sector)

S	$I_0(S)$	$I_B(S)$	S	$I_0(S)$	$I_B(S)$	S	$I_0(S)$	$I_B(S)$	S	$I_0(S)$	$I_B(S)$
3.437	2.5844		8.081	3.0054	2.9382	12.569	3.0185	2.9010	17.004	2.9978	2.9451
3.559	2.5566		8.203	2.9911	2.9340	12.690	3.0090	2.9022	17.123	3.0073	2.9465
3.682	2.5354		8.325	2.9701	2.9300	12.810	2.9965	2.9033	17.242	3.0158	2.9479
3.804	2.5327		8.447	2.9478	2.9260	12.931	2.9787	2.9045	17.361	3.0199	2.9494
3.927	2.5604		8.568	2.9257	2.9223	13.051	2.9598	2.9057	17.480	3.0222	2.9509
4.049	2.6116		8.690	2.9122	2.9189	13.172	2.9419	2.9070	17.599	3.0218	2.9524
4.172	2.6693		8.812	2.9033	2.9156	13.292	2.9260	2.9082	17.718	3.0196	2.9541
4.294	2.7525		8.933	2.9037	2.9126	13.413	2.9131	2.9094	17.836	3.0155	2.9558
4.417	2.8225		9.055	2.9112	2.9097	13.533	2.9041	2.9106	17.955	3.0118	2.9575
4.539	2.9249		9.177	2.9218	2.9070	13.653	2.8985	2.9118	18.073	3.0072	2.9594
4.661	3.0147		9.298	2.9301	2.9045	13.774	2.8966	2.9130	18.192	3.0008	2.9613
4.784	3.0870	2.9894	9.420	2.9357	2.9023	13.894	2.8946	2.9142	18.310	2.9930	2.9633
4.906	3.1424	2.9928	9.541	2.9350	2.9005	14.014	2.8956	2.9154	18.429	2.9850	2.9653
5.028	3.1894	2.9955	9.663	2.9272	2.8989	14.134	2.8953	2.9166	18.547	2.9752	2.9675
5.151	3.2261	2.9977	9.784	2.9116	2.8976	14.254	2.8980	2.9178	18.665	2.9649	2.9697
5.273	3.2569	2.9993	9.906	2.8924	2.8964	14.375	2.9001	2.9189	18.784	2.9557	2.9720
5.395	3.2628	3.0004	10.027	2.8706	2.8954	14.495	2.9000	2.9201	18.902	2.9476	2.9744
5.518	3.2727	3.0010	10.149	2.8483	2.8946	14.615	2.8987	2.9213	19.020	2.9401	2.9769
5.640	3.2635	3.0011	10.270	2.8327	2.8940	14.734	2.9009	2.9224	19.138	2.9343	2.9795
5.762	3.2487	3.0007	10.391	2.8182	2.8934	14.854	2.9017	2.9236	19.256	2.9307	2.9821
5.884	3.2195	2.9998	10.512	2.8096	2.8928	14.974	2.9002	2.9247	19.374	2.9299	2.9849
6.007	3.1797	2.9984	10.634	2.8052	2.8924	15.094	2.8992	2.9258	19.492	2.9304	2.9877
6.129	3.1302	2.9967	10.755	2.8042	2.8921	15.214	2.8958	2.9269	19.610	2.9337	2.9907
6.251	3.0720	2.9947	10.876	2.8047	2.8919	15.333	2.8901	2.9280	19.727	2.9368	2.9937
6.373	3.0108	2.9922	10.997	2.8072	2.8919	15.453	2.8851	2.9291	19.845	2.9448	2.9968
6.495	2.9553	2.9895	11.118	2.8134	2.8920	15.573	2.8794	2.9302	19.963	2.9515	3.0000
6.617	2.9038	2.9865	11.239	2.8200	2.8921	15.692	2.8743	2.9313	20.080	2.9609	3.0033
6.740	2.8670	2.9832	11.360	2.8325	2.8925	15.812	2.8732	2.9324	20.198	2.9695	
6.862	2.8441	2.9797	11.482	2.8476	2.8930	15.931	2.8733	2.9335	20.315	2.9798	
6.984	2.8380	2.9760	11.602	2.8681	2.8936	16.051	2.8766	2.9347	20.433	2.9877	
7.106	2.8421	2.9721	11.723	2.8922	2.8943	16.170	2.8842	2.9359	20.550	2.9945	
7.228	2.8624	2.9681	11.844	2.9188	2.8950	16.290	2.8968	2.9371	20.668	3.0058	
7.350	2.8919	2.9639	11.965	2.9476	2.8959	16.409	2.9126	2.9384	20.785	3.0177	
7.472	2.9256	2.9597	12.086	2.9717	2.8968	16.528	2.9312	2.9397	20.902	3.0297	
7.594	2.9564	2.9554	12.207	2.9941	2.8978	16.647	2.9482	2.9410	21.019	3.0420	
7.716	2.9848	2.9511	12.328	3.0108	2.8988	16.766	2.9673	2.9423	21.136	3.0542	
7.837	3.0027	2.9468	12.448	3.0185	2.8999	16.885	2.9846	2.9437	21.253	3.0646	
7.959	3.0090	2.9425									

11 cm Camera Distance (r^3 Sector)

S	$I_0(S)$	$I_B(S)$	S	$I_0(S)$	$I_B(S)$	S	$I_0(S)$	$I_B(S)$	S	$I_0(S)$	$I_B(S)$
8.331	7.3929		17.014	7.0271	6.9006	25.438	6.8783	6.8627	33.495	7.1029	7.0906
8.575	7.2570		17.252	7.0648	6.8961	25.667	6.8766	6.8653	33.713	7.1116	7.0994
8.818	7.2111		17.490	7.0699	6.8919	25.896	6.8763	6.8682	33.930	7.1167	7.1083
9.062	7.1779		17.728	7.0559	6.8879	26.125	6.8752	6.8713	34.147	7.1229	7.1174
9.305	7.2503		17.965	7.0253	6.8842	26.353	6.8752	6.8747	34.364	7.1289	7.1265
9.548	7.2675		18.202	6.9804	6.8809	26.581	6.8737	6.8785	34.580	7.1348	7.1358
9.791	7.1998		18.439	6.9299	6.8777	26.809	6.8747	6.8826	34.796	7.1389	
10.034	7.0811		18.676	6.8675	6.8748	27.036	6.8752	6.8869	35.012	7.1432	
10.277	6.9666		18.913	6.8084	6.8721	27.263	6.8793	6.8915	35.227	7.1464	
10.519	6.8968		19.149	6.7660	6.8695	27.490	6.8825	6.8965	35.442	7.1529	
10.762	6.8845		19.385	6.7427	6.8671	27.717	6.8841	6.9017	35.657	7.1652	
11.004	6.8711	7.0956	19.621	6.7422	6.8649	27.943	6.8896	6.9071	35.871	7.1774	
11.247	6.9014	7.0849	19.857	6.7556	6.8629	28.169	6.9016	6.9128	36.085	7.1909	
11.489	6.9474	7.0746	20.092	6.7767	6.8610	28.395	6.9182	6.9188	36.298	7.2044	
11.731	7.0527	7.0646	20.327	6.7998	6.8594	28.620	6.9353	6.9250	36.511	7.2197	
11.973	7.1841	7.0550	20.562	6.8261	6.8579	28.845	6.9518	6.9314	36.724	7.2351	
12.214	7.2963	7.0455	20.797	6.8631	6.8566	29.070	6.9645	6.9380	36.937	7.2524	
12.456	7.3437	7.0364	21.031	6.8989	6.8554	29.294	6.9750	6.9447	37.149	7.2646	
12.697	7.3096	7.0274	21.266	6.9254	6.8543	29.518	6.9765	6.9515	37.360	7.2796	
12.939	7.2159	7.0187	21.500	6.9446	6.8534	29.742	6.9726	6.9585	37.572	7.2912	
13.180	7.1121	7.0101	21.733	6.9450	6.8526	29.965	6.9673	6.9655	37.782	7.3053	
13.421	7.0171	7.0017	21.967	6.9263	6.8518	30.188	6.9595	6.9726	37.993	7.3154	
13.662	6.9660	6.9935	22.200	6.9006	6.8512	30.411	6.9545	6.9797	38.203	7.3273	
13.902	6.9413	6.9854	22.433	6.8724	6.8507	30.634	6.9482	6.9869	38.413	7.3353	
14.143	6.9322	6.9775	22.666	6.8439	6.8504	30.856	6.9507	6.9941	38.622	7.3461	
14.383	6.9185	6.9698	22.898	6.8197	6.8503	31.077	6.9607	7.0015	38.831	7.3571	
14.623	6.9085	6.9623	23.131	6.8032	6.8504	31.299	6.9746	7.0090	39.040	7.3719	
14.863	6.8975	6.9549	23.363	6.7972	6.8507	31.520	6.9944	7.0167	39.248	7.3885	
15.103	6.8752	6.9478	23.594	6.8020	6.8512	31.741	7.0146	7.0244	39.456	7.4051	
15.342	6.8416	6.9409	23.826	6.8136	6.8518	31.961	7.0325	7.0323	39.664	7.4172	
15.582	6.7980	6.9342	24.057	6.8332	6.8526	32.182	7.0496	7.0403	39.871	7.4293	
15.821	6.7625	6.9279	24.288	6.8493	6.8536	32.401	7.0607	7.0484	40.078	7.4401	
16.060	6.7607	6.9218	24.518	6.8656	6.8549	32.621	7.0717	7.0566	40.284	7.4506	
16.299	6.8022	6.9160	24.749	6.8736	6.8564	32.840	7.0805	7.0649	40.490	7.4657	
16.538	6.8760	6.9106	24.979	6.8773	6.8583	33.059	7.0854	7.0734	40.696	7.4822	
16.776	6.9627	6.9055	25.208	6.8791	6.8604	33.277	7.0945	7.0820			

6.5 cm Camera Distance (r^3 Sector)

S	$I_0(S)$	$I_B(S)$	S	$I_0(S)$	$I_B(S)$	S	$I_0(S)$	$I_B(S)$	S	$I_0(S)$
18.296	4.0160		30.238	3.8777	3.8885	41.002	3.9521	3.9560	50.806	4.2076
18.668	3.9626		30.587	3.8698	3.8883	41.323	3.9594	3.9609	51.096	4.2185
19.039	3.9140		30.936	3.8647	3.8883	41.644	3.9659	3.9660	51.385	4.2286
19.410	3.8895		31.284	3.8696	3.8883	41.963	3.9712	3.9713	51.673	4.2397
19.781	3.8877		31.632	3.8796	3.8884	42.282	3.9783	3.9769	51.960	4.2502
20.150	3.9043		31.978	3.8868	3.8886	42.600	3.9846	3.9827	52.246	4.2599
20.520	3.9250		32.324	3.8943	3.8889	42.916	3.9904	3.9889	52.531	4.2727
20.888	3.9560	3.9386	32.668	3.8995	3.8894	43.232	3.9963	3.9952	52.815	4.2841
21.256	3.9795	3.9346	33.012	3.9007	3.8899	43.547	4.0036	4.0018	53.098	4.2958
21.623	3.9863	3.9309	33.355	3.8992	3.8906	43.860	4.0115	4.0086	53.380	4.3060
21.990	3.9703	3.9274	33.698	3.9001	3.8914	44.173	4.0182	4.0155	53.661	4.3189
22.356	3.9454	3.9240	34.039	3.9003	3.8924	44.485	4.0256	4.0226	53.941	4.3305
22.722	3.9140	3.9208	34.379	3.8952	3.8936	44.796	4.0290	4.0299	54.220	4.3434
23.087	3.8890	3.9179	34.719	3.8929	3.8950	45.106	4.0368	4.0374	54.498	4.3560
23.451	3.8816	3.9150	35.058	3.8903	3.8968	45.415	4.0440	4.0450	54.776	4.3687
23.815	3.8867	3.9123	35.396	3.8899	3.8987	45.723	4.0515	4.0528	55.052	4.3810
24.177	3.9004	3.9098	35.733	3.8902	3.9008	46.029	4.0591	4.0608	55.327	4.3942
24.540	3.9119	3.9074	36.069	3.8944	3.9031	46.335	4.0685	4.0691	55.601	4.4080
24.901	3.9134	3.9052	36.404	3.9003	3.9055	46.640	4.0762	4.0774	55.874	4.4191
25.262	3.9112	3.9031	36.738	3.9080	3.9082	46.944	4.0825		56.146	4.4329
25.622	3.9080	3.9011	37.072	3.9123	3.9110	47.247	4.0921		56.417	4.4451
25.982	3.9059	3.8993	37.404	3.9177	3.9139	47.549	4.1022		56.687	4.4582
26.341	3.9008	3.8976	37.736	3.9215	3.9169	47.850	4.1106		56.956	4.4691
26.699	3.8953	3.8960	38.067	3.9241	3.9201	48.150	4.1212		57.224	4.4833
27.056	3.8937	3.8946	38.397	3.9274	3.9233	48.449	4.1303		57.492	4.4947
27.412	3.8868	3.8933	38.726	3.9298	3.9267	48.747	4.1398		57.758	4.5078
27.768	3.8870	3.8922	39.054	3.9339	3.9303	49.044	4.1511		58.023	4.5222
28.123	3.8849	3.8912	39.381	3.9355	3.9341	49.340	4.1598		58.287	4.5390
28.478	3.8904	3.8904	39.707	3.9358	3.9381	49.636	4.1697		58.550	4.5559
28.831	3.9041	3.8898	40.032	3.9382	3.9423	49.930	4.1802		58.812	4.5736
29.184	3.9110	3.8894	40.356	3.9414	3.9467	50.223	4.1878		59.074	4.5908
29.536	3.9042	3.8890	40.680	3.9469	3.9513	50.515	4.1986		59.334	4.6047
29.887	3.8903	3.8888								

APPENDIX E

Experimental Leveled Intensity and Background Intensity Functions for PCl_5*

---

* Only data points for which background intensities, $I_B(s)$, are given were used in the structural analysis.

21 cm Camera Distance (r^3 Sector)

S	$I_0(S)$	$I_B(S)$	S	$I_0(S)$	$I_B(S)$	S	$I_0(S)$	$I_B(S)$	S	$I_0(S)$	$I_B(S)$
3.437	2.6290		8.081	2.3732	2.6344	12.569	2.6337	2.6307	17.004	2.6546	2.6713
3.559	2.6575		8.203	2.3489	2.6331	12.690	2.6695	2.6311	17.123	2.6504	2.6726
3.682	2.7016		8.325	2.3514	2.6318	12.810	2.7041	2.6316	17.242	2.6477	2.6740
3.804	2.7659		8.447	2.3797	2.6305	12.931	2.7321	2.6321	17.361	2.6486	2.6754
3.927	2.8481		8.568	2.4297	2.6291	13.051	2.7539	2.6327	17.480	2.6515	2.6768
4.049	2.9280		8.690	2.4961	2.6277	13.172	2.7658	2.6334	17.599	2.6539	2.6783
4.172	2.9805		8.812	2.5694	2.6264	13.292	2.7667	2.6342	17.718	2.6582	2.6797
4.294	3.0229		8.933	2.6399	2.6252	13.413	2.7551	2.6351	17.836	2.6609	2.6811
4.417	3.0132		9.055	2.7029	2.6241	13.533	2.7341	2.6360	17.955	2.6641	2.6826
4.539	3.0006		9.177	2.7500	2.6232	13.653	2.7066	2.6370	18.073	2.6668	2.6841
4.661	2.9470	2.7005	9.298	2.7758	2.6224	13.774	2.6713	2.6381	18.192	2.6688	2.6856
4.784	2.8560	2.6985	9.420	2.7824	2.6219	13.894	2.6342	2.6391	18.310	2.6711	2.6871
4.906	2.7396	2.6964	9.541	2.7698	2.6222	14.014	2.6001	2.6402	18.429	2.6729	2.6886
5.028	2.6174	2.6942	9.663	2.7458	2.6227	14.134	2.5708	2.6414	18.547	2.6754	2.6902
5.151	2.4990	2.6920	9.784	2.7155	2.6233	14.254	2.5495	2.6424	18.665	2.6791	2.6917
5.273	2.4040	2.6896	9.906	2.6856	2.6240	14.375	2.5376	2.6435	18.784	2.6853	2.6932
5.395	2.3230	2.6872	10.027	2.6575	2.6249	14.495	2.5364	2.6446	18.902	2.6931	2.6946
5.518	2.2876	2.6847	10.149	2.6383	2.6257	14.615	2.5438	2.6457	19.020	2.7016	2.6961
5.640	2.2829	2.6822	10.270	2.6298	2.6265	14.734	2.5611	2.6468	19.138	2.7109	
5.762	2.3170	2.6796	10.391	2.6300	2.6272	14.854	2.5844	2.6479	19.256	2.7202	
5.884	2.3808	2.6769	10.512	2.6349	2.6275	14.974	2.6089	2.6491	19.374	2.7281	
6.007	2.4682	2.6742	10.634	2.6432	2.6276	15.094	2.6365	2.6502	19.492	2.7335	
6.129	2.5682	2.6714	10.755	2.6514	2.6278	15.214	2.6615	2.6515	19.610	2.7370	
6.251	2.6721	2.6687	10.876	2.6527	2.6278	15.333	2.6807	2.6527	19.727	2.7367	
6.373	2.7696	2.6659	10.997	2.6499	2.6279	15.453	2.6958	2.6540	19.845	2.7330	
6.495	2.8590	2.6632	11.118	2.6377	2.6279	15.573	2.7070	2.6553	19.963	2.7284	
6.617	2.9233	2.6604	11.239	2.6199	2.6280	15.692	2.7125	2.6566	20.080	2.7227	
6.740	2.9701	2.6577	11.360	2.5968	2.6281	15.812	2.7165	2.6579	20.198	2.7149	
6.862	2.9905	2.6551	11.482	2.5738	2.6282	15.931	2.7148	2.6592	20.315	2.7072	
6.984	2.9858	2.6525	11.602	2.5505	2.6284	16.051	2.7101	2.6605	20.433	2.6983	
7.106	2.9578	2.6499	11.723	2.5332	2.6286	16.170	2.7042	2.6618	20.550	2.6917	
7.228	2.9073	2.6475	11.844	2.5226	2.6288	16.290	2.6971	2.6631	20.668	2.6876	
7.350	2.8398	2.6451	11.965	2.5198	2.6291	16.409	2.6890	2.6645	20.785	2.6890	
7.472	2.7584	2.6429	12.086	2.5261	2.6294	16.528	2.6822	2.6658	20.902	2.6933	
7.594	2.6681	2.6409	12.207	2.5429	2.6297	16.647	2.6724	2.6672	21.019	2.6997	
7.716	2.5780	2.6391	12.328	2.5684	2.6300	16.766	2.6665	2.6685	21.136	2.7090	
7.837	2.4939	2.6374	12.448	2.5984	2.6303	16.885	2.6594	2.6699	21.253	2.7227	
7.959	2.4231	2.6359									

11 cm Camera Distance (r^3 Sector)

S	$I_0(S)$	$I_B(S)$	S	$I_0(S)$	$I_B(S)$	S	$I_0(S)$	$I_B(S)$	S	$I_0(S)$	$I_B(S)$
8.331	3.3176		17.014	3.6339	3.6642	25.438	3.7073	3.6962	33.495	3.8354	3.8448
8.575	3.4231	3.7435	17.252	3.6234	3.6639	25.667	3.7138	3.6988	33.713	3.8424	3.8498
8.818	3.6467	3.7396	17.490	3.6276	3.6637	25.896	3.7180	3.7015	33.930	3.8487	3.8548
9.062	3.8349	3.7357	17.728	3.6353	3.6635	26.125	3.7182	3.7043	34.147	3.8568	3.8599
9.305	3.9648	3.7319	17.965	3.6421	3.6633	26.353	3.7150	3.7073	34.364	3.8653	3.8650
9.548	3.9625	3.7281	18.202	3.6467	3.6633	26.581	3.7092	3.7103	34.580	3.8741	3.8701
9.791	3.8692	3.7243	18.439	3.6490	3.6633	26.809	3.7019	3.7135	34.796	3.8818	3.8752
10.034	3.7684	3.7207	18.676	3.6557	3.6633	27.036	3.6975	3.7168	35.012	3.8882	3.8804
10.277	3.7116	3.7170	18.913	3.6725	3.6634	27.263	3.6990	3.7202	35.227	3.8905	3.8855
10.519	3.7102	3.7135	19.149	3.6955	3.6636	27.490	3.7048	3.7237	35.442	3.8943	3.8908
10.762	3.7380	3.7100	19.385	3.7171	3.6639	27.717	3.7142	3.7273	35.657	3.8985	3.8961
11.004	3.7295	3.7067	19.621	3.7247	3.6642	27.943	3.7288	3.7310	35.871	3.9023	3.9014
11.247	3.6944	3.7034	19.857	3.7117	3.6646	28.169	3.7441	3.7348	36.085	3.9056	3.9069
11.489	3.6224	3.7002	20.092	3.6828	3.6651	28.395	3.7539	3.7387	36.298	3.9100	3.9124
11.731	3.5662	3.6972	20.327	3.6454	3.6656	28.620	3.7606	3.7427	36.511	3.9145	3.9180
11.973	3.5451	3.6942	20.562	3.6159	3.6661	28.845	3.7604	3.7467	36.724	3.9195	3.9237
12.214	3.5763	3.6914	20.797	3.6037	3.6667	29.070	3.7582	3.7509	36.937	3.9277	3.9295
12.456	3.6525	3.6888	21.032	3.6093	3.6674	29.294	3.7556	3.7551	37.149	3.9364	3.9355
12.697	3.7514	3.6863	21.266	3.6306	3.6681	29.518	3.7526	3.7594	37.360	3.9434	
12.939	3.8379	3.6840	21.500	3.6607	3.6689	29.742	3.7534	3.7638	37.572	3.9506	
13.180	3.8820	3.6818	21.733	3.6882	3.6698	29.965	3.7571	3.7682	37.782	3.9577	
13.421	3.8559	3.6798	21.967	3.7106	3.6707	30.188	3.7638	3.7727	37.993	3.9651	
13.662	3.7699	3.6779	22.200	3.7183	3.6717	30.411	3.7691	3.7772	38.203	3.9709	
13.902	3.6547	3.6762	22.433	3.7132	3.6727	30.634	3.7744	3.7818	38.413	3.9757	
14.143	3.5525	3.6746	22.666	3.6973	3.6739	30.856	3.7818	3.7865	38.622	3.9813	
14.383	3.4964	3.6731	22.898	3.6760	3.6751	31.077	3.7887	3.7911	38.831	3.9868	
14.623	3.5093	3.6717	23.131	3.6606	3.6764	31.299	3.7967	3.7959	39.040	3.9951	
14.863	3.5695	3.6705	23.363	3.6550	3.6779	31.520	3.8039	3.8006	39.248	4.0025	
15.103	3.6511	3.6694	23.594	3.6576	3.6794	31.741	3.8114	3.8054	39.456	4.0095	
15.342	3.7169	3.6684	23.826	3.6672	3.6811	31.961	3.8155	3.8103	39.664	4.0189	
15.582	3.7535	3.6675	24.057	3.6759	3.6829	32.182	3.8201	3.8151	39.871	4.0253	
15.821	3.7580	3.6667	24.288	3.6812	3.6849	32.401	3.8251	3.8200	40.078	4.0312	
16.060	3.7421	3.6661	24.518	3.6838	3.6869	32.621	3.8278	3.8249	40.284	4.0372	
16.299	3.7126	3.6655	24.749	3.6856	3.6890	32.840	3.8288	3.8299	40.490	4.0481	
16.538	3.6797	3.6650	24.979	3.6903	3.6913	33.059	3.8298	3.8348	40.696	4.0576	
16.776	3.6525	3.6645	25.208	3.6989	3.6937	33.277	3.8326	3.8398			

6.5 cm Camera Distance (r^3 Sector)

S	$I_0(S)$	$I_B(S)$	S	$I_0(S)$	$I_B(S)$	S	$I_0(S)$	$I_B(S)$	S	$I_0(S)$
18.296	4.4962	4.4954	30.238	4.4710	4.4841	41.002	4.5842	4.5815	50.806	4.8182
18.668	4.5054	4.4950	30.587	4.4799	4.4853	41.323	4.5916	4.5868	51.096	4.8309
19.039	4.5355	4.4946	30.936	4.4865	4.4866	41.644	4.5947	4.5923	51.385	4.8360
19.410	4.5785	4.4942	31.284	4.4938	4.4880	41.963	4.5996	4.5979	51.673	4.8462
19.781	4.5740	4.4939	31.632	4.4985	4.4895	42.282	4.6030	4.6035	51.960	4.8546
20.150	4.5193	4.4934	31.978	4.4994	4.4911	42.600	4.6067	4.6093	52.246	4.8636
20.520	4.4504	4.4929	32.324	4.4985	4.4927	42.916	4.6119	4.6153	52.531	4.8748
20.888	4.4254	4.4923	32.668	4.5008	4.4945	43.232	4.6186	4.6213	52.815	4.8833
21.256	4.4488	4.4915	33.012	4.4952	4.4964	43.547	4.6269	4.6274	53.098	4.8920
21.623	4.4986	4.4907	33.355	4.4919	4.4985	43.860	4.6358	4.6337	53.380	4.9035
21.990	4.5410	4.4897	33.698	4.4921	4.5007	44.173	4.6443	4.6401	53.661	4.9133
22.356	4.5413	4.4884	34.039	4.4983	4.5030	44.485	4.6477	4.6466	53.941	4.9240
22.722	4.5061	4.4870	34.379	4.5064	4.5055	44.796	4.6547	4.6533	54.220	4.9374
23.087	4.4654	4.4857	34.719	4.5138	4.5080	45.106	4.6598	4.6601	54.498	4.9474
23.451	4.4491	4.4843	35.058	4.5188	4.5106	45.415	4.6674	4.6670	54.776	4.9579
23.815	4.4599	4.4831	35.396	4.5193	4.5133	45.723	4.6723	4.6741	55.052	4.9683
24.177	4.4733	4.4821	35.733	4.5191	4.5161	46.029	4.6798	4.6813	55.327	4.9782
24.540	4.4733	4.4811	36.069	4.5170	4.5191	46.335	4.6888	4.6887	55.601	4.9917
24.901	4.4750	4.4803	36.404	4.5162	4.5221	46.640	4.6956	4.6962	55.874	5.0028
25.262	4.4824	4.4797	36.738	4.5191	4.5253	46.944	4.7034	4.7039	56.146	5.0142
25.622	4.4943	4.4792	37.072	4.5253	4.5286	47.247	4.7121	4.7119	56.417	5.0254
25.982	4.4976	4.4789	37.404	4.5319	4.5321	47.549	4.7203		56.687	5.0375
26.341	4.4892	4.4787	37.736	4.5379	4.5357	47.850	4.7296		56.956	5.0481
26.699	4.4726	4.4786	38.067	4.5443	4.5396	48.150	4.7383		57.224	5.0590
27.056	4.4606	4.4785	38.397	4.5480	4.5436	48.449	4.7460		57.492	5.0681
27.412	4.4550	4.4786	38.726	4.5510	4.5478	48.747	4.7534		57.758	5.0777
27.768	4.4705	4.4788	39.054	4.5535	4.5522	49.044	4.7602		58.023	5.0912
28.123	4.4883	4.4791	39.381	4.5533	4.5567	49.340	4.7696		58.287	5.1047
28.478	4.4991	4.4796	39.707	4.5576	4.5614	49.636	4.7780		58.550	5.1189
28.831	4.5008	4.4803	40.032	4.5611	4.5662	49.930	4.7891		58.812	5.1360
29.184	4.4906	4.4811	40.356	4.5687	4.5712	50.223	4.7979		59.074	5.1528
29.536	4.4782	4.4820	40.680	4.5774	4.5763	50.515	4.8081		59.334	5.1654
29.887	4.4685	4.4830								

APPENDIX F

Corrected Experimental Leveled Intensity and Background Intensity Functions for PCl_5*

---

* Only data points for which background intensities, $I_B(s)$, are given were used in the structural analysis. The 21 cm camera distance intensity functions was corrected for 15 mole % $POCl_3$ and 30 mole % HCl impurity; the 11 and 6.5 cm camera distance intensity functions were both corrected for 8 mole % $POCl_3$ and 16 mole % HCl impurity.

21 cm Camera Distance (r^3 Sector)

S	$I_0(S)$	$I_B(S)$	S	$I_0(S)$	$I_B(S)$	S	$I_0(S)$	$I_B(S)$	S	$I_0(S)$	$I_B(S)$
3.437	2.5323		8.081	2.2159	2.5064	12.569	2.5143	2.5069	17.004	2.5159	2.5451
3.559	2.5615		8.203	2.1837	2.5052	12.690	2.5503	2.5076	17.123	2.5121	2.5466
3.682	2.6021		8.325	2.1826	2.5041	12.810	2.5859	2.5083	17.242	2.5108	2.5480
3.804	2.6609		8.447	2.2123	2.5031	12.931	2.6147	2.5091	17.361	2.5144	2.5496
3.927	2.7373		8.568	2.2687	2.5021	13.051	2.6376	2.5098	17.480	2.5207	2.5511
4.049	2.8097		8.690	2.3460	2.5012	13.172	2.6499	2.5106	17.599	2.5264	2.5526
4.172	2.8506		8.812	2.4331	2.5004	13.292	2.6504	2.5113	17.718	2.5342	2.5542
4.294	2.8843		8.933	2.5180	2.4997	13.413	2.6370	2.5121	17.836	2.5395	2.5558
4.417	2.8618		9.055	2.5950	2.4990	13.533	2.6132	2.5128	17.955	2.5450	2.5575
4.539	2.8450		9.177	2.6532	2.4984	13.653	2.5821	2.5136	18.073	2.5491	2.5591
4.661	2.7874	2.5544	9.298	2.6854	2.4978	13.774	2.5419	2.5144	18.192	2.5515	2.5609
4.784	2.6925	2.5520	9.420	2.6937	2.4974	13.894	2.4997	2.5152	18.310	2.5537	2.5626
4.906	2.5733	2.5498	9.541	2.6773	2.4971	14.014	2.4610	2.5160	18.429	2.5544	2.5643
5.028	2.4509	2.5475	9.663	2.6455	2.4969	14.134	2.4278	2.5169	18.547	2.5555	2.5661
5.151	2.3341	2.5454	9.784	2.6045	2.4967	14.254	2.4041	2.5177	18.665	2.5574	2.5679
5.273	2.2435	2.5433	9.906	2.5628	2.4967	14.375	2.3916	2.5186	18.784	2.5624	2.5697
5.395	2.1651	2.5413	10.027	2.5223	2.4967	14.495	2.3919	2.5195	18.902	2.5691	2.5715
5.518	2.1352	2.5393	10.149	2.4924	2.4967	14.615	2.4023	2.5204	19.020	2.5767	2.5733
5.640	2.1343	2.5374	10.270	2.4762	2.4968	14.734	2.4246	2.5214	19.138	2.5855	
5.762	2.1724	2.5356	10.391	2.4720	2.4970	14.854	2.4542	2.5224	19.256	2.5948	
5.884	2.2389	2.5337	10.512	2.4755	2.4973	14.974	2.4849	2.5234	19.374	2.6026	
6.007	2.3281	2.5320	10.634	2.4856	2.4976	15.094	2.5193	2.5244	19.492	2.6078	
6.129	2.4290	2.5302	10.755	2.4982	2.4980	15.214	2.5502	2.5255	19.610	2.6112	
6.251	2.5333	2.5285	10.876	2.5052	2.4984	15.333	2.5737	2.5267	19.727	2.6105	
6.373	2.6312	2.5269	10.997	2.5092	2.4989	15.453	2.5917	2.5278	19.845	2.6061	
6.495	2.7229	2.5252	11.118	2.5035	2.4994	15.573	2.6044	2.5290	19.963	2.6010	
6.617	2.7892	2.5236	11.239	2.4919	2.4999	15.692	2.6095	2.5302	20.080	2.5948	
6.740	2.8407	2.5220	11.360	2.4738	2.5004	15.812	2.6122	2.5315	20.198	2.5864	
6.862	2.8665	2.5204	11.482	2.4551	2.5010	15.931	2.6076	2.5327	20.315	2.5783	
6.984	2.8676	2.5189	11.602	2.4341	2.5016	16.051	2.5988	2.5340	20.433	2.5688	
7.106	2.8452	2.5173	11.723	2.4185	2.5022	16.170	2.5884	2.5353	20.550	2.5622	
7.228	2.7986	2.5159	11.844	2.4082	2.5028	16.290	2.5765	2.5366	20.668	2.5586	
7.350	2.7327	2.5144	11.965	2.4049	2.5035	16.409	2.5636	2.5380	20.785	2.5616	
7.472	2.6495	2.5130	12.086	2.4099	2.5042	16.528	2.5527	2.5394	20.902	2.5681	
7.594	2.5534	2.5116	12.207	2.4255	2.5048	16.647	2.5387	2.5408	21.019	2.5768	
7.716	2.4545	2.5102	12.328	2.4500	2.5055	16.766	2.5303	2.5422	21.136	2.5888	
7.837	2.3593	2.5089	12.448	2.4790	2.5062	16.885	2.5213	2.5436	21.253	2.6058	
7.959	2.2765	2.5076									

11 cm Camera Distance (r^3 Sector)

S	$I_0(S)$	$I_B(S)$	S	$I_0(S)$	$I_B(S)$	S	$I_0(S)$	$I_B(S)$	S	$I_0(S)$	$I_B(S)$
8.331	3.1595		17.014	3.4927	3.5322	25.438	3.5744	3.5625	33.495	3.6956	3.7036
8.575	3.2668	3.5925	17.252	3.4837	3.5320	25.667	3.5797	3.5650	33.713	3.7030	3.7086
8.818	3.5024	3.5897	17.490	3.4915	3.5319	25.896	3.5828	3.5676	33.930	3.7094	3.7136
9.062	3.7030	3.5869	17.728	3.5029	3.5318	26.125	3.5821	3.5702	34.147	3.7176	3.7186
9.305	3.8427	3.5842	17.965	3.5126	3.5317	26.353	3.5783	3.5730	34.364	3.7259	3.7237
9.548	3.8401	3.5814	18.202	3.5182	3.5317	26.581	3.5722	3.5758	34.580	3.7344	3.7288
9.791	3.7374	3.5786	18.439	3.5199	3.5317	26.809	3.5649	3.5788	34.796	3.7416	3.7340
10.034	3.6240	3.5759	18.676	3.5251	3.5317	27.036	3.5609	3.5819	35.012	3.7474	3.7392
10.277	3.5573	3.5732	18.913	3.5405	3.5318	27.263	3.5631	3.5850	35.227	3.7488	3.7445
10.515	3.5526	3.5705	19.149	3.5627	3.5319	27.490	3.5698	3.5883	35.442	3.7519	3.7499
10.762	3.5845	3.5679	19.385	3.5841	3.5319	27.717	3.5799	3.5917	35.657	3.7558	3.7553
11.004	3.5830	3.5654	19.621	3.5915	3.5321	27.943	3.5951	3.5951	35.871	3.7592	3.7608
11.247	3.5565	3.5630	19.857	3.5778	3.5322	28.169	3.6108	3.5987	36.085	3.7624	3.7664
11.489	3.4907	3.5606	20.092	3.5479	3.5324	28.395	3.6202	3.6024	36.298	3.7669	3.7720
11.731	3.4381	3.5584	20.327	3.5096	3.5327	28.620	3.6262	3.6062	36.511	3.7714	3.7778
11.973	3.4173	3.5562	20.562	3.4799	3.5330	28.845	3.6248	3.6101	36.724	3.7766	3.7836
12.214	3.4467	3.5540	20.797	3.4686	3.5333	29.070	3.6214	3.6140	36.937	3.7851	3.7895
12.456	3.5207	3.5520	21.032	3.4758	3.5338	29.294	3.6179	3.6181	37.149	3.7940	3.7956
12.697	3.6182	3.5500	21.266	3.4993	3.5343	29.518	3.6142	3.6222	37.360	3.8010	
12.939	3.7044	3.5481	21.500	3.5313	3.5349	29.742	3.6150	3.6264	37.572	3.8080	
13.180	3.7489	3.5463	21.733	3.5598	3.5356	29.965	3.6190	3.6306	37.782	3.8148	
13.421	3.7217	3.5446	21.967	3.5821	3.5365	30.188	3.6262	3.6348	37.993	3.8217	
13.662	3.6327	3.5430	22.200	3.5884	3.5374	30.411	3.6320	3.6391	38.203	3.8269	
13.902	3.5135	3.5415	22.433	3.5810	3.5385	30.634	3.6376	3.6434	38.413	3.8310	
14.143	3.4078	3.5401	22.666	3.5623	3.5398	30.856	3.6451	3.6477	38.622	3.8360	
14.383	3.3507	3.5388	22.898	3.5386	3.5411	31.077	3.6520	3.6522	38.831	3.8408	
14.623	3.3666	3.5377	23.131	3.5221	3.5426	31.299	3.6597	3.6566	39.040	3.8489	
14.863	3.4326	3.5367	23.363	3.5167	3.5442	31.520	3.6663	3.6611	39.248	3.8561	
15.103	3.5211	3.5358	23.594	3.5209	3.5458	31.741	3.6733	3.6657	39.456	3.8629	
15.342	3.5920	3.5350	23.826	3.5328	3.5476	31.961	3.6766	3.6703	39.664	3.8723	
15.582	3.6308	3.5343	24.057	3.5435	3.5495	32.182	3.6806	3.6749	39.871	3.8784	
15.821	3.6340	3.5338	24.288	3.5503	3.5514	32.401	3.6852	3.6796	40.078	3.8840	
16.060	3.6144	3.5333	24.518	3.5535	3.5535	32.621	3.6876	3.6843	40.284	3.8895	
16.299	3.5798	3.5329	24.749	3.5552	3.5556	32.840	3.6884	3.6891	40.490	3.9003	
16.538	3.5421	3.5326	24.979	3.5593	3.5578	33.059	3.6894	3.6939	40.696	3.9095	
16.776	3.5119	3.5323	25.208	3.5671	3.5602	33.277	3.6925	3.6987			

6.5 cm Camera Distance (r^3 Sector)

S	$I_0(S)$	$I_B(S)$	S	$I_0(S)$	$I_B(S)$	S	$I_0(S)$	$I_B(S)$	S	$I_0(S)$
18.296	4.5399	4.5630	30.238	4.5060	4.5199	41.002	4.6216	4.6178	50.806	4.8571
18.668	4.5470	4.5583	30.587	4.5168	4.5212	41.323	4.6290	4.6229	51.096	4.8701
19.039	4.5756	4.5539	30.936	4.5243	4.5226	41.644	4.6316	4.6282	51.385	4.8748
19.410	4.6201	4.5497	31.284	4.5319	4.5242	41.963	4.6363	4.6336	51.673	4.8851
19.781	4.6145	4.5459	31.632	4.5360	4.5258	42.282	4.6394	4.6392	51.960	4.8935
20.150	4.5555	4.5423	31.978	4.5357	4.5275	42.600	4.6432	4.6449	52.246	4.9025
20.520	4.4821	4.5389	32.324	4.5338	4.5294	42.916	4.6485	4.6508	52.531	4.9140
20.888	4.4577	4.5358	32.668	4.5362	4.5314	43.232	4.6555	4.6569	52.815	4.9225
21.256	4.4858	4.5329	33.012	4.5305	4.5334	43.547	4.6642	4.6631	53.098	4.9312
21.623	4.5412	4.5303	33.355	4.5277	4.5356	43.860	4.6736	4.6695	53.380	4.9430
21.990	4.5859	4.5279	33.698	4.5286	4.5379	44.173	4.6822	4.6761	53.661	4.9528
22.356	4.5825	4.5257	34.039	4.5357	4.5403	44.485	4.6850	4.6829	53.941	4.9637
22.722	4.5403	4.5237	34.379	4.5442	4.5428	44.796	4.6918	4.6898	54.220	4.9775
23.087	4.4942	4.5219	34.719	4.5514	4.5454	45.106	4.6968	4.6969	54.498	4.9875
23.451	4.4780	4.5203	35.058	4.5557	4.5482	45.415	4.7045	4.7042	54.776	4.9980
23.815	4.4936	4.5189	35.396	4.5551	4.5510	45.723	4.7093	4.7117	55.052	5.0085
24.177	4.5119	4.5177	35.733	4.5543	4.5540	46.029	4.7172	4.7194	55.327	5.0184
24.540	4.5136	4.5166	36.069	4.5518	4.5570	46.335	4.7266	4.7273	55.601	5.0324
24.901	4.5151	4.5157	36.404	4.5513	4.5602	46.640	4.7335	4.7354	55.874	5.0436
25.262	4.5211	4.5150	36.738	4.5550	4.5635	46.944	4.7414	4.7436	56.146	5.0551
25.622	4.5317	4.5144	37.072	4.5621	4.5669	47.247	4.7502	4.7521	56.417	5.0664
25.982	4.5333	4.5140	37.404	4.5693	4.5705	47.549	4.7583		56.687	5.0786
26.341	4.5234	4.5138	37.736	4.5754	4.5741	47.850	4.7676		56.956	5.0892
26.699	4.5059	4.5137	38.067	4.5817	4.5779	48.150	4.7763		57.224	5.0999
27.056	4.4945	4.5137	38.397	4.5848	4.5818	48.449	4.7839		57.492	5.1088
27.412	4.4901	4.5139	38.726	4.5872	4.5858	48.747	4.7911		57.758	5.1181
27.768	4.5084	4.5142	39.054	4.5894	4.5900	49.044	4.7979		58.023	5.1318
28.123	4.5279	4.5147	39.381	4.5888	4.5943	49.340	4.8075		58.287	5.1455
28.478	4.5386	4.5152	39.707	4.5935	4.5987	49.636	4.8161		58.550	5.1599
28.831	4.5390	4.5159	40.032	4.5973	4.6033	49.930	4.8276		58.812	5.1777
29.184	4.5264	4.5168	40.356	4.6054	4.6080	50.223	4.8365		59.074	5.1951
29.536	4.5124	4.5177	40.680	4.6147	4.6128	50.515	4.8468		59.334	5.2077
29.887	4.5021	4.5188								